Self-Assembled Peptides as Biomolecular Assemblers for Biomedical Applications

University of Kansas

2022

Sarah Kay Woolfolk (VanOosten)

ADVISOR, COMMITTEE CHAIR

Candan Tamerler, Ph.D.

COMMITTEE MEMBERS

Michael Johnson, Ph.D.

Gibum Kwon, Ph.D.

Malcolm Snead D.D.S., Ph.D.

Paulette Spencer, D.D.S., Ph.D.

Self-Assembled Peptides as Biomolecular Assemblers for Biomedical Applications

By
Sarah Kay Woolfolk (VanOosten)
M.S. BioEngineering, University of Kansas, 2016

Submitted to the graduate degree program of Bioengineering and the Graduate Faculty of the University of Kansas in partial fulfillment of the requirements for the degree of Doctor of Philosophy.

Chair: Candan Tamerler, Ph.D.

Michael Johnson, Ph.D.

Gibum Kwon, Ph.D.

Malcolm Snead D.D.S., Ph.D.

Paulette Spencer, D.D.S., Ph.D.

Defense Date: January 27, 2022

The dissertation committee for Sarah Kay Woolfolk certifies that this is the approved version of the following dissertation:

Self-Assembled Peptides as Biomolecular Assemblers for Biomedical Applications

_____

Chair: Candan Tamerler, Ph.D.

Date Approved: January 31, 2022

Abstract

In Nature, molecular self-assembly plays a critical role in the formation of complex biological structures and functions and is omnipresent in biological materials and systems. The dynamic interactions driven by the molecular self-assembly have been at the core of highly organized structures spanning the nano-, micro-, and macroscopic scales. Mimicking the self-assembly process in biological systems at the molecular scale led to the emerging field of molecular biomimetics, building upon the significant advances in biology, chemistry, material sciences, engineering, and medicine over the past three decades. The premise of molecular biomimetics is the development of hybrid engineering principles, where biomolecular tools can be incorporated in the design of advanced materials, processes, and systems. Recognized as the fundamental building blocks in biological systems, peptides and proteins play a key role in molecular recognition and self-assembly. Over the past few decades, solid-binding peptides have been identified and designed as molecular assemblers with material-selective affinities. These peptides demonstrate the ability to self-assemble at the surfaces and interfaces of solid materials and guide additional moieties to be anchored at site-specific positions. Building upon their bio-enabled surface and interfacial properties, several of these solid-binding peptides have been shown to develop novel hybrid materials. With inherent advantages over conventional chemical methods including ease of design and synthesis and modular design potential to offer multi-functional properties, these solid binding peptides have attracted increasing attention as a promising bio-enabled approach to design self-assembled, bioactive materials and systems for various applications across biotechnology, nanotechnology, and biomedical sciences.

Vast libraries of solid-binding peptides, known also as genetically engineered peptides for inorganics (GEPIs), have been identified in the past decades using principles of combinatorial

biology and protocols such as phage- and cell-surface display technologies. Identified peptides are subject to extensive qualitative and quantitative characterization to investigate their material-binding properties under different conditions. Peptide binding and assembly properties are merged with the computational approaches to investigate their sequence-structure-function properties. The iterative design of the peptides builds upon detailed experimental and computational approaches to enhance their properties specific to materials and desired applications.

Using high-affinity peptides and building upon their modular design potential at complex biomaterial interfaces, multifunctional biohybrid platforms can be designed where additional biological activities can be incorporated. Each application introduces new challenges with respect to their unique surface or interface in addition to the function in a desired environment. The peptide self-assembly depends on several factors ranging from physicochemical to environmental factors, and biological environments introduce another level of complexity due to several molecular events taking place. Peptide binding to biomaterial surfaces and interfaces under biological environments needs to be investigated in detail. Similarly, multi-domain activity of the peptides also requires significant exploration into *in vitro* and *in vivo* performances to ensure the robust multifunctional activities of the resultant molecular assemblies are maintained.

Herein, ***we explored engineered peptide design incorporated with different bioactive domains to address unique biomedical challenges to investigate them as effective and robust multi-functional biomolecular assemblers for selected biomedical applications under conditions ranging from*** **in vitro** ***to*** **in vivo** ***environments.*** This hypothesis is supported by the inclusion of three publications, presented herein, where a variety of peptide-enabled biomolecular systems were studied as biohybrid technologies for different applications. These applications include: 1) Capturing bioactivity in polymer fiber mats toward the design of novel, tunable biomaterials. Here,

bioactive shape memory polymer (SMP) fiber mats were developed as a self-assembled biohybrid material system. Nanofibers composed of poly(l-lactide)/poly(methyl methacrylate) (PLLA/PMMA) were produced using pressurized infusion gyration and incorporated a fusion fluorescence protein tagged with mineral binding peptide. Peptide-enabled design allowed for binding to hydroxyapatite nanoparticles as well as offered mineralization capability towards developing a tunable soft to hard material transition; 2) Imbalance of free biometal ions are recognized to play a critical role in neurodegenerative diseases. A peptide-enabled nanoprobe design was developed as a potential imaging tool to monitor free biometals associated with neurodegenerative diseases in a living zebrafish brain model with both spatial and temporal resolution; and 3) Caries is the most pervasive infectious disease of mankind and early childhood caries (ECC) and resultant destruction of the teeth is recognized as a global health crisis. Silver diamine fluoride (SDF) offers a promising treatment option but causes significant staining of caries-effected dental tissues. A peptide-enabled nanocomposite formation at the interface of SDF-treated dental tissues was developed. A novel bifunctional construct was developed, building upon the peptide binding ability to silver-stained dental tissues, to incorporate a peptide capable of mediated mineralization at this complex interface. The proposed approach offers the potential to overcome the black staining associated with the recently approved SDF caries arresting treatment.

Acknowledgements

It feels surreal to finally be submitting my PhD dissertation. I came to KU with the idea that I would work hard, conduct novel research, and earn a degree, but am leaving with infinitely more. I have experienced numerous successes and challenges both in my academic and personal life throughout my time here at KU and have grown immensely as a person. I am so grateful for this tremendous accomplishment and would not have reached my goals without the support and guidance of the numerous incredible people who have helped me along this journey. I am forever grateful to each of these people mentioned below who have lifted me up and kept me moving forward on the path to a successful academic journey, especially on the most difficult days.

I would first like to thank my advisor, Dr. Candan Tamerler, who has supported me unconditionally and pushed me to achieve more than I ever thought possible. Her understanding, encouragement, and help through both personal and academic struggles throughout my journey here at KU can only be described as above and beyond. She has had my back through thick and thin and I am eternally grateful to have had such an incredibly wise, patient, and fiercely supportive mentor. Thank you, Dr. Tamerler, for taking me on as a student, seeing my potential, teaching me extraordinary science, and helping me to achieve both my Master's and PhD degree – I would not be the person I am today without you and your guidance and mentorship.

I am grateful for my committee members, Dr. Michael Johnson, Dr. Gibum Kwon, Dr. Malcolm Snead, and Dr. Paulette Spencer. Drs. Snead and Spencer have been part of my journey throughout both my Master's and PhD degrees here at KU and I am so fortunate to have had their support and mentorship and access to their wealth of knowledge. Dr. Kwon has provided great insight into my projects and it was also wonderful to work with him as his GTA. I have enjoyed working with Dr. Johnson and his expertise in chemistry has helped boost my knowledge and advance our collaborative works.

I also want to acknowledge the numerous grants and funding sources throughout my time at KU. I have been supported as a GRA and GTA through departmental funds from the University of Kansas Department of Mechanical Engineering and Department of BioEngineering, as well as National Institutes of Health (NIH) grant 1R01DE025476 (PI: P Spencer and C Tamerler), NFR support provided through the University of Kansas, the University of Kansas Research Grant Opportunity program (KU Research GO; Lead PI: M Johnson, Co-PI: C Tamerler), and National Science Foundation-NSF-CHE program research grant 2108448 (PI: C. Berrie, Co-PI: C. Tamerler). I appreciate all of the time and hard work put in by my advisor, Dr. Tamerler, as well as that of Dr. Spencer, Dr. Johnson, and Dr. Berrie to secure these grants and funding opportunities that supported me and my research.

I want to thank all of my current and former lab group members. Dr. Banu Taktak-Karaca for her countless hours teaching me – from the basics to complex protocols and experimental design, her constant guidance and support, patience, and lifelong friendship. I am so thankful for the mentorship and training from wonderful post-docs Dr. Erkan Mozioglu, Dr. Sheng-Xue Xie, Dr. Esra Yuca, and especially Dr. Nilan Kamathewatta for his training, advice, and helping me on the path to finish and Dr. Kyle Boone for his support, numerous scientific discussions, and friendship over the years I've been at KU. I am so grateful for my former lab-mates Dr. Cate Wisdom, Rachel

Lietz, Jack Rogers, and Dr. Onur Caglar for their friendships and wonderful late nights working together. I also have had the privilege to work with fantastic undergraduate students Marcos Barbosa, Tammy Nguyen, Brandon Tomas, Sarah Freeburne, Matthew Kavanaugh, and especially Matthew Jaeschke who helped me tremendously on several of my core PhD projects. I am also thankful for my current lab members and all of their friendships and support, especially over the past couple years. Thank you to Jacob Freitag for your vast wealth of knowledge, problem solving abilities, and willingness to help at any given second. Thank you to Aya Cloyd and Alyssa Curry for your friendship and support over the past few semesters in our lab – I have loved working with you both. I'm grateful for our newest lab member Taylor Bader, who will be taking over some of my projects and our current undergraduate students Kalea Chu and Ishan De – all of whom have bright futures ahead of them.

I am so lucky to have been able to work with amazing collaborators at KU. I am so appreciative of Dr. Charles Ye of IBER for the years of training, support, and guidance. Former IBER members Dr. Xueping Ge, Dr. Leon Song, Dr. Odair Bim, and Dr. Rizacan Sarikaya – I am so thankful for the training and mentorship. A big thank you to Dr. Romana Jarosova for her mentorship on collaborative projects. Thank you to the MAI imaging lab staff – Dr. Eduardo Rosa-Molinar, Dr. Prem Thapa, Dr. Noraida Martinez-Rivera, and former staff Heather Shinogle for the countless hours of training and help with advanced imaging across all of my projects. I was lucky enough to work with Dr. Mark Richter who was an amazing scientist and will forever be missed. To Dr. Cindy Berrie and undergraduate student Sarah Gress whom I have had the pleasure working with this past year. Thank you to Dr. Annie Lee who I met during my time at KUMC – you have supported me and kept a light on for me at my darkest times and I am so grateful for your mentorship and lifelong friendship. I am grateful for Dr. Patrick Grogan and family who helped me start this journey at KU. Thank you to my colleagues and Tamerler lab alumni at University of Washington, especially Dr. Deniz Yucesoy. It has also been incredible to work with our international collaborators at University College of London Dr. Mohan Edirisinghe, Dr. Sunthar Mahalingam, Dr. Siqi Zhang, and Dr. Xiowen Wu.

I am also extremely lucky to have met such fantastic people within the KU BioE program and other graduate programs throughout my time here and would not have made it through without their support and friendships. I am tremendously thankful for Dr. Saba Ghazvini, Dr. Farhana Abedin, Dr. Aparna Chakravarti, and Jeannie Salash – you are all such incredible friends and have supported me immensely along this journey. I also want to thank Dr. Sushma Jadalannagari, Dr. Steve Harrington, Dr. Karthik Ramachandran, Dr. Sonia Rawal, Dr. Mitch VeDepo, Dr. Aishik Chakraborty, Dr. Dwight Deay, Dr. Emily Beck, Dr. Nikki Galvis, Dr. Lindsey Ott, Dr. Robbie Hable, Dr. Saman Modaresi , Dr. Emi Kiyotake, Dr. Jakob Townsend, Dr. Fallon Fitzwater, Dr. Jordan Borrell, Rachel Hattaway, Dr. Renae Davis, Dr. Ember Krech, and Dr. Kelsey Knewtson for their help, friendship, and support over the course of my academic journey. I also want to thank Jen Welch for her friendship and for being the best administrative assistant to ever exist. A special thank you to Phil Elrod for the countless hours of mentorship, guidance, training, life advice, and friendship over the years since you came to KU.

I am so thankful for my life-long besties Rachel Spencer and Amy Alexander and their wonderful families. Rach and Aimes, you are my sisters and our friendships have lasted through

decades. I could not live life without you both and all the trips you have made to visit me down in Kansas to help me not feel so far from home. I love you both so much and your unconditional support has meant the world to me. I am also thankful to my other incredible friends I have made outside academia – from friends back in Minnesota to new friends in Kansas City and Lawrence. These friendships have kept me going and the amazing people in my life have offered me the support I needed to achieve both my academic and personal goals. I cannot believe I could have these friendships that can span from elementary school to new friends that I've made along the way – each of them have played a key role in making me the person I am today, and I am eternally grateful.

An enormous thank you to the Woolfolk family. Since December 2017 they have provided me with a wealth of love and support. I'm so lucky to call them my actual family now, but they gave me a sense of family within days of meeting them all. It was that sense of family that kept me here at KU after a very rough year. I could never express the amount of love I have for my in-laws Mark and Laura Woolfolk as truly my second parents – thank you both especially for your unconditional love and support and for every Sunday dinner and family event you've hosted – it has meant the world to me. I am also thankful to Chess and Nikki Woolfolk for all that they have done for me, especially helping to support me when times were tough. I love you both so much and am so blessed to be an aunt to both Eli and Beau. To Adam and LeiLei Mitchell and your incredible kiddos, Graham and Lenore - I cannot thank you enough for inviting me into your family with open arms and lots of love. Thank you all so much and I am beyond lucky to have married into such an incredible family.

To my parents, Ann and Jim VanOosten… where do I begin? I am beyond blessed to have the most incredible and supportive parents who have taught me and guided me from a young age to set goals and chase my dreams. I never expected to be away from 'home' as long as I have and hate how many things I have missed out on throughout my academic journey at KU. But they have both kept believing in me and have unconditionally supported me mentally, emotionally, financially, and, at times, even physically so that I could achieve this goal of getting my PhD. I cannot imagine trying to do this without their unconditional love, encouragement, and fierce support. They have made countless trips down to be here with me and have kept me afloat when I felt like I was drowning. My extraordinary parents have been there *for* me and *with* me through both my successes and immense challenges in both my personal and academic life. Mom and Dad – I love you both so much and am forever indebted to you both for everything you have helped me with throughout this long and difficult journey. Thank you both for having my back and pushing me forward so that I could achieve every one of my goals. I am also so thankful for my amazing brothers Matthew VanHua and David VanOosten and my incredible sister-in-law Lillian VanHua. Even from opposite coasts, they have provided me with support and encouragement throughout my entire time at KU. I could not have asked for a more loyal and loving family. Thank you, Matt, Lil, and Dave, for helping me along my journey and for shaping me into the person I am today.

Finally, I am thankful for my amazing and handsome husband, John Woolfolk. He has been 'the one' since day one and I am so lucky to be married to my best friend. I am grateful for his unconditional love and support through this whole process and the countless number of times he has had to take on all the housework and errands when I have been buried in my work. He has

encouraged me and pushed me forward when I was falling back and kept me focused on the end goal when I felt overwhelmed. I am beyond lucky to have met him and am so thankful that we have been able to raise our insane animals together. I'm so thankful for our German Shepherd and princess, Freyja Louise, and our rabbit, Gaia, who have both been a constant source of laughter and joy over the years with daily antics. John Scott – you have been my rock and have been there for me on my worst of days to give me a hug and get me to laugh. I am so thankful to you and love you more than words. I cannot wait for our next adventure as parents to our baby boy, who is still in utero at the time of writing this!

I dedicate all of my hard work and this dissertation to my parents, my husband, and my baby boy who is due within two weeks

Research Publications

This dissertation is prepared mainly based upon my co-authored and first-authored journal publications **(P1-P3)** listed below:

P1: *X Wu, S Mahalingam,* ***SK VanOosten****, C Wisdom, C Tamerler, M Edirisinghe, "New Generation of Tunable Bioactive Shape Memory Mats Integrated with Genetically Engineered Proteins", Macromolecular Bioscience, 17(2) (2017).*

This work demonstrated two novelties by first generating shape memory polymer (SMP) fiber mats through the process of pressurized infusion gyration as well as incorporating bioactivity through a genetically engineered bifunctional construct. Poly(l-lactide)/poly(methyl methacrylate) (PLLA/PMMA) binary blends of fibers were first prepared as SMP mats and their morphologies were investigated via scanning electron microscopy to determine the effects of processing parameters. A 50/50 blend was selected and further studied following the incorporation of a green fluorescence protein-hydroxyapatite peptide (GFP-HABP) functionalized hydroxyapatite nanoparticles to bring bioactivity to the fiber mats. Shape memory properties were assessed, and the uniform distribution and sustained function of the bioactive domain within the SMP mat network was confirmed via fluorescence microscopy. An enzyme-mediated mineralization assay and subsequent analysis with Fourier transform infrared (FTIR) and Raman spectroscopies were used to further evaluate the bi-functionality of the engineered protein-peptide construct in the complex 3-D environment. My contributions to this work were in the experimental design to incorporate the bioactive domain, GFP-HABP production, fluorescence imaging, vibrational spectroscopic analysis, and helping to write the manuscript.

P2: *R Jarosova, **SK Woolfolk**, N Martinez-Rivera, MW Jaeschke, E Rosa-Molinar, C Tamerler, MA Johnson, "Engineered Nanoprobes for Spatiotemporal Imaging of Metal Ions in Living Zebrafish Brain Tissue", Submitted to ChemComm, January 2022.*

This paper is currently under review in ChemComm published by the Royal Society of Chemistry

This work demonstrated that a peptide-protein functionalized gold nanoparticle (AuNP) nanosensor could be used for *in vivo* monitoring of key metal ions with both spatial and temporal resolution. The novelty of this work was in the approach to optimize the delivery of red fluorescence protein–gold binding peptide (DsRed-AuBP) functionalized AuNP-based nanoprobes and determine the maintained stability and function within a living brain model for the first time. Fluorescence and two-photon excitation confocal fluorescence microscopies were employed to provide a detailed evaluation of the stability of the bioactive nanoprobes in a living zebrafish brain via the sustained fluorescence signal of the DsRed protein bound via an affinity-peptide. Fluorescence quenching studies in the presence of key free transition metals were completed both *in vivo* and *in vitro*. My contributions to this work were the production of the bifunctional construct and developing of the nanoprobe sensors for optimized in vivo studies, *in vitro* quenching studies, fluorescence imaging and analysis, and helping to write the manuscript.

P3: ***SK Woolfolk**, AK Cloyd, Q Ye, K Boone, P Spencer, ML Snead, C Tamerler, "Peptide Enabled Nanocomposites Offer Biomimetic Reconstruction of Silver Diamine Fluoride Treated Dental Tissues", Submitted to Polymers, January 2022.*

This paper is currently under review in Polymers published by MDPI

The studies conducted in this work aimed to employ a novel bifunctional peptide to offer biomimetic reconstitution of dental tissues treated silver diamine fluoride (SDF), a recently

approved treatment for advanced dental caries. Our approach first confirmed the binding of our established silver-binding peptide (AgBP) conjugated with red fluorescence protein (DsRed) on complex interface of dental tissues using confocal fluorescence microscopy. Amelogenin protein as the most abundant enamel matrix protein is recognized its key role during enamel biomineralization. Building upon our prior art in identification of amelogenin domains, we selected an amelogenin derived peptide (ADP5) that mimics the mineralization kinetics properties of full length amelogenin protein. A novel bifunctional peptide was designed using merged computational and experimental methods, synthesized, and characterized to test multi-functionality. Using this bifunctional peptide, we then functionalized dental tissue slabs and subjected them to an enzyme-mediated mineralization assay and studied the resultant calcium phosphate mineral formation using scanning electron microscopy and energy dispersive X-ray spectroscopy (SEM-EDS). Our results confirmed new mineral synthesis at the complex dental tissue interface. Overall, our approach offers a potential path to overcome the negative aesthetic side effects of SDF staining on dental tissues. My contributions to this work were the developing the protocols, dental tissue preparation, protein-peptide and peptide-peptide selection, production/synthesis, and characterization, imaging and EDS analysis, and writing of the manuscript.

I have also co-authored five additional publications **(P4-P9)** that were not covered in the scope of this dissertation but are listed below:

P4: *E Yuca, SX Xie, L Song, K Boone, NJB Kamathewatta,* ***SK Woolfolk****, P Elrod, P Spencer, C. Tamerler, "Reconfigurable Dual Peptide Tethered Polymer System Offers a Synergistic Solution*

for Next Generation Dental Adhesives", International Journal of Molecular Sciences, 22(12) 6552 (2021).

P5: *P Spencer, Q Ye, NJB. Kamathewatta, SK Woolfolk, BS Bohaty, A Misra, C Tamerler, "Chemometrics-Assisted Raman Spectroscopy Characterization of Tunable Polymer-Peptide Hybrids for Dental Tissue Repair", Frontiers in Materials, 8 (2021).*

P6: *SX Xie, L Song, E Yuca, K Boone, R Sarikaya,* ***SK VanOosten****, A Misra, Q Ye, P Spencer, C Tamerler, "Antimicrobial peptide-polymer conjugates for dentistry", ACS Applied Polymer Materials, 2(3) 1134-44 (2020).*

P7: *SX Xie, K Boone,* ***SK VanOosten****, E Yuca, L Song, X Ge, Q Ye, P Spencer, C Tamerler, "Peptide mediated antimicrobial dental adhesive system", Applied Sciences, 9(3), 557 (2019).*

P8: *C Wisdom,* ***SK VanOosten****, KW Boone, D Khvostenko, PM Arnold, ML Snead, C Tamerler, "Controlling the Biomimetic Implant Interface: Modulating Antimicrobial Activity by Spacer Design", Journal of Molecular and Engineering Materials, 4(1) 1640005 (2016).*

Table of Contents

List of Figures

List of Tables

Chapter 1 Introduction

1.1 Surfaces and Interfaces of Biomaterials

Implantable biomaterials, biomedical devices, and tissue-engineered constructs have become a pillar of modern medicine, most notably over the past three decades. Such materials and devices have been employed to restore, repair, and regenerate irreparable tissue loss or damage, provide mechanical support, promote local function, deliver pharmaceutics, facilitate imaging and diagnostics, or direct native tissue growth, among many other applications.[1-7] However, these advanced techniques, therapeutics, and treatments rely upon the successful integration and initial interaction of biomaterials following their exposure to the complex biological environment. Although often utilized for their bulk properties, it is the *surfaces and interfaces* of biomaterials and subsequent interfacial interactions that ultimately determine the overall success of implantable materials and devices.[1, 4, 6-19] Surfaces of biomaterials have been modified mainly by physical and chemical methods to enhance the interfacial properties. Physiochemical properties, ranging from roughness and degradation to competitive binding, surface charges, and interactions, all play a critical role in directing the biological response to a biomaterial.[6, 20] While physical modification may lead to changes in the surface topographies using different techniques such as etching and machining, chemical modifications may result in changes in hydrophilicity, oxidation, nitrification, ion infusion, single to multi-layer coatings, and surface functionalization using wide range of techniques.[6, 20-24] Overall, these techniques aim to develop a surface and interface offering a favorable biological response. Biomaterial surfaces exposed to the biological environment are subject to protein adsorption; these non-specific interactions may be detrimental to the function of the biomaterials. To avoid non-specific interactions and ensure the desired function of the biomaterial, it has become empirical to couple bioactive moieties at the biomaterial

interface and guide the function toward a desired outcome. Integration of these bioactive cues remains a critical challenge to the advancement in biomaterial design and there is an urgent need for novel approaches aimed to control the displayed activity, synthesis, and functionality at these critical biomaterial interfaces. These complex interactions provide many opportunities to optimize biomaterial design to enable control over interfacial surface properties. Functionalization of biomedical *surfaces* is crucial, but to achieve proper and predictable functional activity of any bioactive moiety relies upon their controlled conformation and orientation.[4, 6, 17, 25, 26]

1.2 Surface Functionalization

Traditional surface functionalization techniques for biomaterials are primarily rooted in chemistry. These methods rely upon physical adsorption of bioactive moieties and/or covalent chemistry to generate a coating or monolayer formation around the relevant bulk material.[23, 24, 27, 28] Surfaces have been functionalized either with small molecules (e.g. thiols, silanes) or macromolecules (polymers) that form self-assembled monolayers (SAMs) have remained a popular technique for decades.[22-24, 27-30] SAMs are immobilized thin films that consist of amphiphilic molecules spontaneously adsorbed onto a substrate. Conventional SAMs feature an affinity-based head group which forms a covalent attachment to a surface, and, separated by a short molecular spacer, display a free functional group at the terminal end for specific surface modification as shown schematically in Figure 1-1(a). Theoretically, on a flat surface, the molecules would covalently bind to the desired surface forming a uniform monolayer as depicted in Figure 1-1(b). Commonly employed thiol-based SAMs boast spontaneous binding affinity to metals and metal oxide surfaces and offer ease of preparation. Unfortunately, thiol-based SAMs have repeatedly shown poor stability due to rapid oxidation under ambient as well as physiological conditions.[22, 24, 29, 30] Alternatively, the silica-binding affinity of silane-based SAMs have

demonstrated tunable wettability and improved physical and chemical stability as compared to their thiol-based counterparts forming monolayers on metals.[22] Silane-based monolayers, however, are highly reactive during assembly, require an involved chemical process, and functionalized silica surfaces have fewer applications for *in vivo* biomaterial implants.[22, 24] The most versatile and stable SAMs for functionalizing biomedical implant interfaces employ long-chain macromolecules with surface-recognition units. Recognized also as polymer brushes, these thicker-film SAMs offer robust stability under physiological conditions, but still require complex preparation and have limited control over the nano-topography.[24, 28] Overall, the complex chemical reactions required for covalent surface functionalization employ harsh solvents and commonly suffer from reduced stability under ambient conditions. Despite the success with the traditional SAM-based surface functionalization techniques, there is a lack of control for the biomolecular orientation (Figure 1-1(c)). The resulting random orientation leads to inconsistent or reduced functional activity. The rigid functionalization approach of SAMs offers reduced compatibility in a biophysical environment which thrives upon dynamic flexibility to achieve proper integration. Overall, these approaches do not address the critical control over molecular orientation which is vital for maintaining bioactivity.[3, 12, 13, 31-33]

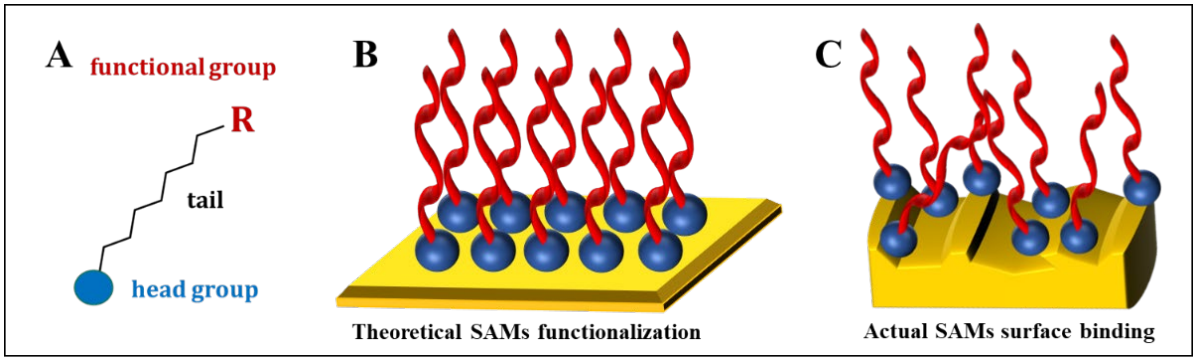

Figure 1-1: Schematic representation of an amphiphilic moiety (a) and the theoretical surface binding and functionalization of SAM molecules (b) versus the actual binding on a non-uniform surface depicting the lack of orientation control over the covalently bonded molecules (c).

1.3 Molecular Biomimetics for Biohybrid Interfaces

Inspired by Nature, molecular biomimetics offers new avenues for design and utilization of multifunctional biomaterials building upon the molecular scale approach to generate bio-hybrid interfaces.[5, 13, 26, 33-36] In Nature, there is a richness of complex materials and systems with remarkable functional properties as a result of their highly organized structures starting at the nanoscale. Biological materials are self-directed in their organization, yet their innate properties are not achievable in purely synthetic systems, even under mimicked biological environments. The molecular recognition is key to their function, which relies on biomolecular interactions. Building upon their uniquely controlled molecular, nano- and micro bio-hybrid structures through molecular recognition, we and many others have applied the molecular biomimetic approach to design biohybrid materials that utilize proteins similar to nature. Inspired by biocomposites that have incorporated both structural and functional proteins and minerals, we identified small peptides for self-assembly of materials with controlled organization and desired function.[5, 13, 26, 33-40] Similar to Nature`s way of successive cycles of mutations and generations, these peptides can be improved with enhanced functionality toward designing self-assembled, self-organized, and self-integrated biomaterial systems. Peptides and proteins have long been recognized as the fundamental building blocks of living systems in nature, their role in molecular recognition and self-assembly have attracted increasing attention as a favorable approach to produce new, hybrid materials with advanced properties for various applications in different areas such as biotechnology, nanotechnology, and biomedical sciences.[26, 33-36, 41-44]

1.4 Peptide-Enabled Surfaces and Interfaces

Self-assembling, short peptide sequences, in particular, have proven to be ideal candidates as molecular assemblers to fabricate new functional hybrid platforms with innate advantages. These

short peptides offer ease of design and synthesis, inherent biocompatibility, and tunable properties without the potential problems or limitations associated with the conventional chemical methods.[3, 13, 32-34, 41, 44-48] Solid binding peptides, also known also as genetically engineered peptides for inorganic surfaces (GEPIs), are isolated using combinatorial biology protocols such as phage- and cell-surface display technologies. GEPIs bind to surfaces through a combination of non-bonded weak interactions, including van der Waals, hydrogen bonding, and Coulombic attraction. However, these non-bonded interactions collectively result in high affinity with dynamic flexibility with the peptide conformation. Peptide conformation onto their affinity surfaces use multiple contact points to create a dynamic and reactive surface interaction.[13, 25, 26, 49] As GEPIs are combinatorially selected, they are subject to extensive qualitative and quantitative molecular characterization merged with the computational approaches prior to their use as molecular assemblers.[10, 18, 33, 34, 37, 50-55] Computational approaches allows to engineer their sequence-structure-function. Dynamically controlled, directed self-assembly of functional moieties through molecular recognition of GEPIs may create robust surface coverage with high material specificity. Building upon the previous combinatorial biology-based techniques, effective peptide sequences have been successfully categorized for their solid materials self-assembly functions.[10, 34, 39, 55-60] Functional hybrid platforms can be further generated using these well-described peptide sequences to display additional biological activities via attached peptides or proteins on key materials for advanced biomaterial design. In our prior studies, we have shown the successful design of multifunctional fusion proteins and peptides, a modular strategy that incorporates the robust capacity of the selected solid-binding peptides.[10, 50, 52, 54, 59, 61-69] These results demonstrated that peptides with material-specific, strong binding, affinity tags provide critical flexibility which allow for a responsive interface and modular design potential

for multi-functionality, while still maintaining critical control over orientation.[14, 26, 33, 35, 39, 52, 63, 67, 69-74]

1.5 Scope of dissertation

Herein, our overall objective is to explore the use of key solid-binding peptides with additional bioactive moieties as robust, dynamic molecular tools that can be utilized at complex biomedical interfaces ensuring the multifunctional activity across both *in vitro* and *in vivo* conditions. ***We hypothesize that solid binding peptides can be engineered with additional biological activities as effective and robust multi-functional molecular assemblers to function under in vitro to in vivo environments to address challenging biomedical problems.***

In the scope of the thesis progression, we focused on three groups of GEPIs to engineer the biomimetic interfacial interactions and include additional functional peptides and proteins to investigate their multifunctional effectiveness in part of biomaterials design and synthesis. Calcium phosphate mineral binding and mineralization peptides (HABP and ADP), gold-binding peptide (AuBP), and silver-binding peptide (AgBP) sequences were selected as the anchoring solid-binding peptides for our studies. Expanding on our prior art, we selected three distinct applications to design and engineer multifunctional peptide constructs and test their effectiveness in selected in vitro and in vivo conditions.

Silver binding peptide (AgBP), gold binding peptide (AuBP), and calcium phosphate mineral binding and mineralization peptides (HABP and ADP) were selected as each offers a unique functionality for specific biomedical applications providing antimicrobial efficacy and anchoring, molecular imaging and biosensing capability, and directed remineralization and biohybrid nanocomposite formation, respectively. Fluorescent proteins including DsRed or GFP were conjugated to the peptides to provide enhanced visualization and bimodal imaging properties.

Figure 1-2 provides a schematic representation of our approach and highlights two of our fusion protein constructs incorporated with selected peptides in sensing and novel biomaterial design. A multi-peptide domain design with peptide-enabled nanopcomposite mineralization was also investigated as a robust interface for a trailblazing dental tissue application.

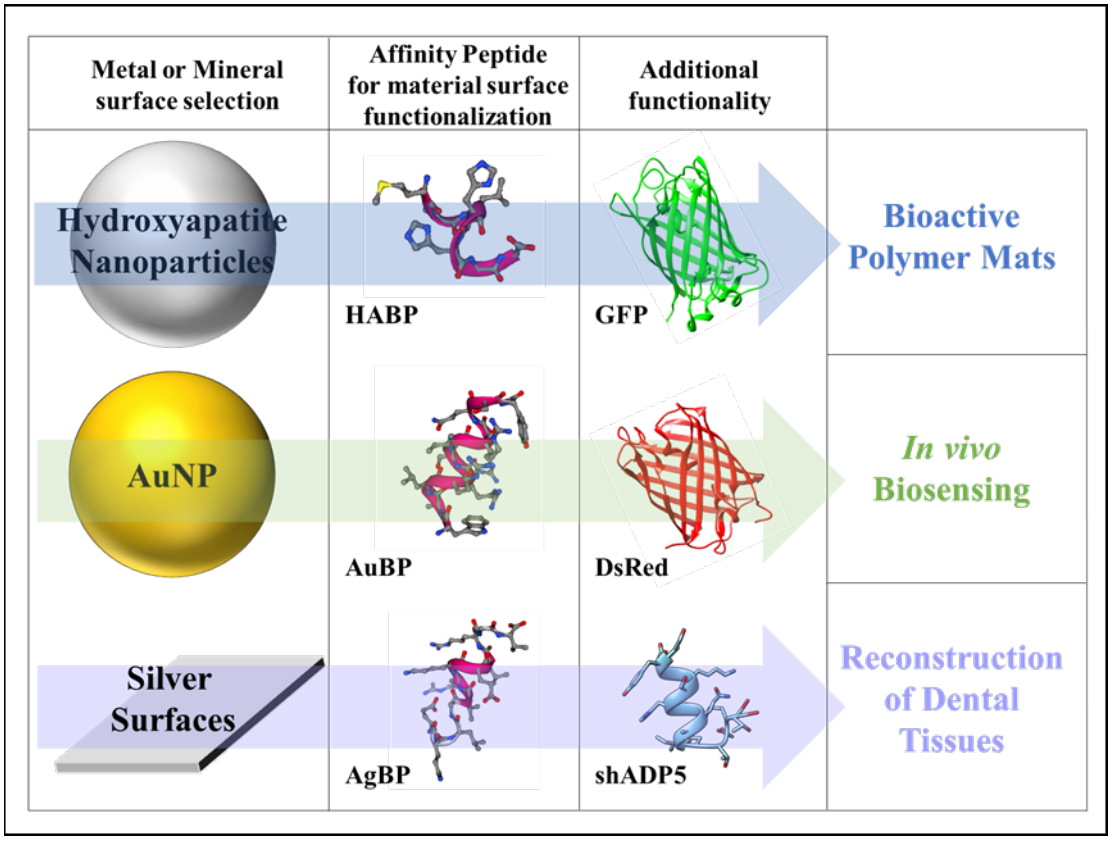

Figure 1-2: Schematic overview of key surfaces functionalized with self-assembling solid-binding peptides conjugated with additional functional proteins or peptides for advanced applications with visualization, biosensing, and remineralization potential for use in novel, bioactive biomaterial design.

To support our hypothesis, **three peer-reviewed publications are included, herein,** with additional features across three distinct applications. In the first publication, we employ GFP-HABP to visualize biofunctional fiber regions that may promote and direct new mineral synthesis in shape memory PLLA/PMMA polymer mats for *in vitro* studies.[51] In this study, we looked to incorporate our bifunctional peptide-protein into a shape memory polymer (SMPs) mat for

enhanced localization (using GFP fluorescence) of hydroxyapatite nanoparticles (functionalized with GFP-HABP). SMPs are a type of smart biomaterials with the ability to alter their shape in response to an environmental stimulus such as temperature, pH, moisture, or light. For decades, SMPs have been proposed for use in many fields, but a promising application has been for minimally invasive surgery applications in the biomedical field.[75, 76] In this international collaboration, we worked with experts as they designed a poly(l-lactide)/poly(methyl methacrylate) (PLLA/PMMA) SMP polymer mat with promising thermally activated, multi-shape memory properties.[77] The ability to include additional biochemical functionality into the SMP to create both a mechanically and bioactive system presented an innovative design opportunity. We employed the use of our GFP-HABP bifunctional construct to allow for directed, self-assembled mineralization properties within the SMP mat to provide localized enhancement via our mineral-binding peptide, HABP. To study the efficacy of this approach and ensure activity and disperse incorporation into the PLLA/PMMA via pressurized gyration, localization was monitored using the GFP fluorescent tag. In this approach, we aimed to explore the sustained bioactivity of both the fluorescent protein and biomineralization potential of our GFP-HABP protein-peptide moiety within a mechanically active PLLA/PMMA SMP fiber mat toward creating a novel biomaterial with tunable soft to hard material transition properties.

In the next publication, we investigated the multi-activity potential of DsRed-AuBP to functionalize gold nanoparticles to be injected into a living zebrafish brain model system to allow for localization and sensing of free metals critical for monitoring neurodegenerative diseases. For over 40 years, gold nanoparticles (AuNPs) have been explored as ideal candidates for biosensing, directed drug delivery, multi-modal imaging, photothermal, and radiotherapy applications due to their innate optical, electronic, physiochemical, and plasmonic properties.[55, 59, 64, 67, 69, 74,

78-85] Numerous reports in recent literature illustrate a critical dependence between specific functional and structure properties such as nanoparticle size, shape, and surface features.[27, 52, 86-88] Functional activity of the AuNP is also highly dependent upon the stabilization method employed. Surface stabilization techniques are required to ensure particles remain discrete, avoiding potential issues such as agglomeration which may further impact their size-dependent functionality. In previous studies, we demonstrated the binding and fluorescence activity of our engineered bifunctional construct on flat gold surfaces to observe nano-patterning arrays.[25, 59, 72] We have further shown the sustained activity of AuNPs functionalized with our DsRed-AuBP protein-peptide construct in *in vitro* environments and embedded within nanofibers.[89] However, the opportunity to use our biofriendly functionalization approach has not been established as a biosensor that may be used within a living system. This application presented several new challenges to ensure that the AuBP would not be displaced in a physiological environment and AuNPs would remain discrete in the complex environment and innate barriers within living brain tissues. A growing body of evidence has implicated the dysregulation of physiologically essential biometals, such as zinc, in the pathogenesis of Alzheimer's disease (AD) and other neurodegenerative disorders.[90-94] Measuring the changes in cytoplasmic zinc levels have received a large amount of attention in sensor development. The use of AuNPs as biosensors has increased in the past few decades due to their inherent optical and electronic properties, yet, limited studies featured the use of functionalized gold nanoparticles for sensing Zn^{2+} ion concentrations. Thus, we aimed to employ the DsRed-AuBP functionalized AuNPs as a nanosensor to monitor changes in free Zn^{2+} via fluorescence quenching in a living zebrafish brain model system. Our results provided insight into a promising platform approach to biosensing with spatial and temporal resolution that has not been previously addressed.

In the final publication, we explored peptide enabled nanocomposite formulation by generating a novel bifunctional peptide that has amelogenin derived peptide for mediating mineralization (shADP5) and an anchoring peptide (AgBP) to address a significant need in a pediatric dentistry application. Hierarchical composite structures often found in biological materials are a result of complex molecular recognition where biomolecules, mainly proteins, play a crucial role. Teeth, in particular, present an extremely challenging example of a heterogeneous, hierarchical, and composite structure in dentistry. Especially within last 5 years, dental materials have seen a plethora of biomimetic approaches in developing next generation restorative biomaterials.[95-97] Dental caries remains the most prevalent infectious disease of mankind, with maternal transmission of cariogenic microbiota and early childhood caries (ECC) widely recognized as a global health crisis [98-109]. ECC is characterized by one or more regions of dental caries in the primary teeth of young children under age five. Extensive reports published by the United States Department of Human Health and Services (USDHHS) and the Centers for Disease Control (CDC) have provided strong evidence supporting the endemic that is the neglect of oral health in America.[107, 110, 111] This neglect and the overall prevalence of ECC disproportionately impacts children of lower socioeconomic status with limited access to dental care.[104, 112-114] Further, due to limited patient cooperation of young children requiring pediatric dental intervention as ECC disease progresses, treatment options are limited and often require the use of general anesthesia – a costly and sometimes dangerous option for children with comorbidities.[100, 115] Early extraction of the carious primary teeth is the current standard of care, but can lead to a negative cascade of issues altering jaw growth and leading to the failure of the remaining teeth to effectively chew with consequential changes in micro- and macro-nutrition that adversely impact the child's health.[115, 116] Alternative treatment options, including the recently approved use of

silver diamine fluoride (SDF), has received attention as a promising approach to circumvent the current standard of care by offering a safe, accessible, and inexpensive method to arrest caries progression in children with ECC [98, 99, 103, 117-119]. A seemingly perfect solution – with one major drawback – SDF permanently stains the caries-effected dental tissues. In one study, this negative side effect was a deterrent for nearly one third of parents of children with ECC interviewed, who deemed that the aesthetic loss was not acceptable under any circumstances.[120, 121] With our previous works in the oral cavity to explore novel, bioactive dental biomaterials, we recognized the immense potential of providing self-assembled peptides for remineralization to mask the silver-stained dental tissues selectively with our AgBP anchoring peptide.

In this exciting, vanguard study, we aimed to employ a novel peptide-peptide bifunctional construct featuring AgBP to bind to the silver of the SDF-stained regions of dental tissues and shADP5 to promote and direct new mineral synthesis at the interface. Our previous works with AgBP showed that selective binding affinity to silver was maintained on well-defined surfaces including nanoparticles (AgNPs).[52, 63, 73] There was no evidence of silver binding peptide capability to anchor to the silver diamine fluoride treated caries. Following the testing the AgBP on SDF treated caries, we engineered a peptide with a spacer to combine with mineralization peptide. In our prior art, we have investigated the mineralization potential of several different peptides, including HABP and various amelogenin derived peptides (ADPs). Building upon our strength, we engineered a short amelogenin derived peptide (shADP5) to couple with an anchoring peptide AgBP.[37, 54, 122-124] Our proof-of-concept studies provided critical insight on the promising potential of novel peptide-peptide constructs and the overall peptide-based modular platform design to mitigate the negative impacts of SDF treatment by working synergistically to mask staining through directed, peptide-mediated remineralization.

1.5.1 Outline

Across Chapters 2 through 4, three core publications are featured to emphasize the multifaceted approach of using affinity-based solid-binding peptides as biomolecular tools for surface functionalization. Each chapter's paper explores a different material-binding peptide to highlight unique opportunities of biomaterial surface design using solid-binding peptides with specific affinity to calcium phosphate, hydroxyapatite, gold, and silver. The significance of each material interface and our innovative approach is described within the preface section for each chapter.

Chapter 2 includes a publication from an international collaboration that explored the dual functionality of our GFP-HABP construct embedded within PLLA/PMMA nanofiber mats to visualize biofunctional fiber regions that may promote and direct new mineral synthesis. Overall, these experiments demonstrated that the produced fluorescent protein-peptide tag constructs are robust and keep their multi-functionality, even under different and complex 3-D environments.[51]

Chapter 3 features our recent publication that explores the use of peptide-protein functionalized gold nanoparticles for use as biosensors in a zebrafish brain model. DsRed-AuBP was employed to functionalize AuNP surfaces to allow for spatial and temporal imaging providing localization and maintained bifunctionality of these biomolecular tools following injection into zebrafish brains. Further experiments were conducted to validate the potential of monitoring key free metals in the brain via fluorescence quenching of the DsRed protein. The dysregulation of physiologically essential biometals, such as zinc, copper, and iron, have been indicated in the pathogenesis of Alzheimer's disease (AD) and other neurodegenerative disorders.

Chapter 4 includes a publication that highlighted the promising results of our proof-of-concept studies utilizing a novel shADP5-AgBP peptide-peptide system as an anchoring system to counter the negative side effects of silver diamine fluoride (SDF) used to combat caries in pediatric

dentistry. SDF treatment is recently approved by FDA (2014), yet the black staining is limiting its wide range usage this easy to employ and effective method. As this is a recently emerging area of research, we were the first to publish our findings that utilize a peptide-based approach to modulate the SDF-stained dental tissues. Future experiments are planned to explore the vast potential of other peptide and protein constructs combined with AgBP as an anchoring peptide to these stained surfaces.

Chapter 5 provides a summary of our key results across the wide range of applications included herein and the impact of this dissertation as a whole. Through our publications, we show the vast potential of bifunctional solid binding peptides to anchor to key biomaterial surfaces to create bioactive interfaces. Our studies have revealed the enormous potential – from biosensing to improved interfacial binding – of our biomolecular systems provides a platform technological approach to novel biomaterial surface functionalization and design.

1.6 References

[1] Anderson JM, Rodriguez A, Chang DT. Foreign body reaction to biomaterials. Seminars in immunology: Elsevier; 2008. p. 86-100.

[2] Khan F, Tanaka M. Designing smart biomaterials for tissue engineering. International journal of molecular sciences 2018;19:17.

[3] Matsuura K. Construction of Functional Biomaterials by Biomolecular Self-Assembly. Bulletin of the Chemical Society of Japan 2017;90:873-84.

[4] Morais JM, Papadimitrakopoulos F, Burgess DJ. Biomaterials/tissue interactions: possible solutions to overcome foreign body response. The AAPS journal 2010;12:188-96.

[5] Zhang S. Fabrication of novel biomaterials through molecular self-assembly. Nature Biotechnology 2003;21:1171-8.

[6] Petersen S. Biofunctionalization. BioNanoMaterials 2017;18.

[7] Delfi M, Ghomi M, Zarrabi A, Mohammadinejad R, Taraghdari ZB, Ashrafizadeh M, Zare EN, Agarwal T, Padil VV, Mokhtari B. Functionalization of polymers and nanomaterials for biomedical applications: Antimicrobial platforms and drug carriers. Prosthesis 2020;2:117-39.

[8] Wisdom EC, Zhou Y, Chen C, Tamerler C, Snead ML. Mitigation of peri-implantitis by rational design of bifunctional peptides with antimicrobial properties. ACS Biomater Sci Eng 2020;6:2682-95.

[9] Yazici H, Habib G, Boone K, Urgen M, Utku FS, Tamerler C. Self-assembling antimicrobial peptides on nanotubular titanium surfaces coated with calcium phosphate for local therapy. Materials Science and Engineering: C 2019;94:333-43.

[10] Yazici H, O'Neill MB, Kacar T, Wilson BR, Oren EE, Sarikaya M, Tamerler C. Engineered Chimeric Peptides as Antimicrobial Surface Coating Agents toward Infection-Free Implants. ACS applied materials & interfaces 2016;8:5070-81.

[11] Yucesoy DT, Hnilova M, Boone K, Arnold PM, Snead ML, Tamerler C. Chimeric peptides as implant functionalization agents for titanium alloy implants with antimicrobial properties. JOM (1989) 2015;67:754-66.

[12] Khatayevich D, Gungormus M, Yazici H, So C, Cetinel S, Ma H, Jen A, Tamerler C, Sarikaya M. Biofunctionalization of materials for implants using engineered peptides. Acta Biomater 2010;6:4634-41.

[13] Sarikaya M, Tamerler C, Jen AKY, Schulten K, Baneyx F. Molecular biomimetics: nanotechnology through biology. Nature Materials 2003;2:577-85.

[14] Yazici H, Fong H, Wilson B, Oren EE, Amos FA, Zhang H, Evans JS, Snead ML, Sarikaya M, Tamerler C. Biological response on a titanium implant-grade surface functionalized with modular peptides. Acta Biomater 2013;9:5341-52.

[15] Zhou Y, Snead ML, Tamerler C. Bio-inspired hard-to-soft interface for implant integration to bone. Nanomedicine 2015;11:431-4.

[16] Zamuner A, Brun P, Scorzeto M, Sica G, Castagliuolo I, Dettin M. Smart biomaterials: Surfaces functionalized with proteolytically stable osteoblast-adhesive peptides. Bioactive Materials 2017;2:121-30.

[17] Spicer CD, Pashuck ET, Stevens MM. Achieving Controlled Biomolecule-Biomaterial Conjugation. Chemical reviews 2018;118:7702-43.

[18] Wisdom C, VanOosten SK, Boone KW, Khvostenko D, Arnold PM, Snead ML, Tamerler C. Controlling the Biomimetic Implant Interface: Modulating Antimicrobial Activity by Spacer Design. J Mol Eng Mater 2016;4.

[19] Major MR, Wong VW, Nelson ER, Longaker MT, Gurtner GC. The foreign body response: at the interface of surgery and bioengineering. Plastic and reconstructive surgery 2015;135:1489-98.

[20] Rahmati M, Silva EA, Reseland JE, Heyward CA, Haugen HJ. Biological responses to physicochemical properties of biomaterial surface. Chemical Society Reviews 2020;49:5178-224.

[21] Devgan S, Sidhu SS. Evolution of surface modification trends in bone related biomaterials: A review. Materials Chemistry and Physics 2019;233:68-78.

[22] Haensch C, Hoeppener S, Schubert US. Chemical modification of self-assembled silane based monolayers by surface reactions. Chemical Society Reviews 2010;39:2323-34.

[23] Hasan A, Pandey LM. Polymers, surface-modified polymers, and self assembled monolayers as surface-modifying agents for biomaterials. Polymer-Plastics Technology and Engineering 2015;54:1358-78.

[24] Hasan A, Pandey L. Self-assembled monolayers in biomaterials. Nanobiomaterials: Elsevier; 2018. p. 137-78.

[25] Corni S, Hnilova M, Tamerler C, Sarikaya M. Conformational Behavior of Genetically-Engineered Dodecapeptides as a Determinant of Binding Affinity for Gold. The Journal of Physical Chemistry C 2013;117:16990-7003.

[26] Tamerler C, Khatayevich D, Gungormus M, Kacar T, Oren EE, Hnilova M, Sarikaya M. Molecular biomimetics: GEPI-based biological routes to technology. Biopolymers 2010;94:78-94.

[27] Heinz H, Pramanik C, Heinz O, Ding Y, Mishra RK, Marchon D, Flatt RJ, Estrela-Lopis I, Llop J, Moya S, Ziolo RF. Nanoparticle decoration with surfactants: Molecular interactions, assembly, and applications. Surface Science Reports 2017;72:1-58.

[28] Raynor JE, Capadona JR, Collard DM, Petrie TA, García AJ. Polymer brushes and self-assembled monolayers: Versatile platforms to control cell adhesion to biomaterials (Review). Biointerphases 2009;4:FA3-FA16.

[29] Love JC, Estroff LA, Kriebel JK, Nuzzo RG, Whitesides GM. Self-assembled monolayers of thiolates on metals as a form of nanotechnology. Chemical reviews 2005;105:1103-70.

[30] Mani G, Johnson DM, Marton D, Dougherty VL, Feldman MD, Patel D, Ayon AA, Agrawal CM. Stability of Self-Assembled Monolayers on Titanium and Gold. Langmuir 2008;24:6774-84.

[31] Briggs BD, Knecht MR. Nanotechnology meets biology: peptide-based methods for the fabrication of functional materials. The journal of physical chemistry letters 2012;3:405-18.

[32] Fukunaga K, Tsutsumi H, Mihara H. Self-assembling peptides as building blocks of functional materials for biomedical applications. Bulletin of the Chemical Society of Japan 2019;92:391-9.

[33] Tamerler C, Sarikaya M. Molecular biomimetics: nanotechnology and bionanotechnology using genetically engineered peptides. Philos Trans A Math Phys Eng Sci 2009;367:1705-26.

[34] Tamerler C, Sarikaya M. Genetically designed Peptide-based molecular materials. ACS Nano 2009;3:1606-15.

[35] Tamerler C, Sarikaya M. Molecular biomimetics: utilizing nature's molecular ways in practical engineering. Acta Biomater 2007;3:289-99.

[36] Mendes AC, Baran ET, Reis RL, Azevedo HS. Self-assembly in nature: using the principles of nature to create complex nanobiomaterials. Wiley Interdisciplinary Reviews: Nanomedicine and Nanobiotechnology 2013;5:582-612.

[37] Gungormus M, Oren EE, Horst JA, Fong H, Hnilova M, Somerman MJ, Snead ML, Samudrala R, Tamerler C, Sarikaya M. Cementomimetics-constructing a cementum-like biomineralized microlayer via amelogenin-derived peptides. Int J Oral Sci 2012;4:69-77.

[38] Hnilova M, So CR, Oren EE, Wilson BR, Kacar T, Tamerler C, Sarikaya M. Peptide-directed co-assembly of nanoprobes on multimaterial patterned solid surfaces. Soft Matter 2012;8:4327-34.

[39] Khatayevich D. Bio-Inorganic Interface Engineering via Solid-Binding Peptides toward Nano-sensing Applications [Ph.D.]. Ann Arbor: University of Washington; 2013.

[40] Tamerler C, Kacar T, Sahin D, Fong H, Sarikaya M. Genetically engineered polypeptides for inorganics: A utility in biological materials science and engineering. Materials Science and Engineering: C 2007;27:558-64.

[41] Chen J, Zou X. Self-assemble peptide biomaterials and their biomedical applications. Bioactive Materials 2019;4:120-31.

[42] Reches M, Gazit E. Molecular self-assembly of peptide nanostructures: mechanism of association and potential uses. Current Nanoscience 2006;2:105-11.

[43] Yuan C, Li S, Zou Q, Ren Y, Yan X. Multiscale simulations for understanding the evolution and mechanism of hierarchical peptide self-assembly. Physical Chemistry Chemical Physics 2017;19:23614-31.

[44] Liu R, Hudalla GA. Using self-assembling peptides to integrate biomolecules into functional supramolecular biomaterials. Molecules (Basel, Switzerland) 2019;24:1450.

[45] Abbas M, Zou Q, Li S, Yan X. Self-Assembled Peptide- and Protein-Based Nanomaterials for Antitumor Photodynamic and Photothermal Therapy. Advanced materials (Deerfield Beach, Fla) 2017;29.

[46] Hamley IW. Small Bioactive Peptides for Biomaterials Design and Therapeutics. Chemical Reviews 2017;117:14015-41.

[47] Lakshmanan A, Zhang S, Hauser CA. Short self-assembling peptides as building blocks for modern nanodevices. Trends in biotechnology 2012;30:155-65.

[48] Li J, Wang J, Zhao Y, Zhou P, Carter J, Li Z, Waigh TA, Lu JR, Xu H. Surfactant-like peptides: From molecular design to controllable self-assembly with applications. Coordination Chemistry Reviews 2020;421:213418.

[49] Yucesoy DT, Khatayevich D, Tamerler C, Sarikaya M. Rationally designed chimeric solid-binding peptides for tailoring solid interfaces. Medical Devices & Sensors 2020;3:e10065.

[50] Ye Q, Spencer P, Yuca E, Tamerler C. Engineered Peptide Repairs Defective Adhesive-Dentin Interface. Macromol Mater Eng 2017;302.

[51] Wu X, Mahalingam S, VanOosten SK, Wisdom C, Tamerler C, Edirisinghe M. New Generation of Tunable Bioactive Shape Memory Mats Integrated with Genetically Engineered Proteins. Macromol Biosci 2017;17.

[52] VanOosten SK, Yuca E, Karaca BT, Boone K, Snead ML, Spencer P, Tamerler C. Biosilver nanoparticle interface offers improved cell viability. Surface innovations 2016;4:121-32.

[53] So CR, Hayamizu Y, Yazici H, Gresswell C, Khatayevich D, Tamerler C, Sarikaya M. Controlling self-assembly of engineered peptides on graphite by rational mutation. ACS Nano 2012;6:1648-56.

[54] Yuca E, Karatas AY, Seker UO, Gungormus M, Dinler-Doganay G, Sarikaya M, Tamerler C. In vitro labeling of hydroxyapatite minerals by an engineered protein. Biotechnol Bioeng 2011;108:1021-30.

[55] So CR, Kulp JL, Oren EE, Zareie H, Tamerler C, Evans JS, Sarikaya M. Molecular recognition and supramolecular self-assembly of a genetically engineered gold binding peptide on Au{111}. ACS Nano 2009;3:1525-31.

[56] Baneyx F, Schwartz DT. Selection and analysis of solid-binding peptides. Current opinion in biotechnology 2007;18:312-7.

[57] Care A, Bergquist PL, Sunna A. Solid-binding peptides: smart tools for nanobiotechnology. Trends in biotechnology (Regular ed) 2015;33:259-68.

[58] Hellner B, Alamdari S, Pyles H, Zhang S, Prakash A, Sprenger KG, De Yoreo JJ, Baker D, Pfaendtner J, Baneyx F. Sequence–Structure–Binding Relationships Reveal Adhesion Behavior of the Car9 Solid-Binding Peptide: An Integrated Experimental and Simulation Study. Journal of the American Chemical Society 2020;142:2355-63.

[59] Hnilova M, Oren EE, Seker UO, Wilson BR, Collino S, Evans JS, Tamerler C, Sarikaya M. Effect of molecular conformations on the adsorption behavior of gold-binding peptides. Langmuir 2008;24:12440-5.

[60] Oren EE, Tamerler C, Sahin D, Hnilova M, Seker UO, Sarikaya M, Samudrala R. A novel knowledge-based approach to design inorganic-binding peptides. Bioinformatics 2007;23:2816-22.

[61] Donatan S, Sarikaya M, Tamerler C, Urgen M. Effect of solid surface charge on the binding behaviour of a metal-binding peptide. Journal of the Royal Society, Interface 2012;9:2688-95.

[62] Cetinel S, Caliskan HB, Yucesoy DT, Donatan AS, Yuca E, Urgen M, Karaguler NG, Tamerler C. Addressable self-immobilization of lactate dehydrogenase across multiple length scales. Biotechnol J 2013;8:262-72.

[63] Sedlak RH, Hnilova M, Grosh C, Fong H, Baneyx F, Schwartz D, Sarikaya M, Tamerler C, Traxler B. Engineered Escherichia coli silver-binding periplasmic protein that promotes silver tolerance. Appl Environ Microbiol 2012;78:2289-96.

[64] Seker UO, Wilson B, Kulp JL, Evans JS, Tamerler C, Sarikaya M. Thermodynamics of engineered gold binding peptides: establishing the structure-activity relationships. Biomacromolecules 2014;15:2369-77.

[65] Seker UO, Wilson B, Sahin D, Tamerler C, Sarikaya M. Quantitative affinity of genetically engineered repeating polypeptides to inorganic surfaces. Biomacromolecules 2009;10:250-7.

[66] So CR, Tamerler C, Sarikaya M. Adsorption, diffusion, and self-assembly of an engineered gold-binding peptide on Au(111) investigated by atomic force microscopy. Angewandte Chemie (International ed in English) 2009;48:5174-7.

[67] Tamerler C, Duman M, Oren EE, Gungormus M, Xiong X, Kacar T, Parviz BA, Sarikaya M. Materials specificity and directed assembly of a gold-binding peptide. Small 2006;2:1372-8.

[68] Hall Sedlak R, Hnilova M, Grosh C, Fong H, Baneyx F, Schwartz D, Sarikaya M, Tamerler C, Traxler B. Engineered Escherichia coli Silver-Binding Periplasmic Protein That Promotes Silver Tolerance2012.

[69] Yuca E, Tamerler C. Self-Assembled Recombinant Proteins on Metallic Nanoparticles as Bimodal Imaging Probes. JOM 2019;71:1281-90.

[70] Duran N, Silveira CP, Duran M, Martinez DS. Silver nanoparticle protein corona and toxicity: a mini-review. Journal of nanobiotechnology 2015;13:55.

[71] Li LL, Qiao ZY, Wang L, Wang H. Programmable construction of peptide-based materials in living subjects: from modular design and morphological control to theranostics. Advanced Materials 2019;31:1804971.

[72] Karaca BT, Meyer J, VanOosten S, Richter M, Tamerler C. Modular Peptide-Based Hybrid Nanoprobes for Bio-Imaging and Bio-Sensing. MRS Online Proceedings Library Archive 2014;1621:155-61.

[73] Hnilova M, Liu X, Yuca E, Jia C, Wilson B, Karatas AY, Gresswell C, Ohuchi F, Kitamura K, Tamerler C. Multifunctional protein-enabled patterning on arrayed ferroelectric materials. ACS Appl Mater Interfaces 2012;4:1865-71.

[74] Hnilova M, Khatayevich D, Carlson A, Oren EE, Gresswell C, Zheng S, Ohuchi F, Sarikaya M, Tamerler C. Single-step fabrication of patterned gold film array by an engineered multi-functional peptide. J Colloid Interface Sci 2012;365:97-102.

[75] El Feninat F, Laroche G, Fiset M, Mantovani D. Shape memory materials for biomedical applications. Advanced Engineering Materials 2002;4:91-104.

[76] Lendlein A, Kelch S. Shape-memory polymers. Angewandte Chemie International Edition 2002;41:2034-57.

[77] Samuel Cd, Barrau S, Lefebvre J-M, Raquez J-M, Dubois P. Designing multiple-shape memory polymers with miscible polymer blends: evidence and origins of a triple-shape memory effect for miscible PLLA/PMMA blends. Macromolecules 2014;47:6791-803.

[78] Elahi N, Kamali M, Baghersad MH. Recent biomedical applications of gold nanoparticles: A review. Talanta 2018;184:537-56.

[79] Chhour P, Naha PC, Cheheltani R, Benardo B, Mian S, Cormode DP. Gold nanoparticles for biomedical applications: synthesis and In vitro evaluation. Nanomaterials in Pharmacology: Springer; 2016. p. 87-111.

[80] Kumar A, Ma H, Zhang X, Huang K, Jin S, Liu J, Wei T, Cao W, Zou G, Liang X-J. Gold nanoparticles functionalized with therapeutic and targeted peptides for cancer treatment. Biomaterials 2012;33:1180-9.

[81] Mandal R, Baranwal A, Srivastava A, Chandra P. Evolving trends in bio/chemical sensor fabrication incorporating bimetallic nanoparticles. Biosensors & bioelectronics 2018;117:546-61.

[82] Selvan ST, Narayanan K. Introduction to Nanotheranostics. Introduction to Nanotheranostics. Singapore: Springer Singapore; 2016.

[83] Slocik JM, Zabinski Jr JS, Phillips DM, Naik RR. Colorimetric response of peptide-functionalized gold nanoparticles to metal ions. Small 2008;4:548-51.

[84] Tamerler C, Oren EE, Duman M, Venkatasubramanian E, Sarikaya M. Adsorption kinetics of an engineered gold binding Peptide by surface plasmon resonance spectroscopy and a quartz crystal microbalance. Langmuir 2006;22:7712-8.

[85] Zong J, Cobb SL, Cameron NR. Peptide-functionalized gold nanoparticles: versatile biomaterials for diagnostic and therapeutic applications. Biomaterials Science 2017;5:872-86.

[86] Franci G, Falanga A, Galdiero S, Palomba L, Rai M, Morelli G, Galdiero M. Silver nanoparticles as potential antibacterial agents. Molecules (Basel, Switzerland) 2015;20:8856-74.

[87] De Matteis V, Cascione M, Toma CC, Leporatti S. Silver Nanoparticles: Synthetic Routes, In Vitro Toxicity and Theranostic Applications for Cancer Disease. Nanomaterials (Basel, Switzerland) 2018;8:319.

[88] Lu Z, Rong K, Li J, Yang H, Chen R. Size-dependent antibacterial activities of silver nanoparticles against oral anaerobic pathogenic bacteria. Journal of Materials Science: Materials in Medicine 2013;24:1465-71.

[89] Zhang S, Karaca BT, VanOosten SK, Yuca E, Mahalingam S, Edirisinghe M, Tamerler C. Coupling infusion and gyration for the nanoscale assembly of functional polymer nanofibers integrated with genetically engineered proteins. Macromolecular rapid communications 2015;36:1322-8.

[90] Bagheri S, Squitti R, Haertle T, Siotto M, Saboury AA. Role of Copper in the Onset of Alzheimer's Disease Compared to Other Metals. Front Aging Neurosci 2017;9:446.

[91] Ward RJ, Dexter DT, Crichton RR. Neurodegenerative diseases and therapeutic strategies using iron chelators. Journal of Trace Elements in Medicine and Biology 2015;31:267-73.

[92] Barnham KJ, Bush AI. Biological metals and metal-targeting compounds in major neurodegenerative diseases. Chemical Society Reviews 2014;43:6727-49.

[93] Qian X, Xu Z. Fluorescence imaging of metal ions implicated in diseases. Chemical Society Reviews 2015;44:4487-93.

[94] Chowdhury S, Rooj B, Dutta A, Mandal U. Review on recent advances in metal ions sensing using different fluorescent probes. Journal of fluorescence 2018;28:999-1021.

[95] Moussa DG, Fok A, Aparicio C. Hydrophobic and antimicrobial dentin: A peptide-based 2-tier protective system for dental resin composite restorations. Acta biomaterialia 2019;88:251-65.

[96] Mukherjee K, Ruan Q, Nutt S, Tao J, De Yoreo JJ, Moradian-Oldak J. Peptide-based bioinspired approach to regrowing multilayered aprismatic enamel. ACS omega 2018;3:2546-57.

[97] Sarikaya R, Song L, Yuca E, Xie S-X, Boone K, Misra A, Spencer P, Tamerler C. Bio-inspired multifunctional adhesive system for next generation bio-addivitely designed dental restorations. Journal of the mechanical behavior of biomedical materials 2020:104135.

[98] Chu C, Lo E. Promoting caries arrest in children with silver diamine fluoride: a review. Oral health & preventive dentistry 2008;6.

[99] Yee R, Holmgren C, Mulder J, Lama D, Walker D, van Palenstein Helderman W. Efficacy of silver diamine fluoride for arresting caries treatment. Journal of dental research 2009;88:644-7.

[100] Çolak H, Dülgergil ÇT, Dalli M, Hamidi MM. Early childhood caries update: A review of causes, diagnoses, and treatments. Journal of natural science, biology, and medicine 2013;4:29.

[101] Dye BA, Hsu K-LC, Afful J. Prevalence and measurement of dental caries in young children. Pediatric dentistry 2015;37:200-16.

[102] Kassebaum NJ, Bernabe E, Dahiya M, Bhandari B, Murray CJ, Marcenes W. Global burden of untreated caries: a systematic review and metaregression. J Dent Res 2015;94:650-8.

[103] Gao SS, Zhao IS, Hiraishi N, Duangthip D, Mei M, Lo E, Chu C. Clinical trials of silver diamine fluoride in arresting caries among children: a systematic review. JDR Clinical & Translational Research 2016;1:201-10.

[104] Anil S, Anand PS. Early Childhood Caries: Prevalence, Risk Factors, and Prevention. Front Pediatr 2017;5:157-.

[105] Institute of Medicine (U.S.). Committee on an Oral Health Initiative. Advancing oral health in America. Washington, D.C.: National Academies Press; 2011.

[106] Albino JaD, B.A. Oral Health In America: Advances and Challenges. 2021.

[107] Dye BA, Albino J, D'Souza RN. Oral health problems are global and need to be addressed in the USA. Lancet 2022;399:127-8.

[108] Balakrishnan M, Simmonds RS, Tagg JR. Dental caries is a preventable infectious disease. Aust Dent J 2000;45:235-45.

[109] Caufield PW, Li Y, Dasanayake A. Dental caries: an infectious and transmissible disease. Compend Contin Educ Dent 2005;26:10-6.

[110] Health UDo, Committee HSOHC. US Department of health and human services oral health strategic framework, 2014–2017. Public health reports 2016;131:242-57.

[111] Health UDo, Services H. Oral health in America: a report of the Surgeon General. Rockville, MD: US Department of Health and Human Services, National Institute of Dental and Craniofacial Research, National Institutes of Health 2000;63:74-94.

[112] Shiboski CH, Gansky SA, Ramos-Gomez F, Ngo L, Isman R, Pollick HF. The association of early childhood caries and race/ethnicity among California preschool children. Journal of public health dentistry 2003;63:38-46.

[113] Ramos-Gomez FJ, Crystal YO, Ng MW, Crall JJ, Featherstone JDB. Pediatric dental care: prevention and management protocols based on caries risk assessment. J Calif Dent Assoc 2010;38:746-61.

[114] Jain M, Namdev R, Bodh M, Dutta S, Singhal P, Kumar A. Social and behavioral determinants for early childhood caries among preschool children in India. Journal of dental research, dental clinics, dental prospects 2015;9:115.

[115] Berkowitz RJ. Causes, treatment and prevention of early childhood caries: a microbiologic perspective. Journal-Canadian Dental Association 2003;69:304-7.

[116] Casamassimo PS, Thikkurissy S, Edelstein BL, Maiorini E. Beyond the dmft: the human and economic cost of early childhood caries. The Journal of the American Dental Association 2009;140:650-7.

[117] Rosenblatt A, Stamford T, Niederman R. Silver diamine fluoride: a caries “silver-fluoride bullet”. Journal of dental research 2009;88:116-25.

[118] Horst JA, Ellenikiotis H, Milgrom PL. UCSF Protocol for Caries Arrest Using Silver Diamine Fluoride: Rationale, Indications and Consent. J Calif Dent Assoc 2016;44:16-28.

[119] Zhao IS, Gao SS, Hiraishi N, Burrow MF, Duangthip D, Mei ML, Lo EC-M, Chu C-H. Mechanisms of silver diamine fluoride on arresting caries: a literature review. International dental journal 2018;68:67-76.

[120] Crystal Y, Kreider B, Raveis V. Parental expressed concerns about silver diamine fluoride (SDF) treatment. Journal of Clinical Pediatric Dentistry 2019;43:155-60.

[121] Crystal YO, Janal MN, Hamilton DS, Niederman R. Parental perceptions and acceptance of silver diamine fluoride staining. The Journal of the American Dental Association 2017;148:510-8. e4.

[122] Gungormus M, Fong H, Kim IW, Evans JS, Tamerler C, Sarikaya M. Regulation of in vitro calcium phosphate mineralization by combinatorially selected hydroxyapatite-binding peptides. Biomacromolecules 2008;9:966-73.

[123] Yucesoy DT. Peptide-guided Dental Tissue Regeneration for Oral Care 2018.

[124] Ye Q, Spencer P, Yuca E, Tamerler C. Engineered Peptide Repairs Defective Adhesive–Dentin Interface. Macromolecular materials and engineering 2017;302:1600487.

Chapter 2 Bioactive Shape Memory Polymer Mats

*This chapter is adapted from the Research Publication **P1**:*

*X Wu, S Mahalingam, **SK VanOosten**, C Wisdom, C Tamerler, M Edirisinghe, "New Generation of Tunable Bioactive Shape Memory Mats Integrated with Genetically Engineered Proteins", Macromolecular Bioscience, 17(2) (2017).*

2.1 Preface

This chapter utilized a fusion protein composed of green fluorescence protein tagged hydroxyapatite binding peptide (GFP-HABP) which is shown to create self-assembled biohybrid system with hydroxyapatite (HA) nanoparticles embedded within a poly(l-lactide)/poly(methyl methacrylate) (PLLA/PMMA) shape memory polymer fiber mat network. The fluorescence imaging would enable to monitor the homogenous distribution of the GFP-HABP/HA nanoparticle system throughout the nanofibers.

Dr. Edirisinghe`s pioneering work demonstrated that pressurized gyration is one of the promising production techniques for nanofibers, microbubbles, and capsules on a large scale. Working collaboratively with his team as part of our prior art, we applied the pressurized infusion gyration method to create polyethylene oxide (PEO) nanofibers. These PEO nanofibers were shown to incorporate gold nanoparticles that are assembled by the fusion red fluorescence protein system through a gold binding peptide tag (DsRed-AuBP).[1] Our results demonstrated the sustained fluorescence activity of the DsRed protein within these nanofibers and enabled further opportunities to explore to integrate different biohybrid design that may present protein and peptide based functional activities. In this work, we explored *in vitro* peptide enabled mineralization and localization of apatitic nanoparticles in the nanofiber systems using our GFP-HABP construct.

Hydroxyapatite is a ceramic material chemically similar to the inorganic component of bone and human enamel and therefore a key material with many opportunities for advanced biomaterial

design and synthesis.[2-5] Our earlier studies demonstrated that HABP peptide mediate mineralization in addition to its hydroxyapatite affinity. We demonstrated that HABP peptide promote and direct calcium phosphate mineralization by controlling the nucleation and growth kinetics on different environments. This peptide mediated mineralization was not investigated in a nanofiber systems, here we explored its activity to design a bioactive shape memory polymer mat. The PLLA/PMMA-based scaffold developed offered an innovative design toward developing a tunable soft to hard matter transition similar to biomaterials-tissue interface. Bioactive scaffolds were produced with our engineered fusion protein and demonstrated to feature a green fluorescence through the use the GFP protein. The peptide tags in these fluorescence proteins enabled to binding to hydroxyapatite nanoparticles as well as offered mineralization capability. Monitoring localization of the HABP within the fiber scaffolds was performed using GFP fluorescence activity.

The publication featured as Chapter 2 has provided evidence of sustained bifunctionality of both the anchoring HA peptide and the GFP fluorescent moiety in a shape memory nanofiber environment.[6, 7]

2.2 New Generation of Tunable Bioactive Shape Memory Mats Integrated with Genetically Engineered Proteins*

2.2.1 Abstract

Aligned poly(l-lactide)/poly(methyl methacrylate) binary blend fibers and mats loaded with a chimeric green fluorescence protein having a bioactive peptide with hydroxyapatite binding and mineralization property are prepared by pressurized gyration. The effect of processing parameters on the product morphologies, and the shape memory properties of these samples are investigated. Integration of hydroxyapatite nanoparticles into the fiber assembly is self-directed using the hydroxyapatite-binding property of the peptide genetically engineered to green fluorescence protein. Fluorescence microscopy analysis corroborated with Fourier transform infrared spectroscopy (FTIR) data confirms the integration of the chimeric protein with the fibers. An enzyme-based remineralization assay is conducted to study the effects of peptide-mediated mineralization within the fiber mats. Raman and FTIR spectral changes observed following the peptide-mediated mineralization provides an initial step toward a soft-hard material transition. These results show that programmable shape memory properties can be obtained by incorporating genetically engineered bioactive peptide domains into polymer fibers. The schematic overview of the paper is shown in Figure 2-1.

---

*Published as X. Wu, S. Mahalingam, **S.K. VanOosten**, C. Wisdom, C. Tamerler, M. Edirisinghe "New Generation of Tunable Bioactive Shape Memory Mats Integrated with Genetically Engineered Proteins", *Macromolecular Bioscience*, 17(2) (2017). Feature Cover

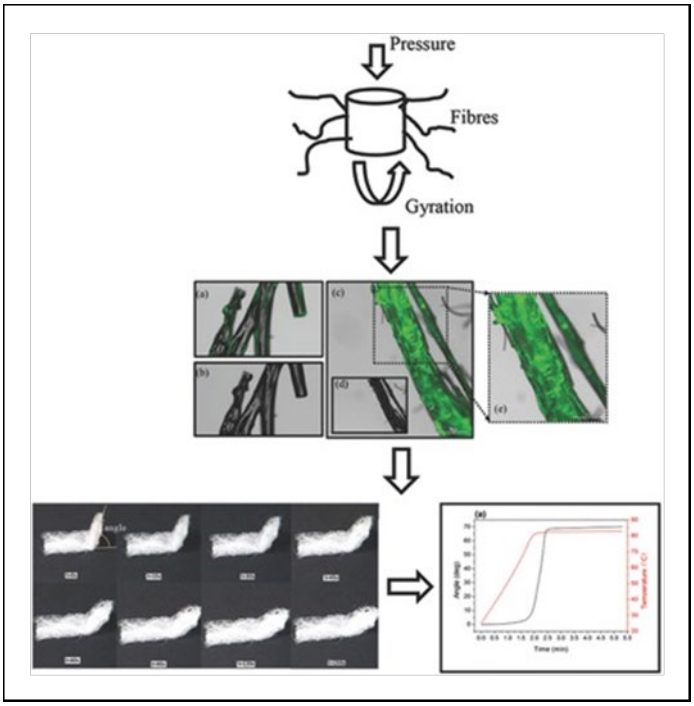

Figure 2-1: Table of contents figure depicting schematic overview of paper.

2.2.2 Introduction

Shape memory polymers (SMPs) are a class of smart materials that are able to change their shape in response to an environmental stimulus such as temperature, pH, moisture, or light. SMPs have been used in many fields including biomedical applications,[8] especially for minimally invasive surgery.[9] Among the numerous SMPs, poly(l-lactide)/poly(methyl methacrylate) (PLLA/PMMA) are recognized as promising thermally activated SMPs with multi-shape memory properties.[10] A new stereo complex crystal was found to be formed between structurally dissimilar chiral PLLA and syndiotactic PMMA.[11] Miscible or immiscible PLLA/PMMA blends could be produced by using different processing conditions such as polymerizing the acrylic monomer in the presence of PLLA or by melt mixing the two polymers (PLLA and PMMA) in bulk.[12, 13]

The solvent-casting process has been able to produce immiscible blends with matrix droplet or continuous morphologies by changing the blend composition, while extrusion melt-processing could obtain miscible PLLA/PMMA blends in a range of compositions.[14] Phase separation method with solutions of two incompatible polydisperse polymers (PLLA/PMMA) in a common solvent (e.g., chloroform) have been studied and revealed new fundamental features such as phase-in-phase or double phase morphology which are absent for solutions of just one polymer with broad molecular weight distribution in a single solvent.[15] A tri-block copolymer of PMMA/PLLA/PMMA was also synthesized and reported to have unique structure and properties.[16] Based on that, PLLA/PMMA blends were shown to be crystallized even at a low temperature of 0 °C under high pressure carbon dioxide. The effect of carbon dioxide on the crystallization behavior and the mechanical properties of PLLA/PMMA blends with various weight fraction of PMMA have been investigated.[17]

Pressurized gyration is one of the promising techniques to successfully form continuous nanofibers and functional microbubbles and capsules on a large scale.[18-20] Over the last two years, it has been a catapult to processing and forming many novel functional materials for biomedical engineering and drug delivery applications.[21-25] This technique relies on centrifugal force and dynamic fluid flow across a small orifice to create instability of a polymer or polymer/protein liquid jet at the liquid–air interface to form the desired products. In addition, by changing the physical properties of the solute–solvent mixture (e.g., surface tension, viscosity) and the processing parameters such as rotating speed and working pressure, the size, size distribution and the morphology of the products could be tailored.[18-20]

The ability to fabricate mechanically active scaffolds with additional biochemical properties presents an intriguing and innovative design opportunity. Herein, we have focused on the directed,

self-assembled mineralization properties of such SMP scaffolds incorporated with a mineral-binding peptide to repair bone defects by providing local stimulation for bone tissue development. We produced these bioactive scaffolds by incorporating a genetically engineered fusion protein, which features a green fluorescence protein tag conjugated with hydroxyapatite binding and mineralization peptide (GFP-HABP). Monitoring localization of the HABP within the fiber scaffolds was performed using GFP. The presence of the bioactive HABP peptide provides control over nucleation and growth of minerals integrated into the PLLA/PMMA scaffold. An enzyme based biomineralization assay was performed to mimic the cellular environment; alkaline phosphatase (AP) was introduced to cleave phosphate groups, catalyzing mineral formation in a calcium rich buffer. In the present study, PLLA/PMMA fibers with or without the GFP-HABP fusion protein were successfully fabricated by using pressurized gyration. The morphology and the shape memory effect of the fiber mats were investigated. Following biomineralization assay, the chemical modification and microstructural changes in the fibers were investigated toward developing a tunable soft to hard matter transition in the shape memory fibers and mats.

2.2.3 Experimental Section

2.2.3.1 Materials

PLLA (amine terminated, average Mn 2500, polydispersity ≤ 1.3), PMMA (average Mn 120,000) were obtained from Sigma-Aldrich, UK. Chloroform with density of 1489 $kg \cdot m^{-3}$ at 25 °C was used as the solvent. Hydroxyapatite nanopowder (particle size ≤ 200 nm) was purchased from Sigma-Aldrich, UK and it was used as received without any modification.

2.2.3.2 Preparation of PLLA/PMMA-Based Fibers

A solution of PLLA/PMMA with composition of 50:50 weight ratio and concentration of 20 wt% in chloroform was prepared in an air tight bottle at ambient temperature (25 °C). Phosphate

buffer saline solution, pH 7.4, was prepared at ambient temperature and added to the purified GFP-HABP engineered protein to achieve a working stock solution of 200×10^{-6}M. GFP-HABP was produced and purified following methods established by Yuca, *et al.*[26] Next, a hydroxyapatite particle solution was added to the protein solution and allowed to incubate under gentle agitation to ensure peptide–particle functionalization. 15g of PLLA/PMMA solution was taken in an air-tight bottle and 0.4 mL of the hydroxyapatite–protein mixture was added while sonicating in a water bath using an ultrasound sonicater (Branson sonifier 250) at a power output of 60% for 15 min. This prevented aggregation of the functionalized hydroxyapatite nanoparticles in the polymer solution.

2.2.3.3 Pressurized Gyration

Figure 2-2 shows the experimental set up of pressurized gyration and the resulting shape memory polymer fibers. The process of pressurized gyration and the theory of the fiber forming have been described in detail elsewhere.[18]

2.2.3.4 Biomineralization

Mineral formation was performed using an AP enzyme-dependent mineralization assay.[5] Briefly, PLLA/PMMA fibers were incubated in a biomineralization buffer (24×10^{-3}M $CaCl_2$, 14.4×10^{-3}M β-GP, 25×10^{-3}M Tris–HCl, pH 7.4). β-GP was hydrolyzed following the addition of AP enzyme, releasing inorganic phosphate ions into the buffer rich in calcium ions which allowed for the Ca/PO_4 mineral formation. Fibers with and without GFP-HABP were incubated at 37 °C under gentle shaking in micro-centrifuge tubes containing biomineralization buffer following the addition of AP enzyme. After 24h, the sample removed from the incubator and AP enzyme was inactivated by heating the tubes to 75 °C for 5 min.

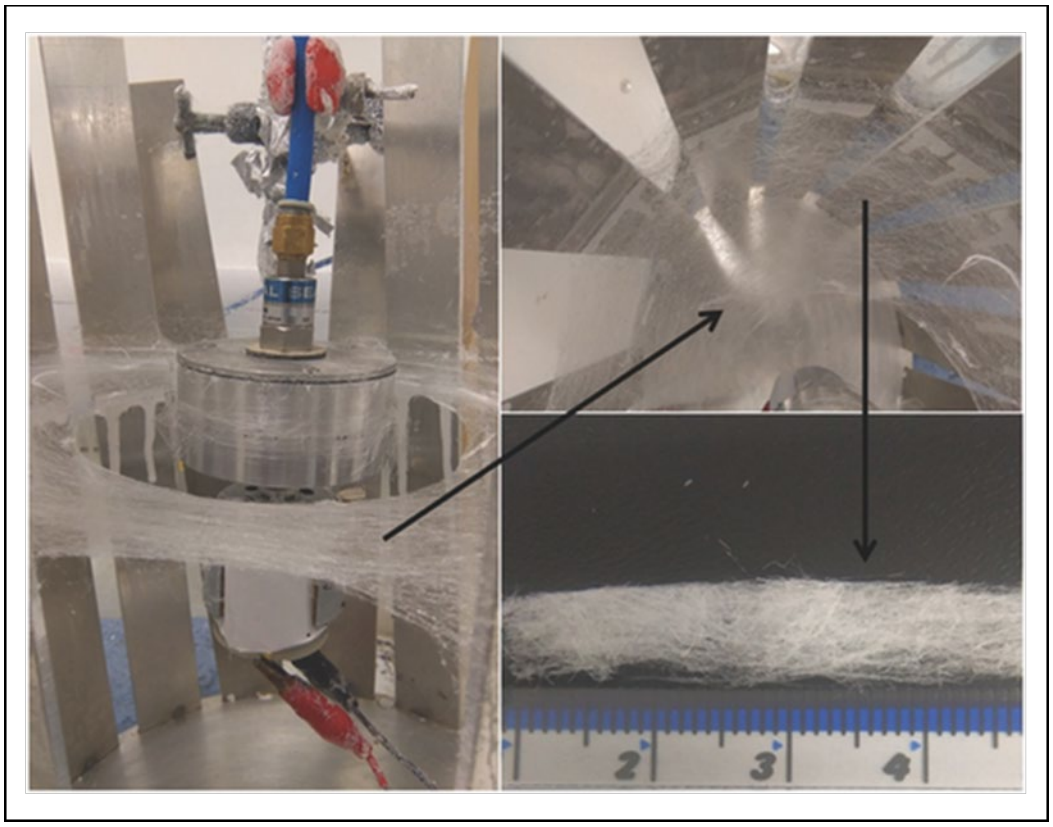

Figure 2-2: The pressurized gyration experimental set-up and the produced shape memory polymer fibers/mats.

2.2.3.5 Characterization

2.2.3.5.1 Morphology

Fibers produced were studied using field emission scanning electron microscopy with an accelerating voltage of 5 kV. Samples were coated with gold using a sputtering machine (sputter time ≈75 s) before loading to the microscope. High and low magnification images were acquired at randomly selected positions (>20) within a sample. About 150 measurements were made at random locations to plot the fiber diameter distribution using Image J software. Additionally, the fibers were characterized using a fluorescence microscope to verify the functional integration of GFP-HABP fusion proteins into the nanofibers via the GFP fluorescence existence. Control and protein-infused fibers were imaged using a 4× objective on a multimodal plate reader (Cytation3,

BioTek, Winooski, VT, USA) and fluorescence intensity within the fibers was quantified using associated Gen5 software.

2.2.3.5.2 Fourier Transform Infrared Spectroscopy (FTIR)

The infrared spectra of fibers were recorded on a Perkin Elmer Spectrum-400 FTIR spectrometer at the ambient temperature between 4000–650 cm^{-1} with a resolution of 4 cm^{-1}. To obtain reasonable signal to noise ratio the average of 20 scans was taken. Samples were analyzed directly on a single bounce diamond (ATR).

2.2.3.5.3 Dynamic Mechanical Analysis (DMA)

Samples subjected to DMA were cut from the aligned fiber films into rectangular specimens of approximately 30 mm × 6.5 mm × 0.25 mm. Analyses were carried out using a DMA (Q800 from TA Instruments) in the film tension mode with an amplitude of 10 μm, a frequency of 1 Hz, a force track of 125%, and a heating rate of 2 °C min^{-1}. The α-relaxation temperature, T_α, is defined at the loss modulus peak.

2.2.3.5.4 Measurements of Shape Memory Properties

The samples (fiber mats) were heated with a hot plate, and then the samples were bended to a certain angle once the temperature reached the stretching temperature (flat to bent). Thereafter, the samples were cooled down very quickly (with a high cooling rate of 10–20 °C min^{-1}) to a temperature lower than 30 °C. Finally, they were heated again. The deformed sample subjected to a lower heating rate, and the shape recovery can be observed as the temperature reached a certain point. The whole process of shape memory testing was recorded using a digital video and the frames of the video was used to calculate the deformed angle at various time intervals, which can be used to evaluate the value of recovery ratio. The stretching temperatures used were 74, 82, 92, or 104 °C. Generally, 74 °C was mostly used because it is quicker to cool down from this point

compared with others. The heating rate was varied between 10 and 20 °C min^{-1}. For quick cooling down, after deformation at the stretching temperature, an ice bath was used rather than just blowing air on it. The heating rate of second ramp was set lower than for the first time, it was set around 5–10 °C min^{-1}.

2.2.3.5.5 Raman Spectroscopy

Following biomineralization experiments, fibers were removed from the biomineralization buffer and allowed to dry, under ambient conditions. Several segments of mineralized and control fibers with and without the GFP-HABP protein were analyzed using confocal micro-Raman spectroscopy (Horiba Jobin Yvon LabRam ARAMIS Micro-Raman) to determine changes in the chemical composition of the fibers. Reference spectra were first collected for untreated fiber samples to identify a characteristic composition of the PLLA/PMMA fiber scaffold. Raman features associated with the polymeric scaffold display distinct peaks defined near 812, 875, 970, 983, 1122, and 1454 cm^{-1}. Spectral scans were taken for control and mineralized samples at 3 μm intervals throughout an area of 12 × 15 μm and the point spectra at each location were studied. Raman spectral features associated with hydroxyapatite mineral (590, 960, 1044, and 1074 cm^{-1}) were compared across all regions to assess compositional differences across all samples. Peak ratios were taken of the 960 and 812 cm^{-1} bands to draw comparisons regarding the biomineralization differences between all samples.

2.2.4 Results and Discussion

2.2.4.1 The Morphologies of PLLA/PMMA Fibers/Mats

The morphology of fibers revealed bead-free, continuous, uniform structures (Figure 2-3 (a),(b)). Single strand pore-free fibers were bundled together and it was also possible to form well-aligned structures due to the high stretching force experienced during gyration. The

interconnection of fibers led to formation of a network-like structure. This may be due to a "fingering instability" at the orifice of the gyration vessel that may not have sufficient shear force to generate break-off of individual fibers.[18] Generally, solvents with a high boiling point evaporate slowly and this causes stretching of a polymeric jet.[27] The fusion of polymer fibers at junctions may be due to solvent evaporation and the variation in solvent evaporation rate in blended fibers. The lower boiling point solvent, (chloroform, 61 °C in this case) has little time to evaporate and solidifies quickly during the spinning process resulting in fusion of fibers at the junction. It is also noteworthy that defect-free fiber morphologies could be produced when the concentration is 2–2.5 times the C_e (the implications of the entanglement concentration).[28] It is very interesting to note that surface of the fibers are pore-free and uniform across all mats. Generally, blended polymeric structures generate porous structures by having different phases that separate from each other due to immiscibility. However, the results here show that the PMMA/PLLA phases are having good miscibility in the chloroform preventing porous structure formation. Additionally, the functionality of the incorporated chimeric protein was determined via measuring the changes in the fluorescence intensity in the region for GFP that is used as a monitoring tool to verify the localization of the hydroxyapatite binding peptide, i.e., HABP. Because the blended polymer scaffolds also display auto-fluorescence in the green region, the intensity was normalized for GFP-HABP-containing fibers with respect to control samples. Figure 2-4 shows fluorescent images of chimeric protein containing fibers. Engineered protein infused fiber scaffold resulted in 20% increase in the average fluorescence intensity when compared to the polymer only control samples. This enhanced and homogenously distributed fluorescence intensity demonstrates the incorporated protein still remains active following introduction to solvents and the polymerization process, resulting in a bioactive fiber.

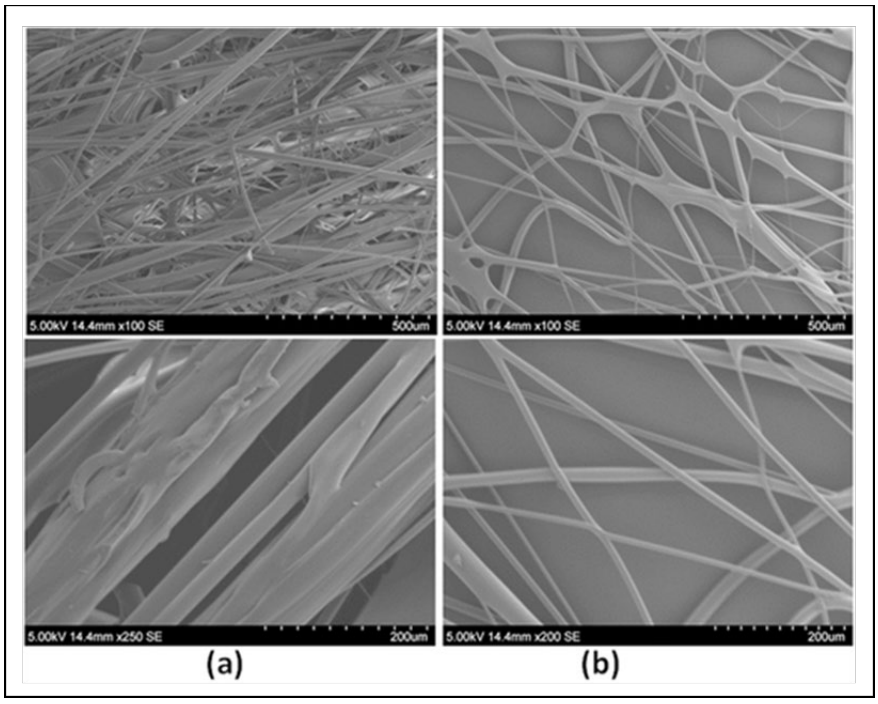

Figure 2-3: Scanning electron micrographs of 50 wt% PLLA/50 wt% PMMA fibers prepared at a rotating speed of 36,000 rpm under different pressure (a) 0.1 MPa, (b) 0.2 MPa.

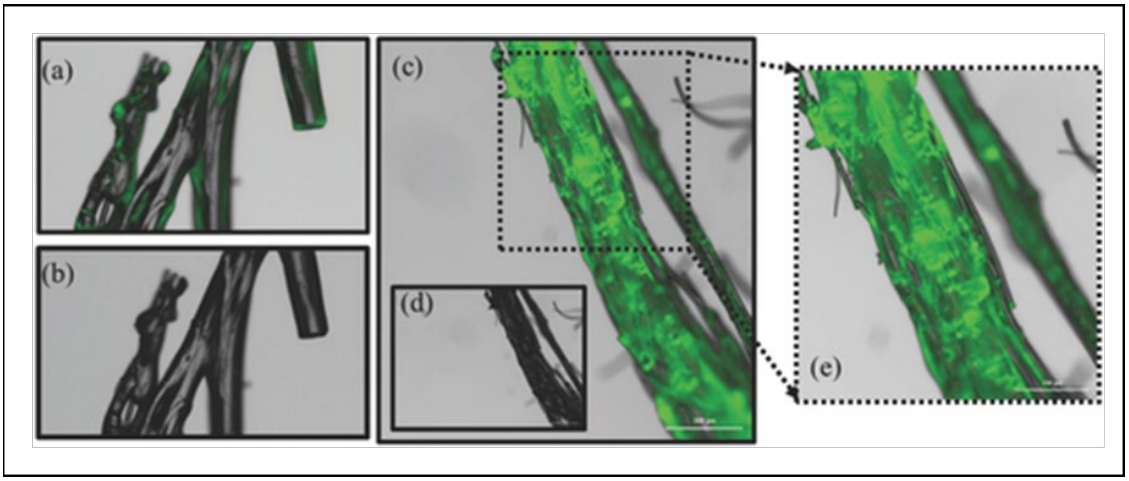

Figure 2-4: (a) Fluorescence and (b) bright field microscopy images of PLLA/PMMA fibers only. (c) Fluorescence and (d) bright field microscopy images of PLLA/PMMA fibers functionalized with GFP-HABP and (e) zoom out image showing the fluorescence intensity is homogenous throughout the protein functionalized fiber.

The fiber diameter analysis of the spun products show an average fiber diameter of 17 μm at a rotating speed of 36 000 rpm and 0.1 MPa working pressure (Figure 2-5).

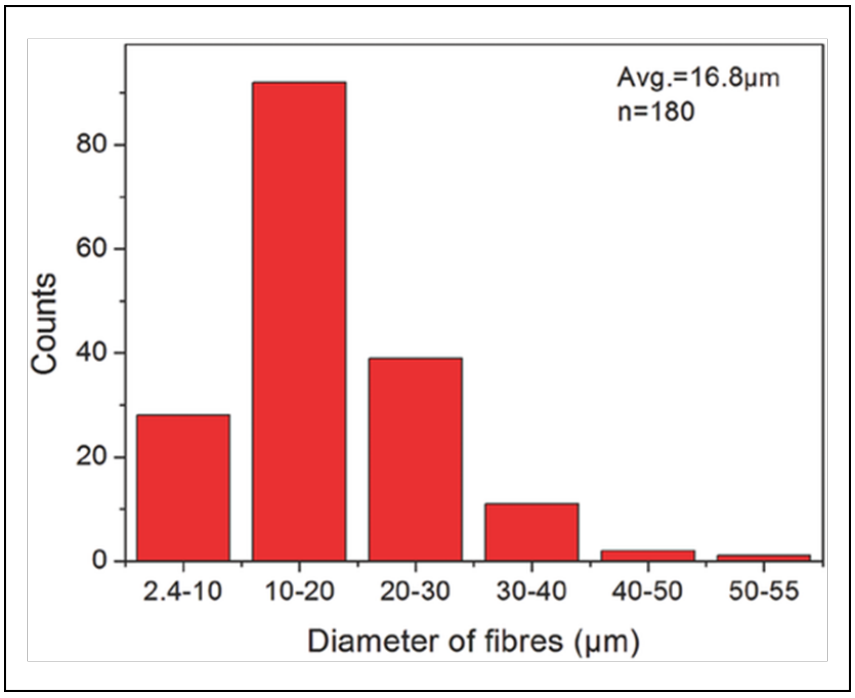

Figure 2-5: Fiber diameter distribution of 50 wt% PLLA/50 wt% PMMA fibers made at a rotating speed of 36,000 rpm and pressure of 0.1 MPa.

2.2.4.2 Thermal-Mechanical Analysis of the PLLA/PMMA Fibers

Figure 2-6(a) shows the storage and loss modulus of the blended fibers as a function of temperature. The storage modulus of the blended fibers initially increased with increasing temperature and reached a maximum value at 45 °C, thereafter it decreased with increasing temperature. The loss modulus and the loss factor may be used interchangeably to measure the characteristic temperatures pertaining to various relaxation processes. Figure 2-6(a) shows two different peaks recorded at 60 and 80 °C. This demonstrates that two different continuous phases appear in the blended fibers at a microscopic level. Actually, these two peaks are related to the glass transition temperature of the PMMA rich phase and the PLLA rich phase in the blended fibers. Generally, microstructure of these blended fibers depends on the weight ratio of original polymers. A transition from polymer rich phase to bicontinuous core/shell structure occurs when the weight ratio increases from 100:0 to 40:60. However, further increase of the weight ratio will

result in discontinuous phase.[29, 30] Moreover, phase separation of polymers depends on the environmental conditions during spinning. At higher relative humidity, the rate of solidification is faster due to water molecules which will act as a non-solvent to polymers. Thus, this leads to higher phase separation than the conditions found at lower relative humidity.[27] Figure 2-6(b) shows the stress–strain behavior of the blended polymer fibers as a function of temperature. The stress (or strain) of the fiber mats were increasing with temperature and shows a maximum value at 45 °C. The stress measured at this temperature was 1.25 MPa with a corresponding strain of 0.25%. Further increasing the temperature reduced the stress (or strain) of the blended polymeric fibers. In Figure 2-6(b), the corresponding tan δ (damping factor) shows a peak between 80 and 90 °C and this is due to glass transition of blended fibers.

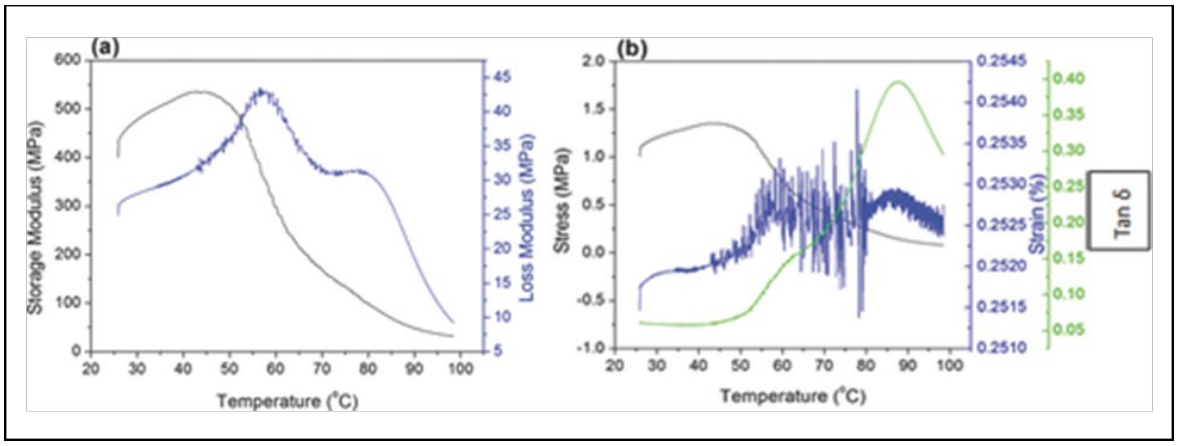

Figure 2-6: (a) Storage and loss modulus of shape memory mats. (b) Stress–strain characteristics of PMMA/PLLA fibers and damping factor Tan δ.

2.2.4.3 Shape Memory Properties of the PLLA/PMMA Mat

Figure 2-7 demonstrates the shape memory effect of the blended polymeric mat. At time 0 s, a flat fiber mat was bent and was observed at a temperature of 74 °C. A gradual recovery process (to flat) occurred and was recorded at different time intervals (every 15 s) up to 150 s. It indicates that the mat clearly recovers its original position.

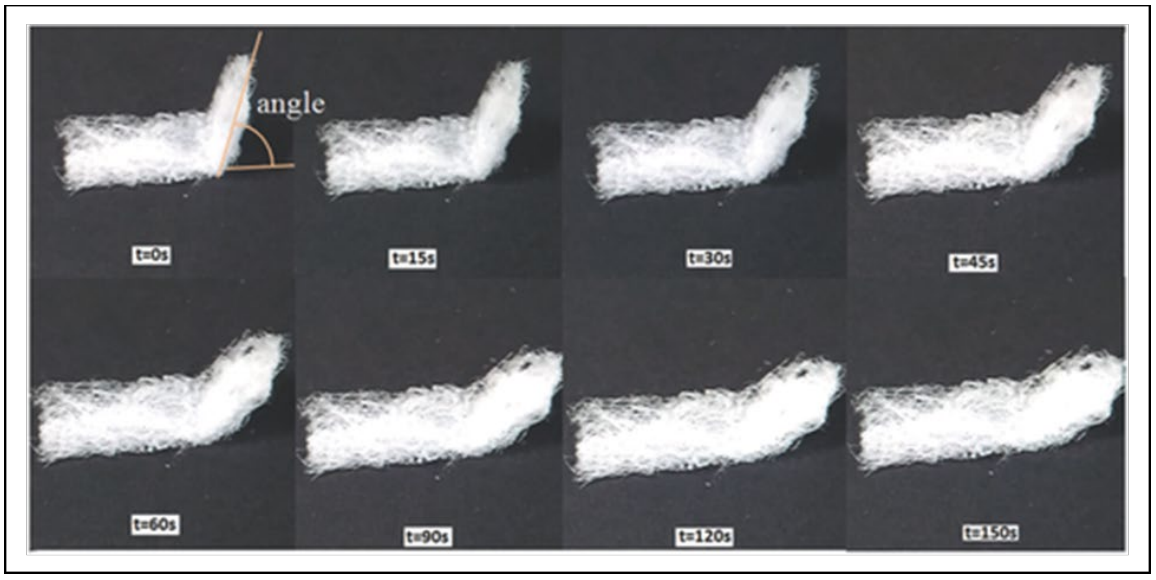

Figure 2-7: Demonstration of the shape memory effect of the polymeric mats prepared in this work.

The acute angle of deformation, i.e., the angle between bending surface and the plate plane (shown in Figure 2-7), and the corresponding strain during each time interval was calculated using digital micrographs and are shown in Figure 2-8. In the initial heating process, this flat fiber mat is not deformed, and the angle is not increased until the temperature reached the stretching point. The angle of deformation increased from 0° to 70° after the temperature reached 82 °C (Figure 2-8(a)). Thereafter, it remained constant. In the cooling down process this angle remained almost constant at ≈70° when reducing the temperature from 82 to 33 °C at a high cooling rate (≈10° min^{-1}) (Figure 2-8(b)). In the reheating process the angle of deformation was again reduced from 70° to 5° when increasing the temperature from 25 to 88 °C (Figure 2-8(c)).

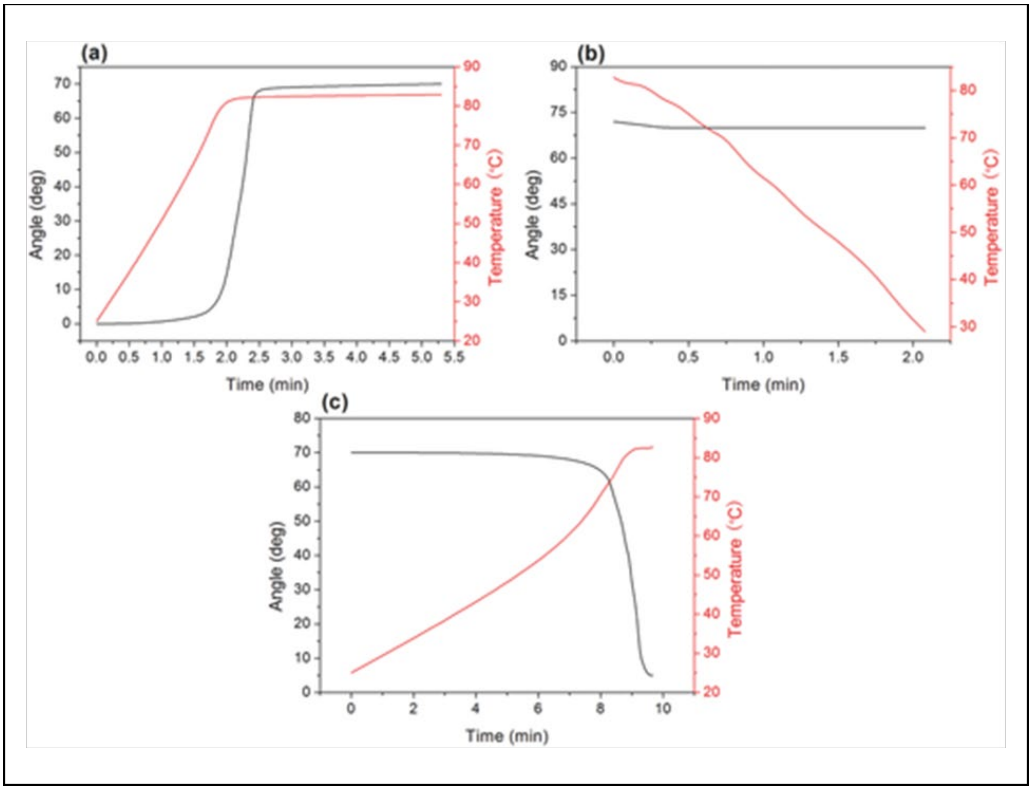

Figure 2-8: Angle of deformation (representing the corresponding strain) during the heat-cool-heat cycle of the polymeric mats (a) heating stage, (b) cooling stage, and (c) reheating stage.

Generally, shape memory polymers show dual-shape memory effect, i.e., they will be able to store different shapes including temporary and permanent. For an effective shape memory effect, one needs to have chemical and/or physical cross-links in the polymer network. The shape memory effect could be enhanced by inducing several distinct glassy and/or melting domains within the polymer chains. The dual shape memory effect of the blended fibers is shown in Figure 2-9 The sample was flat initially, then it was deformed at 94 and 65 °C, respectively, to show the dual shape memory effect. The recovery process of double stretching was observed thereafter where the sample recovers to its original flat position. This indicates that we will be able to tune properties of the polymer blend at different temperatures.

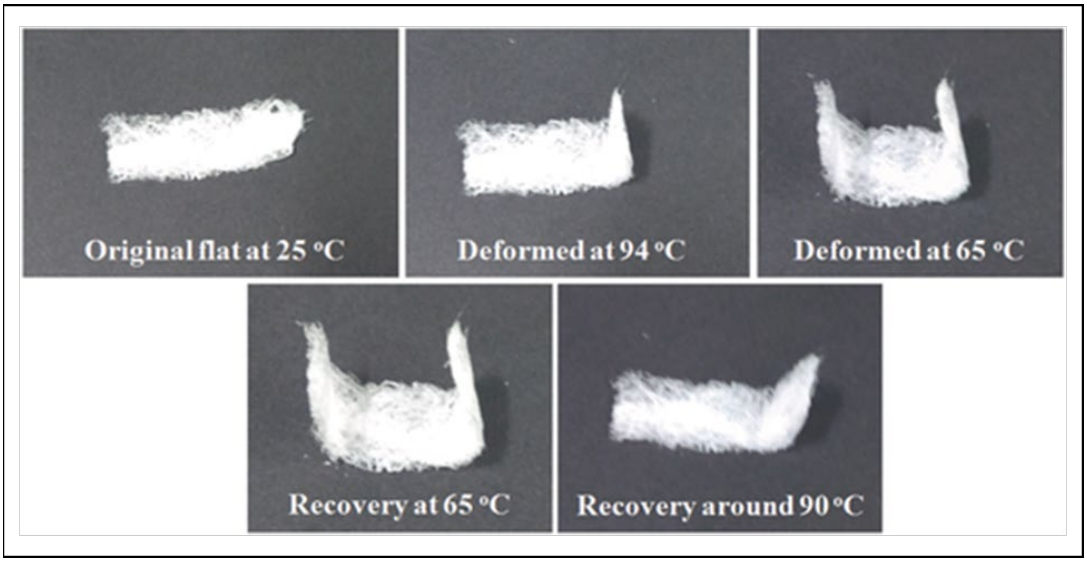

Figure 2-9: Demonstration of the double shape memory effect of the polymeric mats prepared in this work.

2.2.4.4 Biomineralization

Both control and protein-containing fiber mat sections were subjected to a 24h biomineralization assay. Compositional analysis of the mineralized fiber scaffolds was performed via FTIR and Raman spectroscopy. Figure 2-10 shows the FTIR spectra for the dry fibers before mineralization, fibers incubated in biomineralization buffer only (vehicle control), and fibers which were incubated in biomineralization buffer with the addition of AP enzyme to initiate the mineral formation by releasing phosphate ions into calcium rich environment. The PLLA/PMMA blended fibers have several bands attributed to either PLLA or PMMA individually such as peaks at 988, 865, and 842 cm^{-1}, corresponding to O–CH_3 and C–H rocking modes.[10] Due to the overlapping spectral features, notable hydroxyapatite mineral peaks can be observed via shifts in the spectra near 1042 cm^{-1} (v_3), attributed to PO_4.[2, 31] When comparing the spectral shifts between the control and the protein-infused samples treated with AP enzyme, the GFP-HABP-containing fiber scaffold displays a very distinct peak at 1040.5 cm^{-1}, which is much nearer to the mineral peak than the control fiber at 1035.8 cm^{-1}. FTIR bands near the defined phosphate peak at 1042

cm^{-1} indicate the mineral formed in the GFP-HABP sample better represent the composition and structure of the natural hydroxyapatite mineral phase.[2, 10, 31]

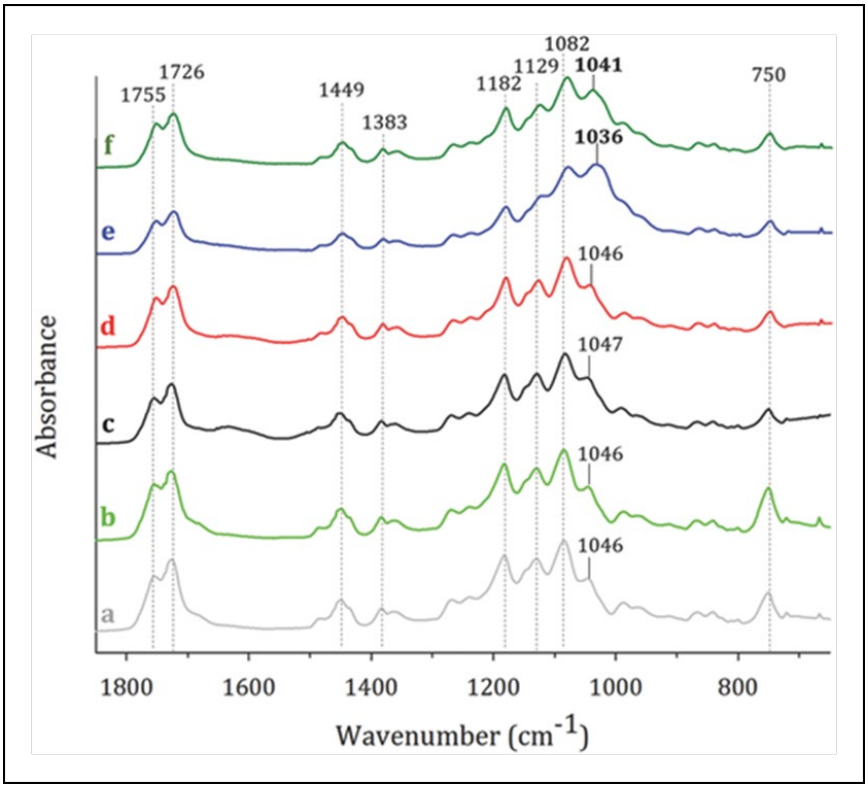

Figure 2-10: FTIR spectra for PLLA/PMMA only and GFP-HABP-functionalized PLLA/PMMA fibers, respectively, alternating. (a,b) Figure includes spectra for the dry fibers before mineralization, (c,d) fibers incubated in biomineralization buffer only (vehicle control), and (e,f) fibers that were incubated in biomineralization buffer with the addition of enzymatic AP. A significant shift is observed near the peak associated with mineral, 1040 cm^{-1} as shown in the (e) PLLA/PMMA only and (f) protein-functionalized PLLA/PMMA fibers which were treated with AP enzyme. These samples are shifted from the other spectra which feature bands at about 1046 cm^{-1}.

Figure 2-11 illustrates the Raman spectra for both PLLA/PMMA-only and PLLA/PMMA with GFP-HABP fibers incubated either in biomineralization buffer only (vehicle control) or biomineralization buffer with the addition of AP enzyme to catalyze mineral formation. The peaks at 812 cm^{-1} are associated with C–O–C symmetric stretching of the PLLA/PMMA polymer blend.[32] The bands at 960 cm^{-1} are characteristic of P–O symmetric stretching in phosphate

groups, as noted in hydroxyapatite mineral.[31] For each mineralized fiber sample, a ratio was taken of the 960 and 812 cm^{-1} bands to measure differences in the degree of mineralization. For the fibers not treated with the AP enzyme, the band ratios were not significantly different for the PLLA/PMMA fiber when compared to the fusion-protein-functionalized fibers. The addition of AP into the mineralization buffer resulted in an increase in the 960/812 peak ratio, as would be predicted. However, the GFP-HABP-functionalized fiber treated with AP displayed a significantly greater contribution at the 960 cm^{-1} mineral peak (comparatively). This increase following the 24 h biomineralization assay indicates the enhanced production of hydroxyapatite mineral within the GFP-HABP infused SMP fiber scaffold when compared to PLLA/PMMA fibers without the fusion protein.

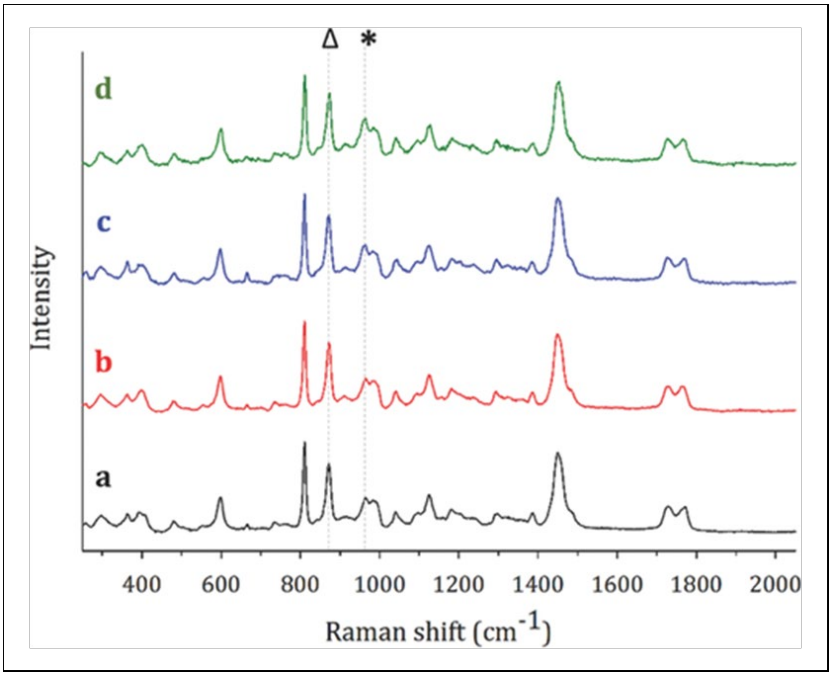

Figure 2-11: Raman spectra for biomineralization assay samples. (a,b) represent spectra for vehicle controls samples (no enzymatic AP added) (a) PLLA/PMMA only fiber and (b) the PLLA/PMMA fiber with GFP-HABP. Raman spectra for the mineralized fibers are shown as (c) and (d). For (c) PLLA/PMMA only fiber and (d) GFP-HABP-functionalized PLLA/PMMA fiber. Line at Δ represents a band associated with PLLA at 875 cm^{-1}. Reference line at * indicates spectral features occurring at the 960 cm^{-1} peak, a distinct hydroxyapatite mineral peak.

2.2.5 Conclusion

PLLA/PMMA composite shape memory fibers were successfully spun using pressurized gyration. The shape memory effect of the fibers was evaluated using a heat-cool-heat cycle. Incorporation of the green fluorescence protein engineered with hydroxyapatite binding peptide into the binary blend fibers resulted in bioactive shape memory fibers using this process. The bonding characteristics of the fiber-proteins were determined. Enzyme based biomineralization studies conducted on the fibers demonstrated that shape memory fibers and mats can have controllable inherent mineralization abilities through integrated bioactivity.

2.3 References

[1] Zhang S, Karaca BT, VanOosten SK, Yuca E, Mahalingam S, Edirisinghe M, Tamerler C. Coupling infusion and gyration for the nanoscale assembly of functional polymer nanofibers integrated with genetically engineered proteins. Macromolecular rapid communications 2015;36:1322-8.

[2] Silva C, Pinheiro A, Miranda M, Góes J, Sombra A. Structural properties of hydroxyapatite obtained by mechanosynthesis. Solid state sciences 2003;5:553-8.

[3] Tamerler C, Sarikaya M. Molecular biomimetics: nanotechnology and bionanotechnology using genetically engineered peptides. Philos Trans A Math Phys Eng Sci 2009;367:1705-26.

[4] Zhou H, Lee J. Nanoscale hydroxyapatite particles for bone tissue engineering. Acta biomaterialia 2011;7:2769-81.

[5] Gungormus M, Fong H, Kim IW, Evans JS, Tamerler C, Sarikaya M. Regulation of in vitro calcium phosphate mineralization by combinatorially selected hydroxyapatite-binding peptides. Biomacromolecules 2008;9:966-73.

[6] Ye Q, Spencer P, Yuca E, Tamerler C. Engineered Peptide Repairs Defective Adhesive-Dentin Interface. Macromol Mater Eng 2017;302.

[7] Spencer P, Ye Q, Song L, Parthasarathy R, Boone K, Misra A, Tamerler C. Threats to adhesive/dentin interfacial integrity and next generation bio-enabled multifunctional adhesives. J Biomed Mater Res B Appl Biomater 2019;107:2673-83.

[8] El Feninat F, Laroche G, Fiset M, Mantovani D. Shape memory materials for biomedical applications. Advanced Engineering Materials 2002;4:91-104.

[9] Lendlein A, Kelch S. Shape-memory polymers. Angewandte Chemie International Edition 2002;41:2034-57.

[10] Samuel Cd, Barrau S, Lefebvre J-M, Raquez J-M, Dubois P. Designing multiple-shape memory polymers with miscible polymer blends: evidence and origins of a triple-shape memory effect for miscible PLLA/PMMA blends. Macromolecules 2014;47:6791-803.

[11] Woo EM, Wang YH. New Complex Crystals of Chiral Poly (L-lactic acid) and Different Tactic Poly (methyl methacrylate). Macromolecular Chemistry and Physics 2012;213:1688-96.

[12] Peres LB, Peres LB, Araújo PHHd, Sayer C, Gonçalves OH. Preparation of PLLA/PMMA and PLLA/PS binary blend nanoparticles by incorporation of PLLA in methyl methacrylate or styrene miniemulsion homopolymerization. Polímeros 2015;25:23-8.

[13] Avella M, Errico ME, Immirzi B, Malinconico M, Falcigno L, Paolillo L. Radical polymerization of methyl methacrylate in the presence of biodegradable poly (l-lactic acid). Preparation of blends, chemical-physical characterization and morphology. Macromolecular Chemistry and Physics 2000;201:1295-302.

[14] Samuel C, Raquez J-M, Dubois P. PLLA/PMMA blends: A shear-induced miscibility with tunable morphologies and properties? Polymer 2013;54:3931-9.

[15] Eckelt J, Enders S, do Carmo Gonçalves M, Queiroz DP, Wolf BA. Polydispersity effects on the phase diagram of the system chloroform/poly-l-(lactic acid)/poly (methyl methacrylate) and morphology of PLA/PMMA films. Fluid phase equilibria 2000;171:219-32.

[16] Shen J, Jiang W, Liu Y, Wei R, Liu X, Zhong Y, Xu J, Li L, Xue G. Synthesis and thermal properties of poly (methyl methacrylate)-poly (L-lactic acid)-poly (methyl methacrylate) tri-block copolymer. Journal of applied polymer science 2012;124:3905-11.

[17] Hirota S-i, Sato T, Tominaga Y, Asai S, Sumita M. The effect of high-pressure carbon dioxide treatment on the crystallization behavior and mechanical properties of poly (l-lactic acid)/poly (methyl methacrylate) blends. Polymer 2006;47:3954-60.

[18] Mahalingam S, Edirisinghe M. Forming of polymer nanofibers by a pressurised gyration process. Macromolecular rapid communications 2013;34:1134-9.

[19] Mahalingam S, Raimi-Abraham BT, Craig DQ, Edirisinghe M. Formation of protein and protein–gold nanoparticle stabilized microbubbles by pressurized gyration. Langmuir 2015;31:659-66.

[20] Orlu-Gul M, Topcu AA, Shams T, Mahalingam S, Edirisinghe M. Novel encapsulation systems and processes for overcoming the challenges of polypharmacy. Current opinion in pharmacology 2014;18:28-34.

[21] Mahalingam S, Xu Z, Edirisinghe M. Antibacterial activity and biosensing of PVA-lysozyme microbubbles formed by pressurized gyration. Langmuir 2015;31:9771-80.

[22] Mahalingam S, Raimi-Abraham BT, Craig DQ, Edirisinghe M. Solubility–spinnability map and model for the preparation of fibres of polyethylene (terephthalate) using gyration and pressure. Chemical Engineering Journal 2015;280:344-53.

[23] Mahalingam S, Ren G, Edirisinghe M. Rheology and pressurised gyration of starch and starch-loaded poly (ethylene oxide). Carbohydrate polymers 2014;114:279-87.

[24] Mahalingam S, Pierin G, Colombo P, Edirisinghe M. Facile one-pot formation of ceramic fibres from preceramic polymers by pressurised gyration. Ceramics International 2015;41:6067-73.

[25] Xu Z, Mahalingam S, Basnett P, Raimi-Abraham B, Roy I, Craig D, Edirisinghe M. Macromol. Mater. Eng. 8/2016. Macromolecular Materials and Engineering 2016;301:881-.

[26] Yuca E, Karatas AY, Seker UO, Gungormus M, Dinler-Doganay G, Sarikaya M, Tamerler C. In vitro labeling of hydroxyapatite minerals by an engineered protein. Biotechnol Bioeng 2011;108:1021-30.

[27] Pai C-L, Boyce MC, Rutledge GC. Morphology of porous and wrinkled fibers of polystyrene electrospun from dimethylformamide. Macromolecules 2009;42:2102-14.

[28] McKee MG, Wilkes GL, Colby RH, Long TE. Correlations of solution rheology with electrospun fiber formation of linear and branched polyesters. Macromolecules 2004;37:1760-7.

[29] Bauer AJ, Wu Y, Li B. Electrospun Poly (ε-caprolactone)/Polyhedral Oligomeric Silsesquioxane-Based Copolymer Blends: Evolution of Fiber Internal Structures. Macromolecular bioscience 2016;16:705-16.

[30] Bauer AJ, Zeng T, Liu J, Uthaisar C, Li B. The Enhanced Encapsulation Capacity of Polyhedral Oligomeric Silsesquioxane-based Copolymers for the Fabrication of Electrospun Core/Shell Fibers. Macromolecular rapid communications 2014;35:715-20.

[31] Chen J, Chu B, Hsiao BS. Mineralization of hydroxyapatite in electrospun nanofibrous poly (L-lactic acid) scaffolds. Journal of Biomedical Materials Research Part A: An Official Journal of The Society for Biomaterials, The Japanese Society for Biomaterials, and The Australian Society for Biomaterials and the Korean Society for Biomaterials 2006;79:307-17.

[32] Vano-Herrera K, Misiun A, Vogt C. Preparation and characterization of poly (lactic acid)/poly (methyl methacrylate) blend tablets for application in quantitative analysis by micro Raman spectroscopy. Journal of Raman spectroscopy 2015;46:273-9.

Chapter 3 Peptide enabled nanoprobes for imaging in living brain tissue

*This chapter is adapted from the Research Publication **P2**:*

*R Jarosova, **SK Woolfolk**, N Martinez-Rivera, MW Jaeschke, E Rosa-Molinar, C Tamerler, MA Johnson, "Engineered Nanoprobes for Spatiotemporal Imaging of Metal Ions in Living Zebrafish Brain Tissue", Submitted to ChemComm, January 2022.*

This paper is currently under review in ChemComm published by the Royal Society of Chemistry

3.1 Preface

This chapter employs an engineered protein-nanoparticle based nanoprobe system as a potential imaging tool to monitor free biometals in living brain tissues using a zebrafish model. Herein, we adapted our previously developed red fluorescence fusion protein produced with a gold binding peptide construct (DsRed-AuBP) to functionalized different sizes of gold nanoparticles (AuNPs) and investigate their potential as a molecular imaging tool in a living brain tissue for the first time.

The homeostatic regulation of free biometals, including zinc, copper, and iron, is critical for maintaining normal neuronal and physiological function and health within the brain. Imbalance of these free biometal ions has been shown to play a critical role in neurodegenerative diseases. The ability to optically control the detection of free biometal ions in biological systems, especially in living brain tissue, has been met with significant challenges. In the last decade, many metal ion sensors, often employed with small organic molecules, peptides, or proteins, have been developed. Limited studies have been conducted to test such metal ions sensors in *in vivo* animal models such as in mice and zebrafish. Further, only a limited number of these sensors allow optical control of the detection with both spatial and temporal precision.

Herein, we describe a multi-functional nanoprobe-based approach to identify and potentially measure these free biometals in living brain tissue. These nanoprobes consist of AuNPs functionalized with DsRed-AuBP protein. To test the nanoprobes stability and free metal ion sensitivity, we have carried out experiments with different metal ions, nanoparticle sizes, and

protein combinations *in vitro* and selected to further explore the effects of Zn^{2+} on our nanoprobes in the living brain tissue studies.

In our studies, we used both epifluorescence and two-photon excitation (2-PE) confocal fluorescence microscopy characterization. Specially, 2-PE microscopy was used to demonstrate that our nanoprobes were both physically and photometrically stable in living brain tissue of zebrafish. We also demonstrated that in the absence of the nanoparticles, fluorescence protein would diffuse instantly. The engineered AuNP nanoprobes provided stability to monitor the nanoprobes in the living brain tissue for a significantly longer time. Furthermore, we demonstrated that the DsRed-labeled nanoprobes exhibited fluorescence quenching upon addition of Zn^{2+}.

Self-assembled bioactive metal nanoprobes offer free metal ion detection by combining orthogonal sensing methods. Due to challenges in the blood brain barrier and working with living tissue, zebrafish brain models are increasingly accepted as attractive models to study disease models and pathogenesis. Our studies demonstrated that the engineered nanoprobes can be applicable for further studies to understand disease pathogenesis using zebrafish brain model system. This paper addresses a growing demand for tunable *ex vivo* and *in vivo* metal ion sensors that can offer spatial and temporal resolution with respect to function.

3.2 Engineered nanoprobes for spatiotemporal imaging of metal ions in living zebrafish brain tissue*

3.2.1 Abstract

Homeostatic regulation of free biometals, such as zinc, copper, and iron, is critical for neuronal function and health. We decorated gold nanoparticles with self-assembled DsRed fluorescent protein, genetically tagged with gold binding peptide, to spatially and temporally resolve biometal levels. Two-photon excitation microscopy confirmed the physical and photometrical stability of these nanoprobes in living zebrafish (*Danio rerio*) brain tissue, while the addition of Zn^{2+} quenched nanoprobe fluorescence. Combining orthogonal sensing methods with our engineered nanoprobes will enable the study of imbalances in homeostatic biometal regulation and contribute to the understanding of neurological disease.

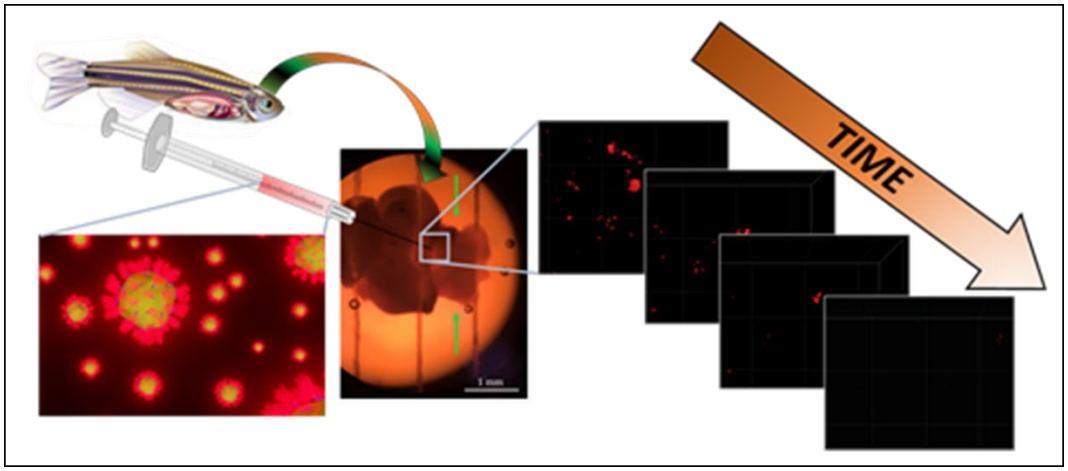

Figure 3-1: Table of contents schematic. Self-assembled bio-hybrid nanoprobes offer biometal imaging with spatial and temporal resolution in living zebrafish brain tissue to study biometal imbalances in homeostatic regulation.

---

* R Jarosova, SK Woolfolk, N Martinez-Rivera, MW Jaeschke, E Rosa-Molinar, C Tamerler, MA Johnson, "Engineered Nanoprobes for Spatiotemporal Imaging of Metal Ions in Living Zebrafish Brain Tissue", *Submitted to ChemComm, January 2022 (In Review)*

3.2.2 Introduction

Free and bound transition metals, including zinc, copper, and iron, influence neuronal function[1, 2] by guiding neuronal communication, memory formation, and sensory processing.[3] These metals exist in bound and unbound form, and their levels as free ions may rapidly fluctuate. For example, about 80-90% of zinc (Zn) exists as an integral part of proteins while the remaining 10-20% exists in its free form (Zn^{2+}) and is stored largely in synaptic vesicles[4], where it undergoes Ca^{2+} dependent exocytosis from subsets of glutamatergic neurons in the hippocampus, amygdala, striatum, and thalamus.[5-9] This release of Zn^{2+}, present in vesicles at 3-30 mM, transiently increases synaptic (100-300 μM) and extracellular (10-20 μM) Zn^{2+} levels.[5] Given their important roles in neuronal health and function, measuring biometals in living brain tissues could contribute immensely to our current understanding of the mechanisms that underlie neurological disease pathology.[10-14]

General categories for measuring Zn^{2+} levels have traditionally included genetically encoded Zn^{2+} indicators (GEZIs) and small molecule sensors (reviewed by Pratt *et al.* 2021).[15] A wide range of genetically encoded Zn^{2+} sensors have been developed to measure Zn^{2+} levels in the cytosol[16] and various organelles, including the endoplasmic reticulum[16], golgi apparatus[16], mitochondrial matrix[17], mitochondrial intermembrane space[18], and secretory vesicles[19]. Additionally, recent work has demonstrated the use of genetically encoded sensors for detecting Zn^{2+} on the extracellular surface in cultured cell preparations.[20] However, optical detection of free metal ion distribution in biological systems, especially in the brain, has proven challenging due to spatial and temporal limitations and inadequate selectivity.

In the past few decades, the use of metal ion sensors using small organic molecules, peptides, and proteins have been explored.[15, 21] The ability to tune these sensors by choice of fluorophore

and chelator are distinct advantages. Nevertheless, problems with using them in complex living brain tissues, including decreased bioavailability due to the inability to cross the blood brain barrier and breakdown by metabolic and catabolic enzymes, may pose a roadblock.

One possible way to address these concerns is by using nanoparticle-based sensing. Among these approaches, gold nanoparticles (AuNPs) are the most used due to their inherent optical and electronic properties, excellent chemical stability, and biological compatibility. Yet, limited studies feature the use of functionalized gold nanoparticles for sensing metal ions. In one application, gold nanoparticles functionalized with N-(2-(bis(pyridine-2-ylmethyl)amino)ethyl)-2-mercaptoacetamide (MDPA) offered bimodal imaging by combining surface enhanced Raman spectroscopy (SERS) and fluorescence spectroscopy, and was used to measure free intracellular Zn^{2+} levels in macrophages.[22] Another study employed chitosan-capped gold nanoparticles to measure Zn^{2+} concentrations in water via shifts in the optical and plasmon resonance peaks.[23] Similarly, uncapped gold nanoparticles have been used to cause visible color changes in solutions containing a targeted Zn^{2+} binding peptide for metal ion selectivity.[24] Optical detection of free metal ion distribution in biological systems, especially in the brain, has proven challenging due to spatial and temporal limitations and inadequate selectivity.

Here, we created nanoprobes composed of genetically engineered protein on gold nanoparticles for metal ion probing functionality with spatial and the temporal resolution in living zebrafish brain tissue (Figure 3-1). The use of whole brains *ex vivo* from this rapidly emerging research model holds key advantages. First, the whole brains are small enough to be kept alive and functional in a superfusion chamber. Because the brain is kept whole, all the neural pathways are preserved. Additionally, the small size of the zebrafish brains facilitates light microscopy imaging measurements while the brains are still alive and is especially amenable to two-photon excitation

(2PE) microscopy, which can image within the opaque tissue of adult brains. For these reasons, this model organism is ideal for the study of free biometals in homeostatic regulation and understanding neurologically relevant disease models using small molecule metal ion sensors.

To generate the self-assembled nanoprobe system, we used peptide motifs generated and applied to bind selectively and with high affinity to gold surfaces and nanoparticles.[25, 26] Genetic incorporation of gold binding peptide as a tag into DsRed fluorescent protein (λ_{ex} = 556 nm, λ_{em} = 590 nm) enabled use of the self-assembled fluorescent gold nanoparticles as bimodal imaging nanoprobes.[27] The resulting nanoprobe was explored as a potential metal ion sensor in living zebrafish brain tissue due to its experimental advantages and the high sequence homology of zebrafish to mammals.[28-30]

3.2.3 Results and Discussion

We first ran *in vitro* quenching assays using different metal ions with nanoprobes that are composed of 15 nm diameter gold nanoparticles functionalized with the fusion DsRed-AuBP protein (Figure 3-2 (a-d)). Figure 3-2(b) shows that the dynamic linear range of the probes with respect to Zn^{2+} extends to about 25 μM (R^2=0.98). Given that expected transient brain concentrations of Zn^{2+} (10-20 μM) fall within the linear dynamic range, our nanoprobes seem well-suited for measurements of extracellular metal release. Analysis by two-way ANOVA revealed significant overall main effects of metal ion identity ($p = 0.007$, $F[3,48] = 6.76$) and concentration ($p < 0.0001$, $F[3,48] = 12.15$) on quenching. Further Tukey *post hoc* testing revealed high selectivity for Zn^{2+} over Mg^{2+} ($p<0.05$ at 10 μM and $p < 0.005$ at 25 μM, two-way ANOVA) and selectivity for Cu^{2+} and Fe^{3+} over Mg^{2+} at 25 μM ($p < 0.05$), (Figure 3-2(d)). This selectivity is important due to the presence of extracellular Mg^{2+} in the extracellular fluid in the brain. Our

results provide a promising concentration-dependent quenching effect on the fluorescence protein displayed on the nanoprobes.

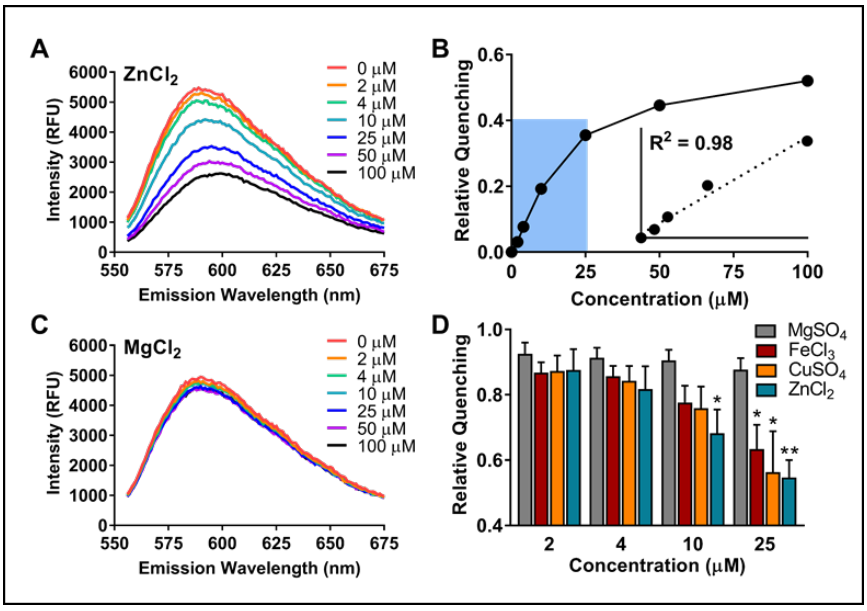

Figure 3-2: Nanoprobe response to metals *in vitro*. (a) Zn^{2+} response curves (0 to 100 µM) and (b) calibration plot (inset from shaded region, 0 to 25 µM). (c) Mg^{2+} response curves (0 to 100 µM) and (d) Quenching vs concentration of added $MgCl_2$, $FeCl_3$, $CuCl_2$, and $ZnCl_2$. Bars on graph indicate mean ± SEM. Statistics: *p<0.05 vs $MgCl_2$, **p<0.005 vs $MgCl_2$, (2-way ANOVA with Tukey *post hoc*, n = 4).

We then injected DsRed-AuBP-AuNPs into living zebrafish whole brains maintained in a superfusion chamber and imaged the nanoprobes with either epifluorescence or 2PE microscopy. Figure 3-3(a) shows an epifluorescence image of injected nanoprobes overlayed on a brightfield image of a zebrafish telencephalon. These nanoprobes tended to disperse over a wide region of the brain immediately following injection. We also injected them into the diencephalon of a living brain from *th2:gfp* zebrafish, which possess fluorescent dopaminergic neurons, and imaged the brain and the adjacent fluorescent dopaminergic neurons with 2PE microscopy (Figures 3-3(b) and (c)). The color differences between the DsRed nanosensors and the GFP allows us to simultaneously observe the nanoprobes and neurons within the same image.

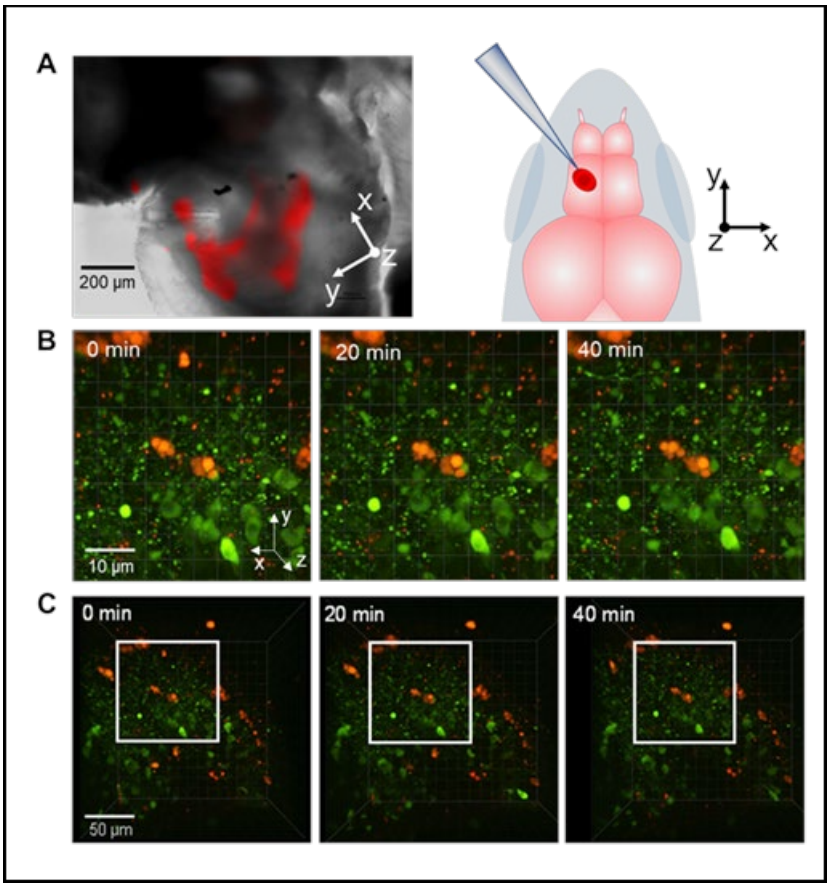

Figure 3-3: DsRed functionalized nanoprobes remain stationery and fluorescent in living zebrafish brain. (a) DsRed-AuBP functionalized nanoparticles, 15 nm diameter injected in the ventral diencephalon area of a viable zebrafish brain. Image obtained by overlaying fluorescence on brightfield images. (b) and (c), DsRed-BP-AuNPs, 15 nm diameter, were picospritzed in living zebrafish brain and imaged with 2PE microscopy. The spatial relationships between the GFP labeled dopamine neurons (green) and nanoprobes (red) are unchanged. For all images, x-axis, caudal, y-axis, lateral, z-axis, ventral.

Possible barriers to using our nanoprobes to sense Zn^{2+} or other metals include peptide fluorophore degradation by photobleaching or protease activity and movement of nanoprobes in the brain. To monitor signal degradation and movement, we imaged the nanoprobes by 2PE microscopy for 40 minutes. Our approach allowed us to directly observe nanoparticle clusters and demonstrated that they remained stationary with respect to the dopaminergic neurons (Figures 3-3 (b) and (c)). Also, the nanoprobes continued to fluoresce without noticeable photobleaching for at least 40 min.

To determine the ability of free metal ions to quench fluorescence in living brain tissue, we injected a solution of $ZnCl_2$ in aCSF into whole brains that had previously been injected with DsRed-BP AuNPs, and imaged the nanoprobes with epifluorescence microscopy (Figures 3-4 (a) and (b)). Upon injection of $ZnCl_2$, fluorescence immediately decreased by 41%, indicating that the Zn^{2+} quenched the protein by association with either the metal selective peptide sequence or another location on the DsRed protein.

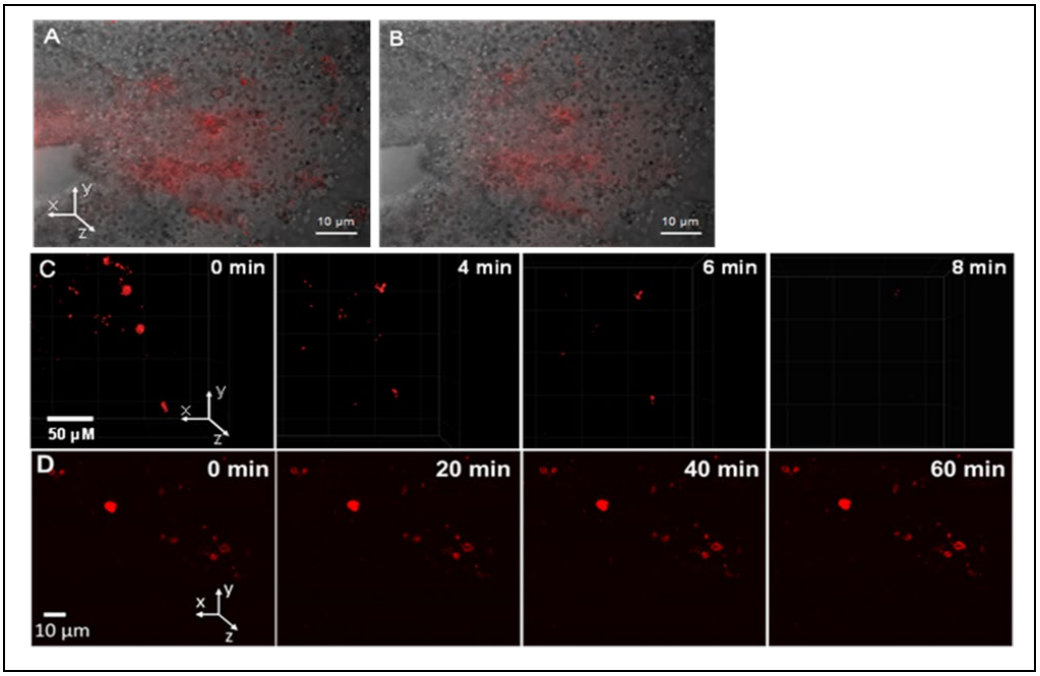

Figure 3-4: Exogenously applied Zn^{2+} rapidly quenches fluorescence. (a) A 15 µL volume of nanoparticles was injected into the telencephalon. (b) Injection of a 10 µL volume of Zn^{2+} at a concentration of 100 µM, resulting in an immediate 41% decrease in total fluorescence. Image obtained by overlaying fluorescence on brightfield images. (c) The brain was perfused with a solution of 100 nM $ZnCl_2$ in aCSF. (d) No Zn^{2+} control. For all images, x-axis, caudal, y-axis, lateral, z-axis, ventral.

We further sought to determine if we could observe the fluorescence quenching of individual nanoparticle clusters. DsRed-BP-AuNPs nanoparticles were injected into the brain and the brain was perfused with $ZnCl_2$ (100 nM) in aCSF while imaging with 2PE (Figures 3-4 (c) and (d)) microscopy. Over the course of 8 min, fluorescence almost completely disappeared, indicating

rapid quenching. On the other hand, the fluorescence of nanoprobes injected without perfusion of Zn^{2+} did not diminish over the course of 60 minutes, demonstrating that the decrease in fluorescence occurred due to quenching of the DsRed protein with Zn^{2+} rather than photobleaching or degradation of the chromophore.

Collectively, these results demonstrate the utility of gold nanoparticles as a stable platform for our custom modified DsRed-BP for the measurement of metals such as Zn^{2+}. For comparison with DsRed-BP-AuNPs, we injected unbound DsRed protein molecules in living zebrafish brains and imaged with 2PE microscopy. In contrast to nanoparticle bound DsRed protein molecules, free DsRed protein molecules tended to disperse throughout the brain. Larger aggregates formed and remained stationary within the brain. To determine if smaller aggregates and individual protein molecules tended to diffuse freely, we chose several larger, stationary aggregates as anchor points, and measured how the fluorescence intensity changes over time at defined regions of interest within a selected panel (Figures 3-5 (a) and (b)). The decreased mobility occurs due to the DsRed protein molecules being tethered to the gold nanoparticles. Over the course of 40 minutes, the fluorescence intensity within the regions of interest decreased significantly (Figure 3-5 (c)), suggesting that free DsRed protein molecules and smaller aggregates tend to diffuse throughout the tissue. These results collectively show that our nanoprobes consisting of gold nanoparticles are better suited for measurements at defined locations within the brain tissue than unbound DsRed protein.

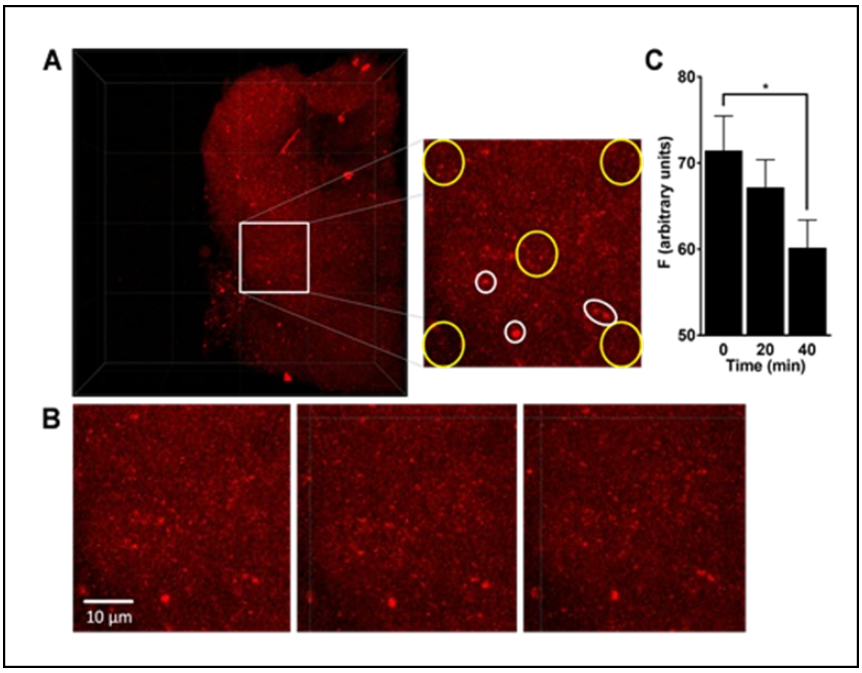

Figure 3-5: DsRed protein diffuses in perfused zebrafish brain. (a) three-dimensional 2PE image of injected DsRed protein in living zebrafish brain. Cutout indicates sampled regions (yellow circles) and reference points (white circles and ellipse). One grid segment = 50 µm. (b) Images of cutout sampled over time. (c) Comparison of fluorescence (F) of pooled regions over time. **p*=0.0091 (two-tailed t-test, n=5 regions sampled per time point). Z-axis slice thickness=80 µm. For all images, x-axis, caudal, y-axis, lateral, z-axis, ventral.

3.2.4 Conclusion

In conclusion, this work provides proof of concept for the use of engineered nanoprobes to track metal ions in living brain tissue with both spatial and temporal resolution. DsRed-AuBP-functionalized AuNP nanoprobes resisted photobleaching and degradation for at least an hour during imaging, remained stationary, and responded to quenching with Zn^{2+} in living brains. The current platform is amenable to combining with other orthogonal methods in which nanoprobes could be tuned to target specific metal ions.

Our proposed probes are versatile and offer to incorporate additional metal binding tags targeting different biometals and combination of small molecules. This work offers a promising, targeted approach to address the growing demand for optical control for *in vivo* sensing of key

metal ions that is adaptable and can be easily implemented with other analytical methods in living tissues. As the multi-functionality of the nanoprobes expands, the novel molecular tools could impact our understanding of the numerous neurological disease states, including Alzheimer's disease, Parkinson's disease, and Huntington's disease.

3.2.5 Materials and methods

3.2.5.1 Animals

Adult *Danio rerio* (zebrafish, transgenic line *th2:gfp*) were housed in the Shankel Structural Biology Center at the University of Kansas, in 3L tanks (20 fish per three-liter system rack tank) and connected to a recirculation filtration system. All tanks were maintained under constant chemical, biological and mechanical filtration, as well as UV sterilizing unit to ensure adequate conditions. The following quality parameters of the reverse osmosis purified system water were controlled and adjusted using Multiparameter Monitoring and Control Instrument 5200A (YSI, Yellow Springs, OH): conductivity (~ 700 µS cm^{-1}), pH (7.2), and temperature (28 °C). The fish were fed twice a day and maintained on a 14:10 light: dark cycle. All protocols and procedures involving zebrafish were approved by the Animal Care and Use Committee of the University of Kansas.

3.2.5.2 Euthanasia, brain perfusion, and extraction

All zebrafish were euthanized by hypothermic shock followed by decapitation. Immediately following euthanasia, whole brains were harvested using previously described method (some citation here) and transferred to a perfusion chambre. The viability of the brain was ensured by continuous flow of oxygenated and heated (28 °C) aCSF. The aCSF consisted of 126 mM NaCl, 2.5 mM KCl, 2.4 mM $CaCl_2$, 1.2 mM $MgCl_2$, 25 mM $NaHCO_3$, and 20 mM HEPES (all Sigma-

Aldrich, St. Louis, MO), and adjusted to a pH of 7.4. Ultrapure water (~18.2 MOhm-cm) was used to prepare all aqueous solutions.

3.2.5.3 Protein-peptide construct methods

The DsRed fluorescent protein conjugated with a gold binding peptide (AuBP) and a maltose-binding protein (MBP) were expressed and purified from recombinant *E. coli* ER2507 cells following previously established protocols [31, 32]. A single colony of the recombinant *E. coli* cells was grown up sequentially into larger volumes (3mL, 10mL, and 400mL) in LB-Miller media with 2% glucose and 100 μg/mL of ampicillin in an incubator (37°C) with continuous shaking. The 400 mL solution of the recombinant *E. coli* cells was inoculated with IPTG (Isopropyl β-D-1-thiogalactopyranoside) with a final concentration of 0.3 mM after an OD_{600} reading of 0.6 was reached. Once inoculated, the cells were incubated with continuous shaking overnight to give the cells time to express the fusion protein. The recombinant *E. coli* cells were then subsequently separated from the media through centrifugation at 4,000g for 30 minutes. The cell pellet was then resuspended in amylose resin column buffer (20 mM Tris–HCl, 200 mM NaCl, 1 mM EDTA, pH 7.4) and lysed through sonication. The lysed cells were spun down through centrifugation at 10,000g for 30 minutes. The supernatant was sterile filtered and loaded onto amylose resin (New England Biolabs, NEB, MA, USA) column to purify the fusion protein using the maltose binding protein tag. Extraneous biomolecules were washed away with column buffer, and the fusion protein was eluted using an elution buffer (column buffer + 10mM of maltose). Using centrifugal filters with a 10 kDa (MilliporeSigma, MO, USA) weight cutoff, the fusion protein was concentrated in Milli-Q sterile filtered water. Samples of various steps of the purification process of MBP-DsRed-AuBP were collected and verified using an SDS-PAGE gel. Then, protein samples were transferred into 1X cleavage buffer containing 20 mMTris-HCl, 100 mM NaCl, 2mM $CaCl_2$

(pH 8.0) by ultrafiltration using the same centrifugal filter tube. 40 µl of 1 mg/ml Factor Xa (NEB, MA, USA) was added to 2.5 mg/ml of fusion protein in 1X cleavage buffer. The cleavage reaction was performed overnight at 16C. A buffer exchange was completed so the cleaved MBP and DsRed-AuBP was back in column buffer and the mixture was added into a fresh amylose resin column. The cleaved MBP fragments bound to the resin and the flow through was collected as pure DsRed-AuBP. The fusion protein was again concentrated in Milli-Q sterile filtered water using centrifugal filters with a 10 kDa MWCO (MilliporeSigma, MO, USA). Following cleavage, the purity of DsRed-AuBP was observed by SDS-PAGE.

3.2.5.4 AuNP functionalization and nanoprobe preparation

Following a previously established protocol, stock, citrate-coated gold nanoparticles (AuNPs) were functionalized with the affinity based DsRed-AuBP construct [32-34]. Briefly, stock AuNPs sized 15 and 50nm (BBI Solutions, ME, USA) were provided at 47.8 and 56.9 ug/mL, respectively, and diluted in water to achieve a concentration of 10 ug/mL. To functionalize AuNPs with the affinity peptide construct, AuNPs were incubated with DsRed-AuBP prepared to achieve a final concentration of 50uM in water. The solution was allowed incubate at room temperature (25C) for 2 hours under gentle shaking conditions, protected from light to allow time for the peptide to bind to the gold surfaces. A wash step was completed to remove excess, unbound protein by pelleting the suspension via 30min centrifugation at 17000g and 1100g for 15 and 50nm AuNPs, respectively and carefully removing the supernatant. The pellet was reconstituted in either Milli-Q water or aCSF media to achieve a final functionalized AuNP concentration of 10ug/mL in solution.

3.2.5.5 *In vitro* fluorescence quenching

To study the quenching effect of key metal ions on the DsRed-AuBP functionalized AuNPs, stock metal ion solutions were prepared. Copper (II) sulfate pentahydrate (CuSO4; Acros Organics), ferric chloride hexahydrate ($FeCl_3$; Fisher Chemical), magnesium sulfate heptahydrate ($MgSO_4$; Fisher Chemical), and zinc chloride ($ZnCl_2$; Acros Organics) were prepared to achieve a working stock concentration of 6mM in 10mL of Milli-Q water and sterile filtered. In a 96-well plate, 100uL of washed, DsRed-AuBP (ex/em 556/590nm) functionalized AuNPs at a final concentration of 10ug/mL were added into each well. Triplicate samples were prepared for each metal ion concentration tested. A 6X concentration of each metal ion was prepared from the working stock so that 20uL could be added to each well immediately prior to experimental measurements to achieve final, in-well ion concentrations of 0, 2, 4, 10, 25, 50, and 100uM. Once the solutions were added, a fluorescence spectral scan was conducted to measure the quenching effect using a Cytation3 multi-modal plate reader. The excitation was kept at 525nm to avoid interference with the emission spectral range from 556 to 680nm. Immediate quenching of the fluorescence signal was noted with increasing ion concentrations.

3.2.5.6 Nanoprobe delivery

DsRed-BP-AuNP was injected into the telencephalon and diencephalon of living zebrafish whole brain with a micropipette linked to a Picospritzer III (Parker, Hollis, NH). The micropipettes were fabricated from glass capillary tubes (1.2 mm D.D and 0.68 mm I.D, 4 in long; A-M System Inc, Carlsborg, WA, USA). The glass capillary tubes were pulled using a PE-22 heated coil puller (Narishige Int. USA, East Meadow, NY, USA) and cut to external diameter of 20 μm. For quenching experiments, a stock solution (10μM) of $ZnCl_2$ (CAS No. 7646-85-7, ≥98%, Sigma-Aldrich, St. Louis, MO) was prepared by dissolving the appropriate analyte mass in modified

artificial cerebrospinal fluid (aCSF). Ultrapure water (~18.2 MOhm-cm) was used to prepare all aqueous solutions.

3.2.5.7 Microscopy

Epifluorescence images were obtained with a Nikon E600Fn Epifluorescence microscope, using either a Plan Fluor 10X/0.30 NA air objective or a Fluor 40X/0.80 NA water immersion objective. Images were collected and analyzed with Metamorph software (Molecular Devices, San Jose, CA). Two-photon imaging was carried out on a customized 3i/Zeiss Axio Examiner.Z1 upright two-photon excitation microscope with a Plan-Apochromat 20X/ 1.0 NA water immersion objective. For imaging of Au, DsRed-Au nanoparticles, and its combination with GFP labeled neurons, excitation wavelength of 850, 920, and 950 nm were used, respectively. The activity of the nanoparticles (viability and movement) in the living brain were monitored by continuous imagining in 10 min intervals for period lasting up to 2 hours. The resulting 2-photon images were analyzed and post-processed using 3i SlideBook 6.0, ImageJ software, and Adobe Photoshop.

3.3 References

[1] Howell GA, Welch MG, Frederickson CJ. Stimulation-induced uptake and release of zinc in hippocampal slices. Nature 1984;308:736-8.

[2] Stewart GR, Frederickson CJ, Howell GA, Gage FH. Cholinergic denervation-induced increase of chelatable zinc in mossy-fiber region of the hippocampal formation. Brain Res 1984;290:43-51.

[3] Goldberg JM, Lippard SJ. Challenges and Opportunities in Brain Bioinorganic Chemistry. Acc Chem Res 2017;50:577-9.

[4] Wang L, Yin YL, Liu XZ, Shen P, Zheng YG, Lan XR, et al. Current understanding of metal ions in the pathogenesis of Alzheimer's disease. Transl Neurodegener 2020;9:10.

[5] Frederickson CJ, Bush AI. Synaptically released zinc: physiological functions and pathological effects. Biometals 2001;14:353-66.

[6] Frederickson CJ. Neurobiology of zinc and zinc-containing neurons. Int Rev Neurobiol 1989;31:145-238.

[7] Slomianka L. Neurons of origin of zinc-containing pathways and the distribution of zinc-containing boutons in the hippocampal region of the rat. Neuroscience 1992;48:325-52.

[8] Ketterman JK, Li YV. Presynaptic evidence for zinc release at the mossy fiber synapse of rat hippocampus. J Neurosci Res 2008;86:422-34.

[9] Takeda A, Fuke S, Tsutsumi W, Oku N. Negative modulation of presynaptic activity by zinc released from Schaffer collaterals. J Neurosci Res 2007;85:3666-72.

[10] Bagheri S, Squitti R, Haertle T, Siotto M, Saboury AA. Role of Copper in the Onset of Alzheimer's Disease Compared to Other Metals. Front Aging Neurosci 2017;9:446.

[11] Ward RJ, Dexter DT, Crichton RR. Neurodegenerative diseases and therapeutic strategies using iron chelators. Journal of Trace Elements in Medicine and Biology 2015;31:267-73.

[12] Barnham KJ, Bush AI. Biological metals and metal-targeting compounds in major neurodegenerative diseases. Chemical Society Reviews 2014;43:6727-49.

[13] Qian X, Xu Z. Fluorescence imaging of metal ions implicated in diseases. Chemical Society Reviews 2015;44:4487-93.

[14] Chowdhury S, Rooj B, Dutta A, Mandal U. Review on recent advances in metal ions sensing using different fluorescent probes. Journal of fluorescence 2018;28:999-1021.

[15] Pratt EPS, Damon LJ, Anson KJ, Palmer AE. Tools and techniques for illuminating the cell biology of zinc. Biochim Biophys Acta Mol Cell Res 2021;1868:118865.

[16] Qin Y, Dittmer PJ, Park JG, Jansen KB, Palmer AE. Measuring steady-state and dynamic endoplasmic reticulum and Golgi Zn2+ with genetically encoded sensors. Proc Natl Acad Sci U S A 2011;108:7351-6.

[17] Park JG, Qin Y, Galati DF, Palmer AE. New sensors for quantitative measurement of mitochondrial Zn(2+). ACS Chem Biol 2012;7:1636-40.

[18] Fudge DH, Black R, Son L, LeJeune K, Qin Y. Optical Recording of Zn(2+) Dynamics in the Mitochondrial Matrix and Intermembrane Space with the GZnP2 Sensor. ACS Chem Biol 2018;13:1897-905.

[19] Vinkenborg JL, Nicolson TJ, Bellomo EA, Koay MS, Rutter GA, Merkx M. Genetically encoded FRET sensors to monitor intracellular Zn2+ homeostasis. Nat Methods 2009;6:737-40.

[20] Chen Z, Ai HW. Single Fluorescent Protein-Based Indicators for Zinc Ion (Zn(2+)). Anal Chem 2016;88:9029-36.

[21] Yang Z, Loh KY, Chu Y-T, Feng R, Satyavolu NSR, Xiong M, et al. Optical control of metal ion probes in cells and zebrafish using highly selective DNAzymes conjugated to upconversion nanoparticles. Journal of the American Chemical Society 2018;140:17656-65.

[22] Li D, Ma Y, Duan H, Jiang F, Deng W, Ren X. Fluorescent/SERS dual-sensing and imaging of intracellular Zn(2). Anal Chim Acta 2018;1038:148-56.

[23] Promnimit S, Bera T, Baruah S, Dutta J. Chitosan capped colloidal gold nanoparticles for sensing zinc ions in water. Journal of Nano Research: Trans Tech Publ; 2011. p. 55-61.

[24] Li W, Nie Z, He K, Xu X, Li Y, Huang Y, et al. Simple, rapid and label-free colorimetric assay for Zn2+ based on unmodified gold nanoparticles and specific Zn2+ binding peptide. Chem Commun (Camb) 2011;47:4412-4.

[25] Hnilova M, Karaca BT, Park J, Jia C, Wilson BR, Sarikaya M, et al. Fabrication of hierarchical hybrid structures using bio-enabled layer-by-layer self-assembly. Biotechnol Bioeng 2012;109:1120-30.

[26] Hnilova M, Oren EE, Seker UO, Wilson BR, Collino S, Evans JS, et al. Effect of molecular conformations on the adsorption behavior of gold-binding peptides. Langmuir 2008;24:12440-5.

[27] Yuca E, Tamerler C. Self Assembled Recombinant Proteins on Metallic Nanoparticles As Bimodal Imaging Probes. JOM (1989) 2019;71:1281-90.

[28] Ko S-K, Chen X, Yoon J, Shin I. Zebrafish as a good vertebrate model for molecular imaging using fluorescent probes. Chemical Society Reviews 2011;40:2120-30.

[29] Kalueff AV, Stewart AM, Gerlai R. Zebrafish as an emerging model for studying complex brain disorders. Trends in pharmacological sciences 2014;35:63-75.

[30] Li W, Fang B, Jin M, Tian Y. Two-photon ratiometric fluorescence probe with enhanced absorption cross section for imaging and biosensing of zinc ions in hippocampal tissue and zebrafish. Analytical chemistry 2017;89:2553-60.

[31] Karaca BT, Meyer J, VanOosten S, Richter M, Tamerler C. Modular Peptide-Based Hybrid Nanoprobes for Bio-Imaging and Bio-Sensing. MRS Online Proceedings Library Archive 2014;1621:155-61.

[32] Zhang S, Karaca BT, VanOosten SK, Yuca E, Mahalingam S, Edirisinghe M, et al. Coupling infusion and gyration for the nanoscale assembly of functional polymer nanofibers integrated with genetically engineered proteins. Macromolecular rapid communications 2015;36:1322-8.

[33] Karaca BT, Hnilova M, Tamerler C. Addressable biological functionalization of inorganics: Materials-selective fusion proteins in bio-nanotechnology. Bio-Inspired Nanotechnology: Springer; 2014. p. 221-55.

[34] Yuca E, Tamerler C. Self-Assembled Recombinant Proteins on Metallic Nanoparticles as Bimodal Imaging Probes. JOM 2019;71:1281-90.

Chapter 4 Peptide enabled nanocomposites for reconstruction of dental tissues

*This chapter is adapted from the Research Publication **P3**:*

***SK Woolfolk**, AK Cloyd, Q Ye, K Boone, P Spencer, ML Snead, C Tamerler, "Peptide Enabled Nanocomposites Offer Biomimetic Reconstruction of Silver Diamine Fluoride Treated Dental Tissues", Submitted to Polymers, January 2022.*

This paper is currently under review in Polymers published by MDPI

4.1 Preface

Early childhood caries (ECC) is the most prevalent chronic disease in children worldwide. We explored a pediatric dental challenge by engineering a novel bi-functional peptide that is composed of silver binding peptide (AgBP) and amelogenin derived peptide (ADP). Silver diamine fluoride (SDF) has been recently approved by FDA in preventive dentistry for arresting ECC disease progression. Although SDF treatment is easy to deploy with minimum cost, lesions treated with SDF are permanently stained black due to oxidative silver staining. The loss of aesthetics has been documented and in interviews with parents of ECC patients who would qualify for SDF treatment, roughly one third found the treatment unacceptable under any circumstances.

To offer a potential therapeutic solution, we investigated the potential affinity of AgBP on silver-stained dental tissues. Once we demonstrated successful binding to the SDF treated tissues, we designed a bifunctional peptide to target SDF-stained caries lesions and provide an interface to mediate mineralization. Building upon our prior art, we utilized an amelogenin derived peptide sequence, specifically, shADP5, conjugated to AgBP via a short linker sequence. Amelogenin is one of the major proteins in dental tissues and plays a key role in enamel formation and mineralization. The ADP5 sequence has been shown to mimic the ability of amelogenin to mediate fast mineralization. Our results demonstrated that our novel bifunctional peptide allowed for extensive remineralization by forming a peptide-enabled nanocomposite film on the SDF-treated carious dental tissues.

4.2 Peptide enabled nanocomposites offer biomimetic reconstruction of silver diamine fluoride treated dental tissues*

4.2.1 Abstract

Caries is the most ubiquitous infectious disease of mankind and early childhood caries (ECC) is the most prevalent chronic disease in children worldwide, with the resulting destruction of the teeth recognized as a global health crisis. The FDA has recently approved the off-label use of silver diamine fluoride (SDF) for arresting caries. SDF offers a safe, accessible, and inexpensive approach to arrest caries progression in children with ECC. However, treated lesions are stained black. The black staining associated with SDF treatment has limited the widespread adoption of this technique. The staining severely compromises aesthetics; parents/patients may find the black staining unacceptable. Targeting SDF silver-stained tooth surfaces, we developed a biohybrid calcium phosphate nanocomposite interface building upon the self-assembly of synthetic biomimetic peptides. Here, an engineered bifunctional peptide composed of a silver binding peptide (AgBP) that provides anchoring to the silver-stained tooth surface is covalently joined to an amelogenin derived peptide (ADP) to deliver the amelogenin protein functions to promote rapid formation of a calcium phosphate isomorph nanocomposite. Our results demonstrated that the bifunctional peptide was effective in remineralizing the biomineral destroyed by caries on slabs of SDF-stained tooth tissues. The proposed engineered peptide approach offers a biomimetic path for remineralization of the SDF-stained dental tissues producing a biomimetic calcium phosphate nanocomposite interface competent to be esthetically restored using commonly available adhesive dental composites, to restore mastication, improve health and reduce social stigma.

---

* SK Woolfolk¸ AK Cloyd, Q Ye, K Boone, P Spencer, ML Snead, C Tamerler, "Peptide Enabled Nanocomposites Offer Biomimetic Reconstruction of Silver Diamine Fluoride Treated Dental Tissues", *Submitted to Polymers, January 2022 (In Review)*

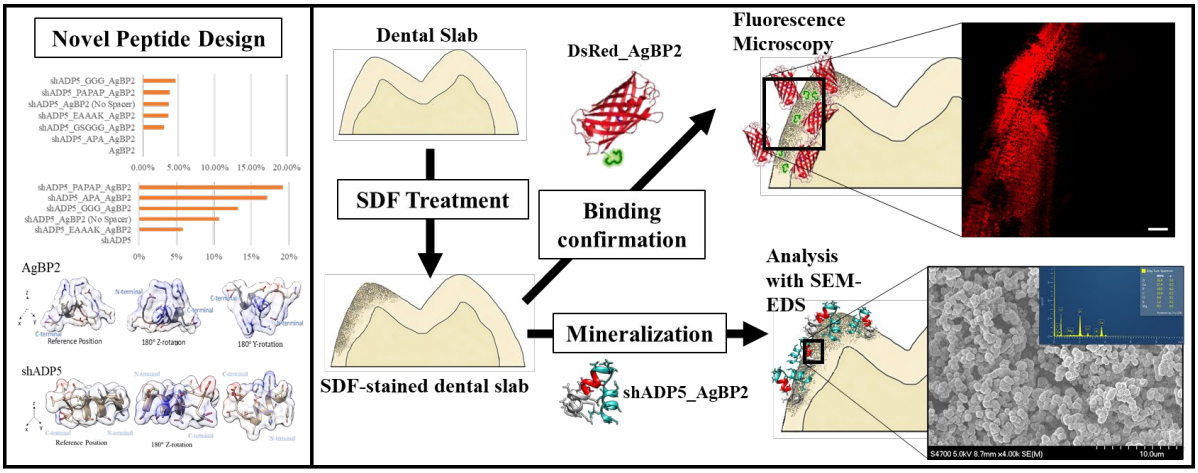

Figure 4-1: Table of contents figure depicting schematic overview of paper.

4.2.2 Introduction

Caries is the most prevalent infectious disease of mankind [1], with maternal transmission of cariogenic microbiota [1, 2]. Early childhood caries (ECC) is widely recognized as a global health crisis, with dental caries still the most prevalent chronic disease in children worldwide [3-12]. Impacting young children under age five, ECC is characterized by the presence of one or more caries lesions of the primary teeth. ECC has a higher prevalence in children of lower socioeconomic groups with limited access to dental care [9, 13-15]. In the United States, the prevalence of ECC is estimated to be between 3 and 6% of all pre-school aged children, a value which is consistent with literature reviews confirming rates from 1-12% in the most developed countries worldwide [9, 14, 16, 17]. However, the worse health outcomes are disproportionately skewed to certain populations as the risk of ECC in disadvantaged populations and less developed countries can be as high as 70% [9, 13, 14, 18]. Once a child develops caries lesions, treatment traditionally requires surgical intervention to remove diseased tooth structure followed by restoring the form and function of the tooth using various dental materials. As the ECC disease progresses, treatment options diminish and are often very costly. There can be several barriers to traditional restorative treatment including behavioral issues due to age and/or limited ability to cooperate,

access to care, and financial constraints. Children with severe early childhood caries must commonly be treated under general anesthesia [5, 18, 19]. Due to the high cost and potential comorbidities, general anesthesia may not be an option for all ECC patients. The treatment of advanced ECC cases may involve premature extraction of deciduous teeth. Early extraction of the primary teeth (aka deciduous teeth) can alter jaw growth, leading to the failure of the remaining teeth to function properly during mastication with consequential changes in micro- and macro-nutrition that adversely impact child health [18, 20]. Therefore, alternative treatment options that circumvent the cascade of failure described above have been the focus of attention in the dental public health community.

Fluorides have proven useful to slow the progression of dental caries by replacing the hydroxyl group with fluoride in the carbonated hydroxyapatite biomineral of the teeth, thereby inhibiting the caries-associated demineralization of teeth [3, 21-23]. Recently, the use of silver diamine fluoride (SDF) has received attention by offering a safe, accessible, and inexpensive approach to arrest caries progression in children with ECC [3, 4, 8, 24-26]. SDF has been used worldwide for decades but was approved for dental use by the FDA in 2014 [24, 27, 28]. Although the exact mechanism for the action of SDF has not been resolved, silver metal ions deposited on the dental tissues have notable antimicrobial properties and have been utilized in medicine and dentistry [29, 30]. More recently, silver microwires have been described in teeth after application of SDF, presumably replacing the defects that are the result of demineralization which is associated with the caries process [31].

Unlike surgical interventions which require skilled professionals, SDF treatments can be applied by a wider-range of health care providers [32] and focuses on limiting the disease progression by mitigating the bacteria known to cause dental caries and progression associated with ECC, as well

as protecting teeth from further degradation [3, 4, 21, 24, 26, 28, 33, 34]. Commonly available as a 38% solution, numerous case studies worldwide have shown the overwhelming benefit of single or bi-annual SDF treatments for caries arrest, with a focus for use of SDF in primary teeth of children affected by ECC [3, 8, 26, 28, 33, 35, 36]. SDF is inexpensive, application takes minutes, and it does not require significant patient cooperation. However, there remains major drawbacks to the wide-spread use of SDF for ECC and caries arrest. SDF treatments causes permanent, black staining of carious tissue. The loss of aesthetics was documented by a study by Crystal, *et. al.*, who interviewed parents of children who would qualify for SDF treatment and found that roughly one third of parents found the treatment unacceptable under any circumstances [37]. In addition to staining, parents must be advised that SDF must be reapplied for disease control. SDF treatment has been shown to reduce effective bonding of adhesive dental composite materials commonly used to mask the staining and restore the function of the carious teeth [38].

Recent advances in peptide design have resulted in predictable-, tunable-multifunctional peptides shown to self-assemble on complex surfaces, ranging from metal to minerals to produce an interface serving to modulate synthetic functions that favorably direct biomimetic synthesis [39-41]. Our group, and others, have identified peptides using combinatorial biology, such as phage display and bioinformatics, to specifically target solid materials including metals, metal oxide, minerals and polymers [40, 41]. We demonstrate that different peptides can be deployed to combat bacteria, direct remineralization of defective enamel and dentin, and as key bioactive components of novel dental biomaterials to facilitate tissue integration [42-50]. In particular, we previously identified a silver binding peptide (AgBP; EQLGVRKELRGV) and demonstrated its self-assembly properties on silver-nanoparticles and silver-surfaces when in the presence of an additional bioactive moiety. We demonstrated the use of this silver-binding peptide in bioimaging

and biosensing applications [46, 51, 52]. Using phage display, our group identified hydroxyapatite binding peptides (HABPs) and demonstrated their ability to control both the kinetics and crystallite morphology of calcium phosphate deposition [53]. Applying knowledge-based bioinformatic design, we created HABP scoring matrices and an algorithm to identify regions of similarity between natural proteins and combinatorically selected peptides [54]. The amino acid sequences of these combinatorically selected hydroxyapatite binding peptides (HABPs) were used in a knowledge-based approach to identify the functional domains in amelogenin for tissue repair and restoration [53]. During enamel formation, amelogenin is the most abundant enamel matrix protein and is recognized to exert a dominant role during enamel biomineralization [55-57]. A bioinformatics search identified several amelogenin domains within the full-length amelogenin protein predicted to participate in controlling biomineralization and these were referred to as amelogenin derived peptides (ADPs). ADP5 was demonstrated the capacity to modulate mineralization kinetics in a manner closely matching the function of the full length amelogenin protein [53].

Here, we explore an engineered peptide nanocomposite for biomimetic reconstruction of SDF treated tooth slabs in order to mitigate the negative side-effect, i.e., black staining associated with SDF treatment. Starting with a 22-amino acid long human amelogenin derived peptide hADP, it was engineered further to allow for improved water solubility, while still preserving the rapid and robust mineral forming properties [42, 58]. The resulting shorter sequence, denoted as shADP5 (SYEKSHSQAINTDRT), was selected for the current studies due to its increased solubility, greater ease of synthesis and reduced cost. By coupling shADP5 with AgBP during synthesis, we engineered a novel multifunctional peptide that binds to SDF-stained regions on dental tissue slabs and facilitates remineralization at the exposed dentin and enamel tissue surfaces. Our results

highlight one approach that bifunctional peptides can offer – the peptides can work synergistically with the silver deposits to help protect and rebuild damaged dental tissues while adding a new layer of calcium phosphate biomimetic mineral. Our peptide based biomimetic nanocomposite approach could synergize with the recent FDA approved use of silver diamine fluoride (SDF) treatment by mitigating its adverse effect, i.e., black staining of the treated caries lesion and offering a safe, accessible, easy to apply, and inexpensive approach to arrest caries progression in children with ECC.

4.2.3 Materials and Methods

4.2.3.1 Peptide design and synthesis

The initial selection of the silver binding peptide sequence using FliTrx (Invitrogen, MA, USA) bacterial surface display has been reported by our group [51, 52]. The strong-binding AgBP2 (EQLGVRKELRGV) 12 amino acid sequence was selected for these studies, as it has shown robust selectivity and binding capacity to silver surfaces in previous work [46, 51, 52].

Binding confirmation studies were completed using DsRed-AgBP2 to visualize binding to the SDF-stained tooth slab samples by the florescent reporter, DsRed. Production of DsRed-labeled solid binding peptides has been reported in previous publications [59, 60].

For the bioactive portion of this work for remineralization, we selected a peptide, shADP5 (SYEKSHSQAINTDRT) which has also been studied [42, 58]. The ADP5 amino acid sequence was identified by bacterial phage display and the amino acid sequence of strong hydroxyapatite-binding peptide candidates were compared by similarity to the sequence of the native amelogenin protein [42]. Mineralization kinetics and resulting crystallite morphology for selected hydroxyapatite-binding peptides were studied and the ADP peptide identified as optimal for

mimicking the kinetic and morphology for hydroxyapatite formation of the native amelogenin protein [42, 58].

The studies herein combine these two well-characterized peptides to create a bifunctional peptide, shADP5-AgBP2. The two peptide sequences were joined by a short, flexible spacer (EAAAK) designed using biocomputational modeling and confirmation studies to ensure individual activities were maintained in the bi-functional peptide. shADP5-AgBP was synthesized using standard Fmoc solid-phase peptide synthesis by the AAPPTec Focus XC (AAPPTec, KY, USA) automated peptide synthesizer, following previous published protocols [48, 49, 61]. Following synthesis, the peptide was cleaved from the resin and side-chain-deprotected using a cleavage cocktail (trifluoroacetic acid/phenol/ethanedithiol/triisopropylsilane/water (87.5 : 5 : 2.5 : 2.5 : 2.5)) for 2 hours and precipitated in cold ether. Crude peptides were purified using reverse-phase HPLC (Waters, MA, USA) equipped with a 10μm C18 silica Luna column (250×10mm, Phenomenex Inc., CA, USA). The pure, bifunctional shADP5-AgBP2 peptide was lyophilized and stored at −20°C.

4.2.3.2 Peptide functionalization

Lyophilized peptide stocks were selected and reconstituted in milli-Q water immediately prior to experiments with both silver-coated silica substrates and dental slabs. Stock solutions were prepared to ensure a final maximum concentration of 100uM could be achieved. Substrates or slabs were submerged into a solution containing 50uM peptide and allowed 2-4 hours gently shaking at room temperature to ensure the binding of AgBP. This excess concentration was used to ensure ample peptide was available for binding to the Ag-coated surfaces and the silver-stained dental slabs.

4.2.3.3 Silver-coated silica substrates

To confirm the selectivity and specificity for silver-binding of bifunctional peptides, preliminary studies were conducted on silver-coated silica substrates. Silica wafers were cut into 1cm square pieces using a diamond scribe and a published protocol for electroless deposition of silver onto silica was followed [62, 63]. Briefly, the Si(111) wafers were cleaned in a hydrogen peroxide and sulfuric acid solution (3:7) for 20 minutes, rinsed thoroughly with milli-Q water, and dried with N_2 gas prior to use. A pre-etching step was employed prior to Ag deposition, where a large drop of 5% NH_4F solution was placed on the surface of the cleaned silica substrate for 30s and removed carefully with N_2 gas. Then a plating solution was prepared with 0.020M NH_4F and 0.010M $AgNO_3$, this was also placed onto the pre-etched silica substrates for about 60s to allow for silver deposition. After the reaction occurred, the substrates were washed with milli-Q water.

4.2.3.4 Dental slab preparation

Dental slab specimens were prepared following a detailed protocol in previous publications [43, 64, 65]. The specimens consisted of extracted human molars. These teeth would otherwise be discarded, no patient identifiers are associated with the teeth and thus, this is not considered human subjects research. The extracted teeth were stored at 4°C in 0.9% wt/vol NaCl containing 0.002% sodium azide. Teeth exhibiting carious lesions were selected and slabs of the dental bioceramic composite tissues, enamel and dentine, were prepared via sectioning using a water-cooled low-speed diamond-blade saw (Buehler, Lake Bluff, IL). The sectioning process was as follows: the root structure was removed by sectioning gingival to the cemento-enamel junction and perpendicular to the long axis of the tooth; slabs of 1.4mm thickness were prepared by sectioning parallel to the long axis of the tooth. The slabs were stored in a modified PBS buffer (20mM

Na_2HPO_4, 137mM NaCl, 2.7mM KCl, and 1.8mM KH_2PO_4; pH 7.4) at 4°C until experimental use.

4.2.3.5 SDF treatment protocol

SDF was applied to dental slabs following the detailed guidelines published by the UCSF Caries Arrest Committee [25, 34]. Briefly, the prepared dental slabs were removed from the modified PBS buffer, rinsed with milli-Q purified water and gently dried with compressed air to reveal suitable carious regions of the dental slab. A single drop of commercially available 38% SDF solution (Dengen Caries Arrest; Dengen Dental, Bahadurgarh, Haryana, India) was placed into a fresh plastic dish. A microbrush applicator head was dipped into the solution and touched to the side of the dish to remove excess fluid by surface tension. The SDF was applied to the dental slab, allowed to absorb for 1 minute and the treated slab was gently rinsed with milli-Q purified water. The slab was placed back into modified PBS buffer and incubated at 37C for 6 hours to mimic the oral environment, to allow for SDF penetration into the slab. The progressive darkening of the treated regions due to precipitation of silver and fluoride from the SDF was noted.

4.2.3.6 Enzyme-mediated biomineralization

To investigate the calcium phosphate nucleation facilitated by the shADP5 peptide, an alkaline phosphatase (AP) mineralization model was followed [42]. This model mimics the biological process, wherein inorganic phosphate is cleaved from organic phosphate by naturally occurring AP and subsequently reacts to free calcium. Briefly, samples functionalized with shADP5 or control samples without peptide were submerged in a biomineralization buffer containing 14.4mM β-glycerophosphate (β-GP) and 24mM Ca^{2+} in 25mM Tris-HCl at pH 7.4. Mineralization reactions were initiated by adding bacterial alkaline phosphatase (fastAP; ThermoFisher, USA) to the solutions to achieve a final concentration of $1.4x10^{-6}$ g/mL and allowed to react at 37°C for 2 hours

to form a calcium phosphate mineral layer on the sample surface. Samples were removed from the solution and allowed to air dry prior to microscopic and spectroscopic analyses.

4.2.3.7 Fluorescence and optical microscopy

Optical microscopic images of dental slabs and Ag-coated silica substrates were taken at 10X magnification on a Nikon SMZ800 StereoMicroscope (Nikon Instruments Inc., NY, USA) system equipped with a Q-Imaging MicroPublisher 5.0 RTV camera (Teledyne QImaging, Teledyne Photometrics, AZ, USA). Images were processed with the Q-Capture software (Teledyne Photometrics, AZ, USA).

Fluorescence images were acquired using a Leica TCS SPE Laser Scanning Confocal DM6-Q upright microscope (Leica Microsystems, NC, USA) using a 10X Leica Infinity corrected objective. DsRed fluorescence was captured using a laser excitation of 561nm. Images were processed using the Leica LAS-X imaging software.

4.2.3.8 Scanning electron microscopy (SEM) with energy dispersive X-ray spectroscopy (EDS)

To image the mineral morphology, surface coverage, and to determine the Ca/P ratios of the precipitated material, a Hitachi SU8230 Field Emission Scanning Electron Microscope (Hitachi High-Tech America, IL, USA) equipped with a silicon drift EDS detector (X-Max, Oxford Instruments, MA, USA) was used. SEM imaging was completed at 5kV and EDS measurements made with an acceleration voltage of 10kV, to improve signal. Prior to SEM/EDS analysis, samples were sputter-coated with 5nm iridium using a Quorum sputter coating system (Q150, Quorum, UK). EDS analysis was performed using AZtec software (Oxford Instruments, MA, USA) and values averaged across a minimum of three regions for each sample.

4.2.4 Results

4.2.4.1 Silver binding peptide assembles onto SDF-treated slabs of dental tissues

Restoring dental tissue requires addressing multiple challenges simultaneously. We have previously shown the specific and selective binding attributes of a silver binding peptide (AgBP; EQLGVRKELRGV) to anchor to silver nanoparticles and surfaces [46, 51, 52]. However, these surfaces are very different with respect to composition and surface features as compared to the silver diamine treated dental tissues. The silver binding peptide was investigated for its specific targeting and binding properties onto the SDF treated slabs of carious dental tissues.

In our prior art, we developed genetically engineered fluorescence fusion proteins that self-assemble on metallic nanomaterials as bimodal imaging nanoprobes [52, 60, 66, 67]. Engineered fusion green and red fluorescent proteins (GFP and DsRed, respectively) were developed by genetically incorporating silver binding (AgBP) and gold binding peptides (AuBP). Fluorescent labelling commonly requires additional labeling steps, whereas the genetic fusion of metal binding peptide tags in the red and green fluorescence proteins as a fusion partner offered to spot the location of the peptides in a single step to confirm the protein assembly process. Compared to control experiments (GFP and DsRed), metal binding peptide tagged, i.e. GFP-AgBP and DsRed-AgBP and DsRed-AuBP fusion proteins resulted in a strong fluorescent intensity on the surfaces confirming metal binding peptides as essential component for the assembly process. Here, we employed DsRed-AgBP fusion protein for direct visualization of silver binding ability of AgBP via the DsRed fluorescence reporter protein onto the SDF treated slabs of dental tissue. The DsRed protein without a AgBP tag was used as the control (Figure 4-2). Control sample that included DsRed protein alone on the SDF treated tooth slabs resulted in minor fluorescent, whereas a significant red fluorescent signal observed on the SDF treated tooth slabs assembled by DsRed-

AgBP. The results confirmed that the silver binding property of the AgBP was preserved for silver stained areas following the silver diamine treatment of dental tissues.

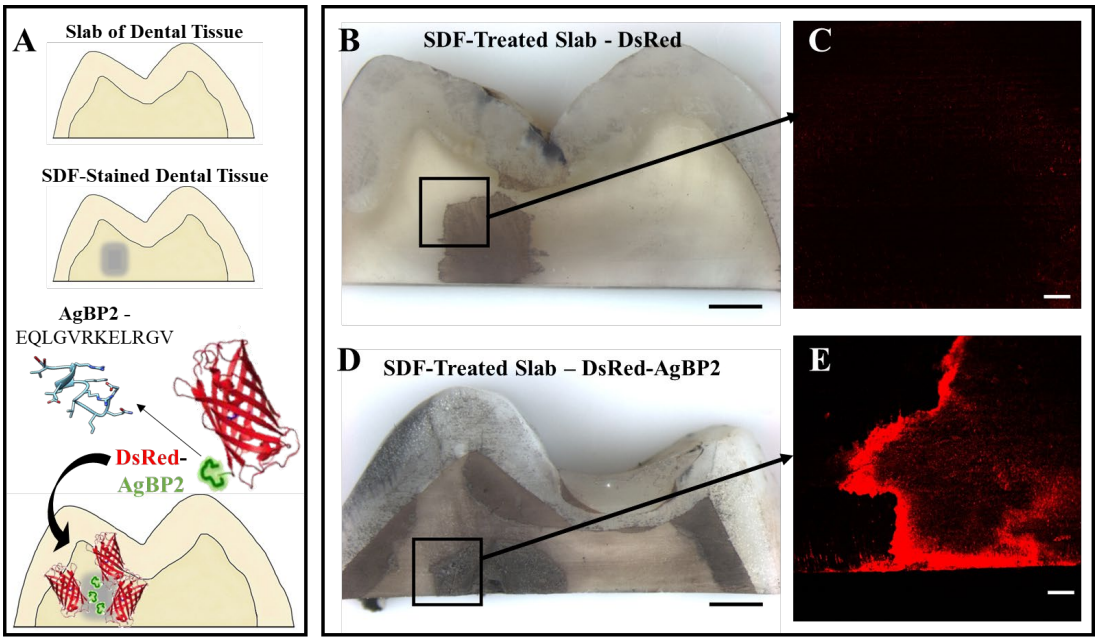

Figure 4-2: Slab of dental tissues treated with SDF, AgBP assembled on silver stains visualized by fluorescence intensity (a); SDF-treated slabs monitored by fluorescence microscopy (Control; (b) & (c)) and DsRed-AgBP2 (d) & (e)) following gentle wash step. Scale bars are 1000mm for optical images and 100µm for fluorescence images.

4.2.4.2. Bifunctional peptide design targeting SDF treated dental tissues

Building upon the AgBP binding on silver stained dental tissue, we selected the next functional peptide domain as an amelogenin derived peptide, shADP5 (SYEKSHSQAINTDRT), which has been previously to have a fast remineralization kinetics similar to amelogenin protein.[42, 58] The ADP5 peptide was resulted in cell-free formation of a robust hydroxyapatite mineral layer on demineralized, human dentin root surfaces [42]. The 22-amino acid long ADP5 sequence was then further engineered to allow for greater water solubility while still preserving the rapid and robust mineral forming properties [42, 58]. When combining different peptide functionality, i.e., mineralization and metal binding, the challenge to address is to design a spacer, which minimizes

the interference between the domains. Therefore, we next investigated spacer sequence as the linking sequence between the domains to combine shADP5 with AgBP. Spacers are known to influence domain activity through length and flexibility.[68] In our previous studies, candidate flexible spacers in peptide design resulted in successful multifunctional peptide functionality (GGG, GSGGG) [69, 70]. Further candidate spacers that provide rigid short linkages also resulted in effective peptide functionality, i.e. PAPAP, EAAAK and APA.

We use in-solution structure prediction [71] to estimate the changed folding dynamics of the bifunctional peptide context compared to the single domain context.[72] The structural variations include hydrodynamic size changes between contexts and the changed backbone conformation for each context. Since the hydrodynamic size almost always must increase for multifunctional peptides, their diffusion will be slower compared to single domain counterparts. This limitation can be overcome for systems in which the material surface-peptide interaction offer competitive advantage for surface assembly. Also, the change in the backbone context may influence the free energy of adsorption as well as desorption. We searched for spacers that induce the minimal change in the folding dynamics for each of the domains [73-75]. The distances between the single domain (2 clustered representatives for AgBP2 and 5 cluster representatives for shADP5) compared to the bifunctional peptides (5 cluster representatives for each sequence) is characterized by the mean sum of squares across the single domain residues (Figure 4-3). These mean sums of squares were scaled by the minimum value. When these percentages were sum, spacer EAAAK results in the smallest predicted backbone change (9.4%) followed by APA (17%) and the GGG spacer (18%). No spacer resulted in a summed percentage of 14%. The alpha-helical spacer of EAAAK results in the minimal predicted change in backbone conformation among spacers evaluated.

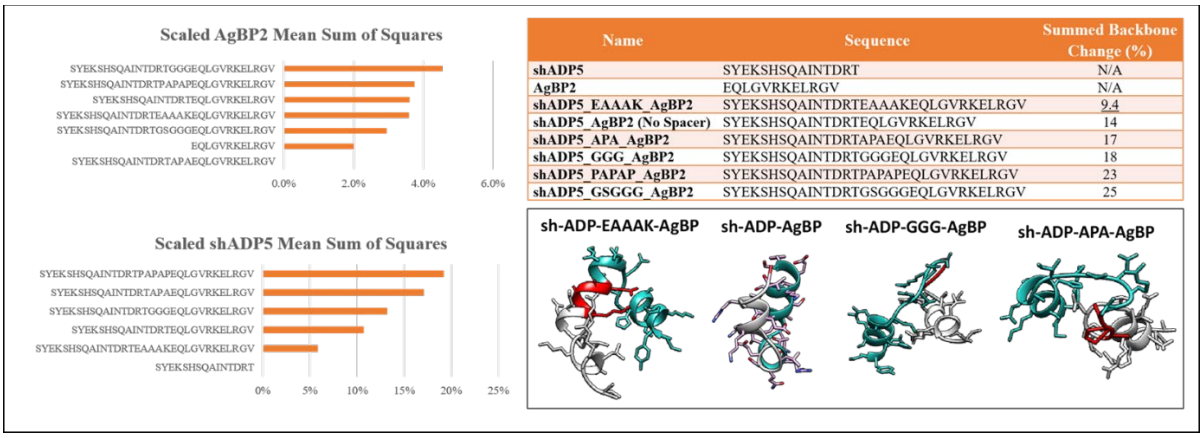

Name	Sequence	Summed Backbone Change (%)
shADP5	SYEKSHSQAINTDRT	N/A
AgBP2	EQLGVRKELRGV	N/A
shADP5_EAAAK_AgBP2	SYEKSHSQAINTDRTEAAAKEQLGVRKELRGV	9.4
shADP5_AgBP2 (No Spacer)	SYEKSHSQAINTDRTEQLGVRKELRGV	14
shADP5_APA_AgBP2	SYEKSHSQAINTDRTAPAEQLGVRKELRGV	17
shADP5_GGG_AgBP2	SYEKSHSQAINTDRTGGGEQLGVRKELRGV	18
shADP5_PAPAP_AgBP2	SYEKSHSQAINTDRTPAPAPEQLGVRKELRGV	23
shADP5_GSGGG_AgBP2	SYEKSHSQAINTDRTGSGGGEQLGVRKELRGV	25

Figure 4-3: Distances between AgBP2 and shADP5 compared to the bifunctional peptides by the mean sum of squares across the single domain residues. Summed backboned change (%) with the representative bifunctional peptide structures are given.

4.2.4.3 Functional activity of shADP5-AgBP2 on Ag-coated silica surfaces

Derived from the amelogenin protein, the most abundant protein associated with enamel formation in mammalian teeth, the shADP5 peptide was selected for use in these studies based on the observed rapid kinetic of calcium phosphate precipitation and favorable mineral crystallite morphology reported in previous studies [53, 76]. Since the bifunctional peptide, shADP5-AgBP2, is a novel peptide, the preservation of activity contributed from both domains was investigated on Ag-coated silica to prevent potential variability among dental tissue.

Figure 4-4 (a) shows representative optical images of the Ag-coated substrates with 50uM shADP5-AgBP or without a peptide (control). The samples were subjected to an enzyme-mediated mineralization protocol, mimicking nature. Alkaline phosphatase enzyme controls the kinetics of the mineralization by cleaving phosphate from an organic phosphate source. The samples were gently washed by water and the formed mineral layer was dried overnight prior to SEM/EDS analysis. Alkaline phosphatase-based mineralization resulted significantly higher mineral coverage in the presence of bifunctional peptide compared to control samples (Figure 4-4 (b) and

(d)). EDS results confirmed the calcium phosphate mineralization, and we calculated the calcium/phosphate ratios to compare potential mineral compositional changes. The mineral layer formed in the presence of bifunctional peptide had an average Ca/P ratio of about 1.40 (Figure 4-4 (f)) as compared to 1.23 control samples (Figure 4-4 (e)). A wide range of distinct calcium phosphate phases exist in mineralized tissues and these phases are commonly classified by the Ca/P molar ratio [77-80]. The molar ratio of 1.40 falls between that of octacalcium phosphate and amorphous calcium phosphate with Ca/P ratios of 1.33 and 1.50, respectively. The results confirmed the bifunctional shADP5-AgBP preserved its mineralization activity. Peptide function is highly dependent upon structure and conformation, with the spacer sequence between the two active domains playing a critical role in allowing each peptide to function to its fullest [81]. Changes to the spacer sequence may allow further optimization of the function of the shADP5 peptide or another mineral-mediating peptide to achieve a specific CaP mineral composition and morphology.

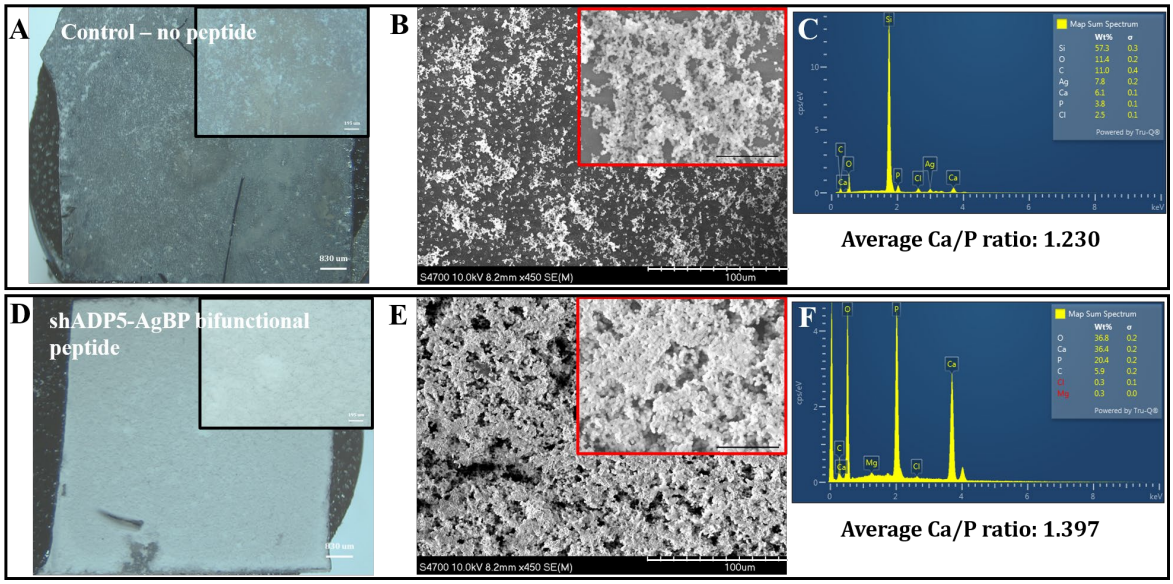

Figure 4-4: Mineralization on silver-coated surfaces. Ag-coated surfaces with no peptide (Control: a-c): Optical microscope images (a), SEM images after 2h AP induced mineralization (b), EDS spectra and average Ca/P ratios for mineralized regions on Control (c); 50µM shADP5-AgBP

treated Ag-coated surface (d), SEM images after 2h AP induced mineralization in the presence of shADP5-AgBP (e), Representative EDS spectra and average Ca/P ratios in the presence of peptide (f). Scale bars are 830µm and 195µm for insets in (a) & (d), and scale bars 100µm and 25µm for insets in (b) & (e).

4.2.4.4 Bifunctional peptide enabled mineralization on SDF-treated dental tissues

Building upon the success of the bifunctional peptide mineralization on Ag coated surfaces, we prepared four SDF treated slabs of carious dental tissue (M&M). The utility of shADP-AgBP peptide on directing the mineralization onto the SDF treated dental tissues was investigated for potential mineral coverage onto the silver-stained areas. The bifunctional peptide solution was applied onto SDF treat surfaces and then placed into mineralization buffer containing fast AP to initiate the biomineralization. Figure 4-5 provides the optical microscope images taken at each experimental stage including untreated, SDF treated and bifunctional peptide applied tooth samples.

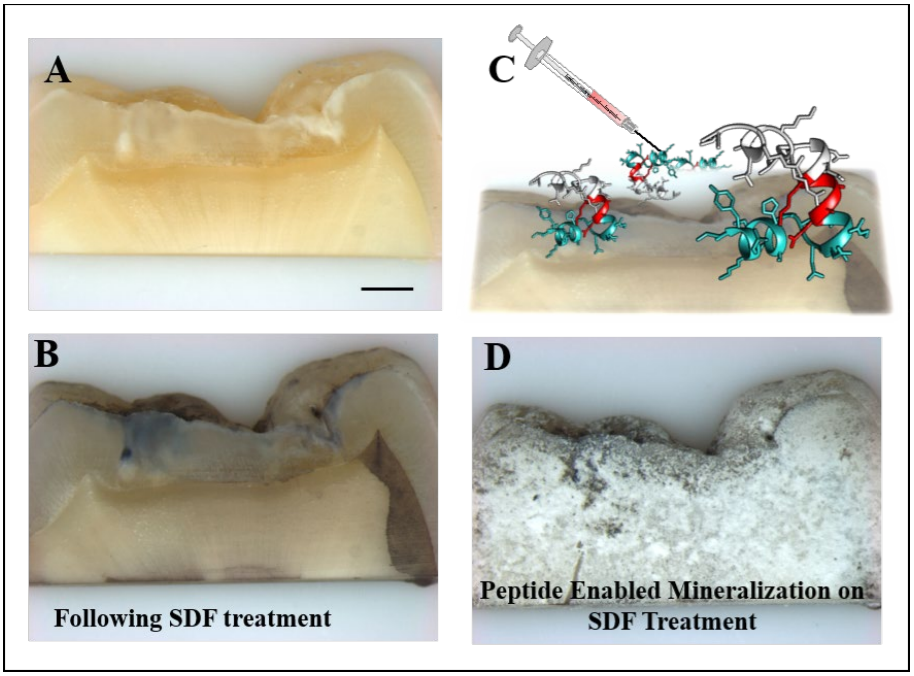

Figure 4-5: The mineralization by the shADP5-AgBP functionalized SDF-treated dental tissue. Optical microscopy images of untreated dental tissue (a), SDF-treated dental tissue (b); Schematics

of bifunctional peptide application on SDF treated dental tissue (c), Peptide enabled mineralization of SDF treated dental tissue. Scalebar is 1000µm.

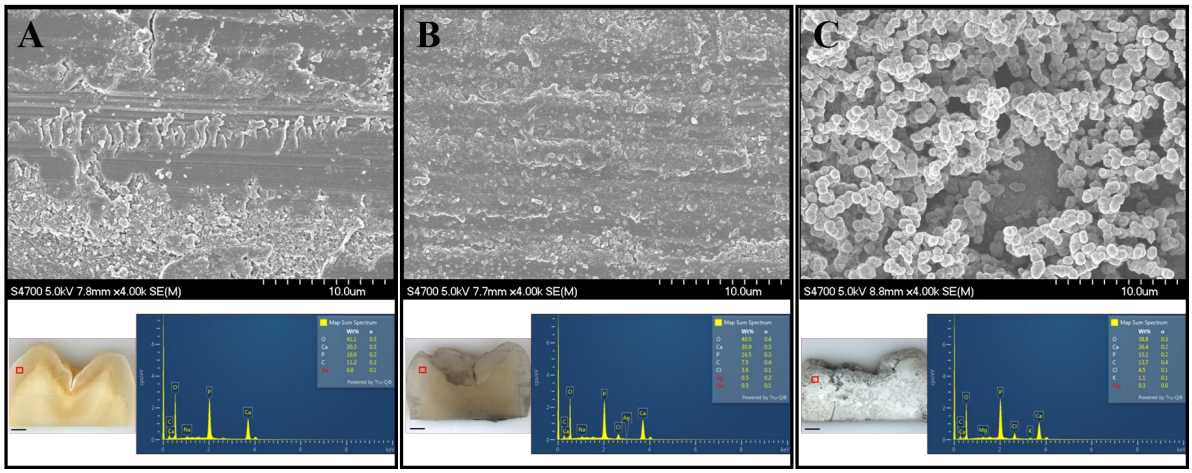

Figure 4-6: SEM images and corresponding EDS spectra on enamel regions on the dental slabs provided with the optical microscopy images. Representative images are shown for samples: untreated sample (a); SDF-treated slab (b); shADP5-AgBP peptide applied SDF-treated slab (c). Scale bar for 10X survey images of dental slabs is 1000µm. Representative EDS spectra to determine Ca/P averages calculated across a minimum of three unique areas for each region studied.

Treated dental slabs were analyzed using SEM/EDS for imaging and compositional analysis. Average Ca/P molar ratios were calculated for each slab in both stained and unstained regions of enamel and dentin to assess mineral formation and compositional changes on the tooth samples in the presence and absence of the shADP5-AgBP2 bifunctional peptide. SEM images with EDS spectra from representative regions of each treated dental slab are shown in Figure 4-6. Differences noted in the mineral morphology on the peptide mediated mineralized sample on Figure 4-6 (c) were attributed to the presence of the mineral-mediating peptide shADP5. Average Ca/P ratios across all dental slab treatment groups in both stained and unstained enamel and dentin regions are reported in Table 4-1.

Table 4-1: Averaged calculated Ca/P ratios of dental tissues in unstained and SDF-stained regions in dentin and enamel across.

			Mineralized Samples (mineral layer formed on surface)	
	Untreated Control	**SDF-treated Control**	**SDF-treated**	**SDF-treated Peptide-functionalized**
Enamel	1.375	1.447	1.092	1.338
Dentin	1.405	1.419	1.066	1.291
SDF-stained enamel	n/a	1.540	1.100	1.257
SDF-stained dentin	n/a	1.546	1.137	1.238

The average Ca/P ratios presented in Table 4-1 allow for direct comparisons between two sets of sample pairs, 1) Untreated control and SDF-treated Control, and 2) Mineralized slabs with and without shADP5-AgBP2 peptide. The formed mineral layer on dental tissue slabs leads to differences in the CaP composition across the two groups, as the first group of data is directly on the dental tissue instead of a new layer of formed mineral. Thus, it is noted that the SDF treatment resulted in slightly higher Ca/P ratios in unstained regions of the tooth compared to its untreated counterpart, with a more notable increase in the enamel region. However, in the stained regions of the SDF-treated control dental slab, a significantly higher Ca/P ratio was demonstrated in both stained enamel and dentin regions as compared to unstained regions of the same slab and the untreated control samples. A 2021 study investigated the effects of SDF on carious primary teeth regions and found SDF treatment promoted pathologic biomineralization by altering physiochemical properties of the tooth structures.[82] Their detailed results included structural and elemental analysis of SDF stained teeth. Our results are consistent with the reported EDS results.[82] The increased Ca/P ratio in the SDF-stained control slab indicates that in these carious

lesions of the tooth, the SDF treatment creates a more stable CaP material, i.e., the Ca/P ratio is closer to a calcium-deficient apatite.[53, 58, 76, 83]

For the enzyme-mediated remineralization group, SDF-treated dental slabs were functionalized with either 0uM or 50uM shADP5-AgBP2 prior to the mineralization protocol. Similar to what was observed with the Ag-coated samples (Figure 4-4), a significant increase in Ca/P ratio was observed in the sample functionalized with the peptide. On average, the Ca/P ratios on the mineralized layer observed in both the peptide-and SDF treated slab as well as the SDF-only treated slabs were about 0.1-0.15 less than what was obtained for the untreated and peptide-functionalized Ag-coated silica slabs. The natural presence of calcium phosphate rich minerals in the dental slabs may alter the availability of free calcium and phosphate in the enzyme-mediated mineralization reaction. However, the same trend was noted, where, in the presence of our shADP5 peptide, the Ca/P ratio was significantly greater than samples not functionalized with peptide, again confirming activity. The differences in the mineralization may be attributed to the anchoring effect of the AgBP2 peptide bound to the stained regions of the dental slab.

4.2.5 Discussion

With recent advances in peptide engineering and tunable design to adapt functions, peptides offer a promising approach to favorably modulate even the most complex surfaces and interfaces. By combining shADP5 with AgBP, we engineered a novel bi-functional peptide that binds to SDF-stained regions on dental slabs and facilitates remineralization at the exposed dentin and enamel surfaces. Our preliminary results highlight just one approach our bifunctional peptides can offer – working synergistically with the SDF to help protect and rebuild damaged dental materials while adding a new layer.

Previously, our group has demonstrated multifunctional capabilities of our solid binding peptides in the oral cavity acting to combat oral bacteria, direct remineralization of dentin and enamel, and as bioactive components of engineered dental biomaterials to improve binding and native tissue integration [42-50]. Limited studies have been published to date focused on masking or reducing the staining of SDF on carious dentin and enamel and have used potassium iodide, composites, or glass ionomer cement [84-86]. Hamdy, *et. al.*, used a calibrated spectrophotometer to monitor changes in tooth color following SDF treatment and found a composite coating was the most successful masking agent at baseline and after an aging protocol of the three treatments [84]. However, the composite treatment that immediately followed SDF application required an etching step and multiple coats of dental composite on the affected surface and the effectiveness of the initial SDF treatment after the composite coverage was not reported. Further, it is known that composite restorations in the oral cavity have a high rate of failure due to cracks and gaps creating spaces for bacterial infiltration causing further decay [87-90]. With the selective and targeted anchoring peptide, AgBP2, one potential improvement to previous studies would be to include our peptide within the composite and/or adhesive to help reinforce interfacial binding between the SDF-treated dental surface and a composite restoration. Our group has recently explored the vast potential of bioactive peptides to improve interfacial integrity and binding of polymeric composites to dental surfaces, but we believe the targeted approach using AgBP2 may be possible for SDF-stained regions on dental tissues [45, 48-50, 91].

Another approach to mask or reduce the staining caused by SDF has focused on remineralization of the affected dentin and enamel. Acid is released by caries-provoking bacteria demineralized the tooth. The fluoride component of SDF treatment promotes natural remineralization of a treated tooth [25, 82, 92]. We, and colleagues, have previously established multiple peptides capable of

directing remineralization of calcium phosphate materials and thus wanted to explore a synergistic approach using bifunctional peptides to anchor to the SDF-treated regions and direct new mineral growth [53, 58, 80, 93-95].

The iterative spacer design process of novel, bifunctional peptides featuring AgBP2 anchoring peptide for targeted binding to SDF is also being studied to ensure optimal and tunable activity of both active domains.

4.2.6 Conclusion

Herein, we report the binding of a silver binding peptide to silver diamine fluoride (SDF) treated human dental tissues. Fluorides have proven useful to slow the progression of dental caries by inhibiting the demineralization of teeth. Recently, the use of silver diamine fluoride (SDF) has received attention as a non-invasive, inexpensive, and easy to use approach for managing cavitated lesions of primary teeth. Early childhood caries is the most prevalent chronic disease in children worldwide. SDF has been used worldwide for decades but was approved for dental use by the FDA in the US in 2014. Widespread adoption of SDF has been slow because SDF stains treated lesions black. Building upon the success of silver binding peptide anchoring onto silver stain on SDF treated dental tissues, we engineered a bifunctional peptide that is composed of silver binding and amelogenin derived peptide domain. Amelogenin protein is recognized with its major role in enamel formation and mineralization. We tested different spacers that will lead to successful domain combination to represent both peptide functionality. The use of affinity-binding peptides to bind to SDF-treated surfaces has not previously been reported to our knowledge and offers a platform approach to target the black staining associated with SDF treated lesions. The novel shADP5-AgBP2 was designed for the first time as the novel, bifunctional peptide and demonstrated the ability to bind and guide formation of calcium phosphate nanocomposite

materials on the dental tissue interface. Future studies must be conducted to tune the peptide sequence to achieve desired mineral composition and morphology to work synergistically with SDF to remineralize affected dentin and enamel. Additional work is focused on employing novel dental adhesives with active AgBP2 binding domains as an alternative approach to mask SDF staining. This work demonstrates the immense potential of bifunctional peptides with their binding selectivity and specificity to mediate surface characteristics of SDF-stained teeth. Overall, this approach demonstrates a novel modular and easily deployable approach toward positive aesthetic outcomes for patients requiring SDF treatment to arrest caries progression.

4.3 References

[1] Caufield PW, Li Y, Dasanayake A. Dental caries: an infectious and transmissible disease. Compend Contin Educ Dent 2005;26:10-6.

[2] Balakrishnan M, Simmonds RS, Tagg JR. Dental caries is a preventable infectious disease. Aust Dent J 2000;45:235-45.

[3] Chu C, Lo E. Promoting caries arrest in children with silver diamine fluoride: a review. Oral health & preventive dentistry 2008;6.

[4] Yee R, Holmgren C, Mulder J, Lama D, Walker D, van Palenstein Helderman W. Efficacy of silver diamine fluoride for arresting caries treatment. Journal of dental research 2009;88:644-7.

[5] Çolak H, Dülgergil ÇT, Dalli M, Hamidi MM. Early childhood caries update: A review of causes, diagnoses, and treatments. Journal of natural science, biology, and medicine 2013;4:29.

[6] Dye BA, Hsu K-LC, Afful J. Prevalence and measurement of dental caries in young children. Pediatric dentistry 2015;37:200-16.

[7] Kassebaum NJ, Bernabe E, Dahiya M, Bhandari B, Murray CJ, Marcenes W. Global burden of untreated caries: a systematic review and metaregression. J Dent Res 2015;94:650-8.

[8] Gao SS, Zhao IS, Hiraishi N, Duangthip D, Mei M, Lo E, Chu C. Clinical trials of silver diamine fluoride in arresting caries among children: a systematic review. JDR Clinical & Translational Research 2016;1:201-10.

[9] Anil S, Anand PS. Early Childhood Caries: Prevalence, Risk Factors, and Prevention. Front Pediatr 2017;5:157-.

[10] Institute of Medicine (U.S.). Committee on an Oral Health Initiative. Advancing oral health in America. Washington, D.C.: National Academies Press; 2011.

[11] Albino JaD, B.A. Oral Health In America: Advances and Challenges. 2021.

[12] Dye BA, Albino J, D'Souza RN. Oral health problems are global and need to be addressed in the USA. Lancet 2022;399:127-8.

[13] Shiboski CH, Gansky SA, Ramos-Gomez F, Ngo L, Isman R, Pollick HF. The association of early childhood caries and race/ethnicity among California preschool children. Journal of public health dentistry 2003;63:38-46.

[14] Ramos-Gomez FJ, Crystal YO, Ng MW, Crall JJ, Featherstone JDB. Pediatric dental care: prevention and management protocols based on caries risk assessment. J Calif Dent Assoc 2010;38:746-61.

[15] Jain M, Namdev R, Bodh M, Dutta S, Singhal P, Kumar A. Social and behavioral determinants for early childhood caries among preschool children in India. Journal of dental research, dental clinics, dental prospects 2015;9:115.

[16] Horowitz HS. Research issues in early childhood caries. Community dentistry and oral epidemiology 1998;26:67-81.

[17] Congiu G, Campus G, Lugliè PF. Early childhood caries (ECC) prevalence and background factors: a review. Oral Health Prev Dent 2014;12:71-6.

[18] Berkowitz RJ. Causes, treatment and prevention of early childhood caries: a microbiologic perspective. Journal-Canadian Dental Association 2003;69:304-7.

[19] Holve S, Braun P, Irvine JD, Nadeau K, Schroth RJ, Bell SL, Calac DJ, Empey A, Nadeau KJ, Oski JA. Early childhood caries in indigenous communities. Pediatrics 2021;147.

[20] Casamassimo PS, Thikkurissy S, Edelstein BL, Maiorini E. Beyond the dmft: the human and economic cost of early childhood caries. The Journal of the American Dental Association 2009;140:650-7.

[21] Chu C, Lo E, Lin H. Effectiveness of silver diamine fluoride and sodium fluoride varnish in arresting dentin caries in Chinese pre-school children. Journal of dental research 2002;81:767-70.

[22] Marinho V. Cochrane reviews of randomized trials of fluoride therapies for preventing dental caries. European Archives of Paediatric Dentistry 2009;10:183-91.

[23] Hiiri A, Ahovuo-Saloranta A, Nordblad A, Mäkelä M. Pit and fissure sealants versus fluoride varnishes for preventing dental decay in children and adolescents. Cochrane Db Syst Rev 2010.

[24] Rosenblatt A, Stamford T, Niederman R. Silver diamine fluoride: a caries “silver-fluoride bullet”. Journal of dental research 2009;88:116-25.

[25] Horst JA, Ellenikiotis H, Milgrom PL. UCSF Protocol for Caries Arrest Using Silver Diamine Fluoride: Rationale, Indications and Consent. J Calif Dent Assoc 2016;44:16-28.

[26] Zhao IS, Gao SS, Hiraishi N, Burrow MF, Duangthip D, Mei ML, Lo EC-M, Chu C-H. Mechanisms of silver diamine fluoride on arresting caries: a literature review. International dental journal 2018;68:67-76.

[27] Crystal YO, Niederman R. Silver diamine fluoride treatment considerations in children's caries management. Pediatric dentistry 2016;38:466-71.

[28] Contreras V, Toro MJ, Elías-Boneta AR, Encarnación-Burgos MA. Effectiveness of silver diamine fluoride in caries prevention and arrest: a systematic literature review. General dentistry 2017;65:22.

[29] Cannon AB. Value of Silver Arsphenamie in the Treatment of Early Syphilis: Conclusions based on a Study of 104 Cases. Journal of the American Medical Association 1934;102:268-73.

[30] Nizami MZI, Xu VW, Yin IX, Yu OY, Chu CH. Metal and Metal Oxide Nanoparticles in Caries Prevention: A Review. Nanomaterials (Basel) 2021;11.

[31] Seto J, Horst JA, Parkinson DY, Frachella JC, DeRisi JL. Enhanced Tooth Structure Via Silver Microwires Following Treatment with 38 Percent Silver Diamine Fluoride. Pediatr Dent 2020;42:226-31.

[32] Milgrom P, Horst JA, Ludwig S, Rothen M, Chaffee BW, Lyalina S, Pollard KS, DeRisi JL, Mancl L. Topical silver diamine fluoride for dental caries arrest in preschool children: A randomized controlled trial and microbiological analysis of caries associated microbes and resistance gene expression. J Dent 2018;68:72-8.

[33] Fung H, Wong MC, Lo EC, Chu C. Arresting early childhood caries with silver diamine fluoride-a literature review. Journal of Oral Hygiene and Health 2013.

[34] Horst J. Silver fluoride as a treatment for dental caries. Advances in Dental Research 2018;29:135-40.

[35] Peng J-Y, Botelho M, Matinlinna J. Silver compounds used in dentistry for caries management: a review. Journal of dentistry 2012;40:531-41.

[36] Duangthip D, Jiang M, Chu CH, Lo EC. Non-surgical treatment of dentin caries in preschool children–systematic review. BMC oral health 2015;15:1-10.

[37] Crystal YO, Janal MN, Hamilton DS, Niederman R. Parental perceptions and acceptance of silver diamine fluoride staining. The Journal of the American Dental Association 2017;148:510-8. e4.

[38] Ko AK, Matsui N, Nakamoto A, Ikeda M, Nikaido T, Burrow MF, Tagami J. Effect of silver diammine fluoride application on dentin bonding performance. Dent Mater J 2020;39:407-14.

[39] Tamerler C, Sarikaya M. Genetically designed Peptide-based molecular materials. ACS Nano 2009;3:1606-15.

[40] Hnilova M, So CR, Oren EE, Wilson BR, Kacar T, Tamerler C, Sarikaya M. Peptide-directed co-assembly of nanoprobes on multimaterial patterned solid surfaces. Soft Matter 2012;8:4327-34.

[41] Hnilova M, Karaca BT, Park J, Jia C, Wilson BR, Sarikaya M, Tamerler C. Fabrication of hierarchical hybrid structures using bio-enabled layer-by-layer self-assembly. Biotechnology and bioengineering 2012;109:1120-30.

[42] Gungormus M, Oren EE, Horst JA, Fong H, Hnilova M, Somerman MJ, Snead ML, Samudrala R, Tamerler C, Sarikaya M. Cementomimetics—constructing a cementum-like biomineralized microlayer via amelogenin-derived peptides. International Journal of Oral Science 2012;4:69-77.

[43] Ye Q, Spencer P, Yuca E, Tamerler C. Engineered Peptide Repairs Defective Adhesive–Dentin Interface. Macromolecular materials and engineering 2017;302:1600487.

[44] Wisdom C, Chen C, Yuca E, Zhou Y, Tamerler C, Snead ML. Repeatedly applied peptide film kills bacteria on dental implants. JOM 2019;71:1271-80.

[45] Xie S-X, Boone K, VanOosten SK, Yuca E, Song L, Ge X, Ye Q, Spencer P, Tamerler C. Peptide Mediated Antimicrobial Dental Adhesive System. Applied Sciences 2019;9:557.

[46] Yuca E, Tamerler C. Self-Assembled Recombinant Proteins on Metallic Nanoparticles as Bimodal Imaging Probes. JOM 2019;71:1281-90.

[47] Fischer NG, Münchow EA, Tamerler C, Bottino MC, Aparicio C. Harnessing biomolecules for bioinspired dental biomaterials. Journal of Materials Chemistry B 2020;8:8713-47.

[48] Xie S-X, Song L, Yuca E, Boone K, Sarikaya R, VanOosten SK, Misra A, Ye Q, Spencer P, Tamerler C. Antimicrobial peptide–polymer conjugates for dentistry. ACS applied polymer materials 2020;2:1134-44.

[49] Yuca E, Xie S-X, Song L, Boone K, Kamathewatta N, Woolfolk SK, Elrod P, Spencer P, Tamerler C. Reconfigurable Dual Peptide Tethered Polymer System Offers a Synergistic Solution for Next Generation Dental Adhesives. International Journal of Molecular Sciences 2021;22:6552.

[50] Sarikaya R, Song L, Yuca E, Xie S-X, Boone K, Misra A, Spencer P, Tamerler C. Bioinspired multifunctional adhesive system for next generation bio-additively designed dental restorations. Journal of the Mechanical Behavior of Biomedical Materials 2021;113:104135.

[51] Hnilova M, Liu X, Yuca E, Jia C, Wilson B, Karatas AY, Gresswell C, Ohuchi F, Kitamura K, Tamerler C. Multifunctional protein-enabled patterning on arrayed ferroelectric materials. ACS applied materials & interfaces 2012;4:1865-71.

[52] VanOosten SK, Yuca E, Karaca BT, Boone K, Snead ML, Spencer P, Tamerler C. Biosilver nanoparticle interface offers improved cell viability. Surface innovations 2016;4:121-32.

[53] Gungormus M, Oren EE, Horst JA, Fong H, Hnilova M, Somerman MJ, Snead ML, Samudrala R, Tamerler C, Sarikaya M. Cementomimetics-constructing a cementum-like biomineralized microlayer via amelogenin-derived peptides. Int J Oral Sci 2012;4:69-77.

[54] Oren EE, Tamerler C, Sahin D, Hnilova M, Seke UO, Sarikaya M, Samudrala R. A novel knowledge-based approach to design inorganic binding peptides. Bioinformatics 2007.

[55] Gibson CW, Yuan ZA, Hall B, Longenecker G, Chen E, Thyagarajan T, Sreenath T, Wright JT, Decker S, Piddington R, Harrison G, Kulkarni AB. Amelogenin-deficient mice display an amelogenesis imperfecta phenotype. J Biol Chem 2001;276:31871-5.

[56] Snead ML. Amelogenin protein exhibits a modular design: implications for form and function. Connect Tissue Res 2003;44 Suppl 1:47-51.

[57] Snead ML, Zhu DH, Lei Y, Luo W, Bringas PO, Jr., Sucov HM, Rauth RJ, Paine ML, White SN. A simplified genetic design for mammalian enamel. Biomaterials 2011;32:3151-7.

[58] Dogan S, Fong H, Yucesoy DT, Cousin T, Gresswell C, Dag S, Huang G, Sarikaya M. Biomimetic tooth repair: amelogenin-derived peptide enables in vitro remineralization of human enamel. ACS Biomaterials Science & Engineering 2018;4:1788-96.

[59] Karaca BT, Meyer J, VanOosten S, Richter M, Tamerler C. Modular Peptide-Based Hybrid Nanoprobes for Bio-Imaging and Bio-Sensing. MRS Online Proceedings Library (OPL) 2014;1621:155-61.

[60] Zhang S, Karaca BT, VanOosten SK, Yuca E, Mahalingam S, Edirisinghe M, Tamerler C. Coupling infusion and gyration for the nanoscale assembly of functional polymer nanofibers integrated with genetically engineered proteins. Macromolecular rapid communications 2015;36:1322-8.

[61] Wisdom EC, Zhou Y, Chen C, Tamerler C, Snead ML. Mitigation of peri-implantitis by rational design of bifunctional peptides with antimicrobial properties. ACS biomaterials science & engineering 2019;6:2682-95.

[62] Edwards CM, Ulapane SB, Kamathewatta NJB, Ashberry HM, Berrie CL. Fabrication and Growth Control of Metal Nanostructures through Exploration of Atomic Force Microscopy-Based Patterning and Electroless Deposition Conditions. The Journal of Physical Chemistry C 2020;124:25588-601.

[63] Ulapane SB, Kamathewatta NJB, Ashberry HM, Berrie CL. Controlled Electroless Deposition of Noble Metals on Silicon Substrates Using Self-Assembled Monolayers as Molecular Resists To Generate Nanopatterned Surfaces for Electronics and Plasmonics. ACS Applied Nano Materials 2019;2:7114-25.

[64] Spencer P, Wang Y. Adhesive phase separation at the dentin interface under wet bonding conditions. Journal of Biomedical Materials Research: An Official Journal of The Society for Biomaterials, The Japanese Society for Biomaterials, and The Australian Society for Biomaterials and the Korean Society for Biomaterials 2002;62:447-56.

[65] Spencer P, Ye Q, Park J, Topp EM, Misra A, Marangos O, Wang Y, Bohaty BS, Singh V, Sene F, Eslick J, Camarda K, Katz JL. Adhesive/Dentin Interface: The Weak Link in the Composite Restoration. Annals of Biomedical Engineering 2010;38:1989-2003.

[66] Hnilova M, Liu X, Yuca E, Jia C, Wilson B, Karatas AY, Gresswell C, Ohuchi F, Kitamura K, Tamerler C. Multifunctional protein-enabled patterning on arrayed ferroelectric materials. ACS Appl Mater Interfaces 2012;4:1865-71.

[67] Karaca BT, Meyer J, VanOosten S, Richter M, Tamerler C. Modular Peptide-Based Hybrid Nanoprobes for Bio-Imaging and Bio-Sensing. MRS Online Proceedings Library Archive 2014;1621:155-61.

[68] Wriggers W, Chakravarty S, Jennings PA. Control of protein functional dynamics by peptide linkers. Peptide Science: Original Research on Biomolecules 2005;80:736-46.

[69] Hnilova M, Khatayevich D, Carlson A, Oren EE, Gresswell C, Zheng S, Ohuchi F, Sarikaya M, Tamerler C. Single-step fabrication of patterned gold film array by an engineered multi-functional peptide. J Colloid Interf Sci 2012;365:97-102.

[70] Wisdom C, VanOosten SK, Boone KW, Khvostenko D, Arnold PM, Snead ML, Tamerler C. Controlling the Biomimetic Implant Interface: Modulating Antimicrobial Activity by Spacer Design. J Mol Eng Mater 2016;4:1640005.

[71] Lamiable A, Thévenet P, Rey J, Vavrusa M, Derreumaux P, Tufféry P. PEP-FOLD3: faster de novo structure prediction for linear peptides in solution and in complex. Nucleic Acids Research 2016;44:W449-W54.

[72] Chen JE, Huang CC, Ferrin TE. RRDistMaps: a UCSF Chimera tool for viewing and comparing protein distance maps. Bioinformatics 2015;31:1484-6.

[73] Chen X, Zaro JL, Shen W-C. Fusion protein linkers: Property, design and functionality. Advanced Drug Delivery Reviews 2013;65:1357-69.

[74] Yazici H, Habib G, Boone K, Urgen M, Utku FS, Tamerler C. Self-assembling antimicrobial peptides on nanotubular titanium surfaces coated with calcium phosphate for local therapy. Materials Science and Engineering: C 2019;94:333-43.

[75] Tan SF, Chee SW, Lin GH, Mirsaidov U. Direct Observation of Interactions between Nanoparticles and Nanoparticle Self-Assembly in Solution. Accounts of Chemical Research 2017;50:1303-12.

[76] Yucesoy DT. Peptide-guided Dental Tissue Regeneration for Oral Care 2018.

[77] Sheikh Z, Abdallah M-N, Hanafi AA, Misbahuddin S, Rashid H, Glogauer M. Mechanisms of in vivo degradation and resorption of calcium phosphate based biomaterials. Materials 2015;8:7913-25.

[78] LeGeros RZ. Calcium phosphate-based osteoinductive materials. Chemical reviews 2008;108:4742-53.

[79] LeGeros RZ, LeGeros JP. Calcium phosphate bioceramics: past, present and future. Key Engineering Materials: Trans Tech Publ; 2003. p. 3-10.

[80] Gungormus M, Fong H, Kim IW, Evans JS, Tamerler C, Sarikaya M. Regulation of in vitro calcium phosphate mineralization by combinatorially selected hydroxyapatite-binding peptides. Biomacromolecules 2008;9:966-73.

[81] Wisdom C, VanOosten SK, Boone KW, Khvostenko D, Arnold PM, Snead ML, Tamerler C. Controlling the Biomimetic Implant Interface: Modulating Antimicrobial Activity by Spacer Design. J Mol Eng Mater 2016;4.

[82] Sulyanto R, Kang M, Srirangapatanam S, Berger M, Candamo F, Wang Y, Dickson J, Ng M, Ho S. Biomineralization of dental tissues treated with silver diamine fluoride. Journal of Dental Research 2021;100:1099-108.

[83] Mei M, Nudelman F, Marzec B, Walker J, Lo E, Walls A, Chu C. Formation of fluorohydroxyapatite with silver diamine fluoride. Journal of dental research 2017;96:1122-8.

[84] Hamdy D, Giraki M, Abd Elaziz A, Badran A, Allam G, Ruettermann S. Laboratory evaluation of the potential masking of color changes produced by silver diamine fluoride in primary molars. BMC Oral Health 2021;21:337.

[85] Fröhlich TT, Gindri LDO, Pedrotti D, Cavalheiro CP, Soares FZM, Rocha RdO. Evaluation of the Use of Potassium Iodide Application on Stained Demineralized Dentin Under Resin Composite Following Silver Diamine Fluoride Application. Pediatric Dentistry 2021;43:57-61.

[86] Roberts A, Bradley J, Merkley S, Pachal T, Gopal J, Sharma D. Does potassium iodide application following silver diamine fluoride reduce staining of tooth? A systematic review. Australian dental journal 2020;65:109-17.

[87] Spencer P, Ye Q, Misra A, Goncalves SdP, Laurence J. Proteins, pathogens, and failure at the composite-tooth interface. Journal of dental research 2014;93:1243-9.

[88] Drummond JL. Degradation, fatigue, and failure of resin dental composite materials. Journal of dental research 2008;87:710-9.

[89] Chisini LA, Collares K, Cademartori MG, de Oliveira LJC, Conde MCM, Demarco FF, Correa MB. Restorations in primary teeth: a systematic review on survival and reasons for failures. International journal of paediatric dentistry 2018;28:123-39.

[90] Elbahie E, Beitzel D, Mutluay MM, Majd H, Yahyazadehfar M, Arola D. Durability of adhesive bonds to tooth structure involving the DEJ. Journal of the Mechanical Behavior of Biomedical Materials 2018;77:557-65.

[91] Spencer P, Ye Q, Song L, Parthasarathy R, Boone K, Misra A, Tamerler C. Threats to adhesive/dentin interfacial integrity and next generation bio-enabled multifunctional adhesives. J Biomed Mater Res B Appl Biomater 2019;107:2673-83.

[92] Tripathi P, Mengi R, Gajare SM, Nanda SS, Wani SA, Kochhar AS. Evaluation of Remineralizing Capacity of P11-4, CPP-ACP, Silver Diamine Fluoride, and NovaMin: An In Vitro Study. The Journal of Contemporary Dental Practice 2021;22:357-60.

[93] Wu X, Mahalingam S, VanOosten SK, Wisdom C, Tamerler C, Edirisinghe M. New Generation of Tunable Bioactive Shape Memory Mats Integrated with Genetically Engineered Proteins. Macromol Biosci 2017;17.

[94] Ye Q, Spencer P, Yuca E, Tamerler C. Engineered Peptide Repairs Defective Adhesive-Dentin Interface. Macromol Mater Eng 2017;302.

[95] Yuca E, Karatas AY, Seker UO, Gungormus M, Dinler-Doganay G, Sarikaya M, Tamerler C. In vitro labeling of hydroxyapatite minerals by an engineered protein. Biotechnol Bioeng 2011;108:1021-30.

Chapter 5 Summary and Future Directions

5.1 Summary

This dissertation was focused on exploring the utilization of bifunctional constructs designed as tunable biomolecular assemblers for biomedically relevant applications ranging from *in vitro* to *in vivo* environments. Modularity offered in this biomolecular design approach builds upon engineering small peptide domains to incorporate desired functions at the challenging biomaterial-tissue interfaces and biological environments. Controlling and/or driving the functionality at these interfaces opens new avenues to develop solutions to different biomedical problems. Motivated with the opportunity to integrate bioactive agents to novel biomaterial interface design, we employed three different groups of solid-binding peptides and further engineered their functionality to develop three distinctive biomaterials design as a solution for different biomedically relevant challenges. Our innovative approach relied upon the successful integration of peptide-protein or peptide-peptide bifunctional constructs with the ability to bind to surfaces dynamically, to form a uniform interfacial layer as well as an additional function. The additional, biomedically relevant functionality can serve for several different purposes, e.g., visualization, localization, monitoring, sensing potential, and guided remineralization at the vulnerable sites to form nanocomposite coatings for utilization under biological environments. We hypothesized ***that solid binding peptides can be engineered with additional biological activities as effective and robust multi-functional molecular assemblers for biomedical applications under conditions ranging from*** **in vitro** ***to*** **in vivo** ***environments.*** This hypothesis was tested and validated across three chapters, herein, each featuring a publication that demonstrated the successful use of our bifunctional constructs in a unique application.

In our design, we employed mineral and metal binding peptides, specifically HABP, AuBP, and AgBP, each of which was shown to have selective affinity to their respective surfaces. However, each biological application and environment may add another level of complexity when these interactions are compared to well defined material surfaces. The anchoring property of these peptides was investigated under different conditions specific to each chosen application. The solid-binding peptides were designed to be an integrated part of fluorescence proteins or other bioactive peptides. The sustained multi-domain activity and function of these biomolecular constructs, i.e., GFP-HABP, DsRed-AuBP, and shADP5-AgBP were explored *in vivo* and *in vitro* and within complex biological environments. Overall, we demonstrated that biomolecular constructs enabled dynamic, robust anchoring and functionalization of key surfaces where bioactivity could be displayed at a complex interface.

In the work that featured the incorporated bioactivity in a PLLA/PMMA shape memory polymer mat, we demonstrated how our bifunctional constructs could be uniformly distributed throughout a complex, 3D fiber network. This bio-enabled approach featured GFP-HABP-decorated hydroxyapatite nanoparticle used as the anchoring surface upon which our HABP construct bound via selective surface affinity to display the fluorescence protein. In this approach, we can monitor the location, distribution, and sustained activity via fluorescence microscopy. To assess the dual functionality of the bioactive construct within the PLLA/PMMA binary blend shape memory fibers, an enzyme-mediated biomineralization assay was employed. SMP fiber mats with and without the GFP-HABP construct were subjected to the assay and mineralized in a buffered solution. The formed calcium phosphate minerals were studied using vibrational spectroscopic analysis, which showed changes to the characteristic mineral peaks in the fibers where the protein-peptide construct was present. This published work demonstrated the dual bioactivity of the

biomolecular constructs within the 3-D network of PLLA/PMMA polymer-based fiber mats and provided a promising platform approach to develop a tunable biomaterial.[1] Future studies are required to determine the sustained activity and compatibility of these bioactive SMPs in a physiologic environment. Further, additional studies may focus on exploring different approaches to incorporate a mineral-mediating peptide allowing for increased accessibility so that the mineralization could be tuned and controlled for the desired soft to hard material transition state.

A bio-enabled approach for monitoring free biometals was demonstrated as part of this dissertation using a zebrafish brain model. Our studies highlighted the sustained bifunctional activity of another fluorescence protein-peptide construct, specifically DsRed-AuBP, used to functionalize AuNPs to be used as bioactive nanoprobes in an *in vivo* environment for the first time. This proof-of-concept study showed the nanoprobes remained stationary and discrete following injection into the zebrafish brain and further resisted photobleaching of the fluorescent moiety during an hour of imaging. The robust, sustained binding of our AuBP anchoring peptide to the AuNP surfaces and active fluorescence moiety allowed us to track the engineered nanoprobes with both spatial and temporal resolution to further study fluorescence quenching response in the presence of added Zn^{2+}. This approach can be further combined with other orthogonal methods where the peptide-functionalized nanoprobes can be designed in future studies to selectively target specific metal ions and dysregulation in a living brain tissue model. Optimized selectivity of bio-enabled nanoprobes offer spatiotemporal imaging opportunities that would have a significant impact toward understanding neurodegenerative disease pathogenesis. Future studies for this project will focus on measuring the metal ion concentrations via fluorescence quenching or through the incorporation of additional metal binding tags to measure specific biometals or key small molecules. Overall, this work opens an avenue for designing modular, multi-functional

biohybrid nanoprobes offering spatiotemporal imaging through the sustained multi-activity in a physiological environment.

Our last application focused on pediatric dentistry and demonstrated a potential use of a novel bifunctional peptide designed using computational and experimental approaches. ECC is the most prevalent disease among children worldwide and the recently approved use of SDF can be employed to arrest dental caries progression in a simple and low-cost manner. However, the treatment faces challenges due to the negative aesthetics arising from the permanent dark staining of caries-effected tissues. With this challenge in mind, we designed a bio-enabled bifunctional peptide system to use at the interface of SDF-treated dental carious tissues featuring an anchoring peptide (AgBP) and a functional peptide (shADP5) to enable remineralization of silver-stained dental tissues. In our study, shADP5-AgBP was iteratively designed and evaluated as an innovative approach to mask the negative cosmetic side effects which can have a significant burden for the children. Directed remineralization of SDF-treated surfaces would be tuned to provide an opportunity for SDF treatment in children with ECC. As this is a recently emerging area of research, the use of a peptide-based approach to modulate the SDF-stained dental surfaces has not previously been reported to our knowledge. We verified the successful binding of AgBP to SDF treated human dental tissues. Different spacers were tested that lead to successful domain combination to represent both peptide functionality and the designed shADP5-AgBP2 bifunctional peptide also demonstrated the ability to guide formation of calcium phosphate nanocomposite materials on the SDF-stained dental tissue interface. Future studies are ongoing to tune the peptide and spacer sequences to achieve a more desirable mineral composition and morphology. We believe there is immense potential to develop an optimized bifunctional peptide that can work synergistically with SDF to remineralize dentin and enamel to provide an interface to reduce the

stained appearance. The successful binding of our anchoring AgBP peptide to SDF-stained regions provides a near-limitless platform to develop an easy to use and cost effective bi- or multi-functional construct toward positive aesthetic outcomes for patients requiring SDF treatment for caries arrest.

5.2 Future Outlook

Herein, we presented multiple examples of the successful incorporation of affinity-binding peptides as a core feature of bifunctional moieties in both *in vivo* and *in vitro* environments. As the field of molecular biomimetics continues to flourish, we aim to further expand our studies to implement our modular design approach to address new applications. Our group, as well as many others, continue to discover and optimize novel peptide sequences capable of specific functions including, but not limited to, selective solid material binding, directed mineral nucleation, antimicrobial activity, cell adhesion, hydrogel formation, anti-cancer therapeutics, and tissue engineering matrix structures.[2-38] Vast libraries have been established for these short bioactive sequences. The ability to form molecular-scale, uniform coverage on both simple and complex biomaterial surfaces and bring additional functionality to those interfaces provides a platform technology for advanced design.

Although this approach is modular, when creating new bifunctional constructs it is critical to design a spacer or linker sequence between the two functional units to ensure each structure, and therefore function, is maintained. Because the function of peptides and proteins are highly dependent upon their structure and conformation, iterative biocomputational design is required to model and predict the spacer or linker sequences allowing optimal conformation of each functional unit. Our group and others have reported on the importance of spacer or linker sequence design and selection to enable robust functionality of both bioactive units.[39-44] Different considerations

should be taken into account when creating novel peptide-peptide constructs versus peptides conjugated with other bioactive moieties to consider size disparities and footprints on a biomaterial surface. For example, spacer length, flexibility/rigidity, and charge units are all key to the selection process and must be considered for each unique construct and application.

With the increasing demand for next-generation, smart biomaterials, future applications aim to incorporate additional moieties moving beyond bifunctionality into a multi-functional approach to peptide-enabled biomaterial surfaces. In those cases, spacer design and the iterative processes of synthesis, characterization, and testing become even more complex. Therefore, we also rely upon advances in biocomputational modeling programs and simulation software to provide better predictions prior to the production or synthesis of peptide-based bi- and multi-functional bioactive constructs. These advanced computational tools are critical to providing a better understanding of the structure-function relationships and simulations to show how these may be impacted under unique environments are critical to advancing peptide and multifunctional peptide designs.

Therefore, although we present bifunctional molecular assemblers featuring solid-binding peptides as a modular platform technology, the successful design of new bi- or multi-functional units requires an advanced iterative biocomputational process, rigorous validation and characterization, and analysis under variable environments. Currently established and novel peptide sequences with surface selectivity and specificity allow for a molecular-scale anchor to biomaterial surfaces with the ability to incorporate additional functionality to design novel biohybrid materials. Tunable, bioactive nano-interfaces with multifunctional design offer unique engineering opportunities to develop novel biomaterials for challenging applications.

5.3 References

[1] Wu X, Mahalingam S, VanOosten SK, Wisdom C, Tamerler C, Edirisinghe M. New Generation of Tunable Bioactive Shape Memory Mats Integrated with Genetically Engineered Proteins. Macromol Biosci 2017;17.

[2] Abbas M, Zou Q, Li S, Yan X. Self-Assembled Peptide- and Protein-Based Nanomaterials for Antitumor Photodynamic and Photothermal Therapy. Advanced materials (Deerfield Beach, Fla) 2017;29.

[3] Acar H, Srivastava S, Chung EJ, Schnorenberg MR, Barrett JC, LaBelle JL, Tirrell M. Self-assembling peptide-based building blocks in medical applications. Advanced drug delivery reviews 2017;110:65-79.

[4] Baig MH, Ahmad K, Saeed M, Alharbi AM, Barreto GE, Ashraf GM, Choi I. Peptide based therapeutics and their use for the treatment of neurodegenerative and other diseases. Biomedicine & Pharmacotherapy 2018;103:574-81.

[5] Boone K, Camarda K, Spencer P, Tamerler C. Antimicrobial peptide similarity and classification through rough set theory using physicochemical boundaries. BMC Bioinformatics 2018;19:469.

[6] Briggs BD, Knecht MR. Nanotechnology meets biology: peptide-based methods for the fabrication of functional materials. The journal of physical chemistry letters 2012;3:405-18.

[7] Care A, Bergquist PL, Sunna A. Solid-binding peptides: smart tools for nanobiotechnology. Trends in biotechnology (Regular ed) 2015;33:259-68.

[8] Chen J, Zou X. Self-assemble peptide biomaterials and their biomedical applications. Bioactive Materials 2019;4:120-31.

[9] Cui H, Webber MJ, Stupp SI. Self-assembly of peptide amphiphiles: From molecules to nanostructures to biomaterials. Peptide Science: Original Research on Biomolecules 2010;94:1-18.

[10] De Santis E, Ryadnov MG. Peptide self-assembly for nanomaterials: the old new kid on the block. Chemical Society Reviews 2015;44:8288-300.

[11] Dogan S, Fong H, Yucesoy DT, Cousin T, Gresswell C, Dag S, Huang G, Sarikaya M. Biomimetic tooth repair: amelogenin-derived peptide enables in vitro remineralization of human enamel. ACS Biomaterials Science & Engineering 2018;4:1788-96.

[12] Fichman G, Gazit E. Self-assembly of short peptides to form hydrogels: Design of building blocks, physical properties and technological applications. Acta Biomaterialia 2014;10:1671-82.

[13] Fosgerau K, Hoffmann T. Peptide therapeutics: current status and future directions. Drug Discovery Today 2015;20:122-8.

[14] Fukunaga K, Tsutsumi H, Mihara H. Self-assembling peptides as building blocks of functional materials for biomedical applications. Bulletin of the Chemical Society of Japan 2019;92:391-9.

[15] Gungormus M, Branco M, Fong H, Schneider JP, Tamerler C, Sarikaya M. Self assembled bi-functional peptide hydrogels with biomineralization-directing peptides. Biomaterials 2010;31:7266-74.

[16] Gungormus M, Oren EE, Horst JA, Fong H, Hnilova M, Somerman MJ, Snead ML, Samudrala R, Tamerler C, Sarikaya M. Cementomimetics-constructing a cementum-like biomineralized microlayer via amelogenin-derived peptides. Int J Oral Sci 2012;4:69-77.

[17] Habibi N, Kamaly N, Memic A, Shafiee H. Self-assembled peptide-based nanostructures: Smart nanomaterials toward targeted drug delivery. Nano Today 2016;11:41-60.

[18] Hamley IW. Small Bioactive Peptides for Biomaterials Design and Therapeutics. Chemical Reviews 2017;117:14015-41.

[19] Hnilova M, Karaca BT, Park J, Jia C, Wilson BR, Sarikaya M, Tamerler C. Fabrication of hierarchical hybrid structures using bio-enabled layer-by-layer self-assembly. Biotechnol Bioeng 2012;109:1120-30.

[20] Karaca BT, Meyer J, VanOosten S, Richter M, Tamerler C. Modular Peptide-Based Hybrid Nanoprobes for Bio-Imaging and Bio-Sensing. MRS Online Proceedings Library Archive 2014;1621:155-61.

[21] Khadka DB, Haynie DT. Protein-and peptide-based electrospun nanofibers in medical biomaterials. Nanomedicine: Nanotechnology, Biology and Medicine 2012;8:1242-62.

[22] Khatayevich D, Gungormus M, Yazici H, So C, Cetinel S, Ma H, Jen A, Tamerler C, Sarikaya M. Biofunctionalization of materials for implants using engineered peptides. Acta Biomater 2010;6:4634-41.

[23] Kyle S, Aggeli A, Ingham E, McPherson MJ. Recombinant self-assembling peptides as biomaterials for tissue engineering. Biomaterials 2010;31:9395-405.

[24] Li J, Xing R, Bai S, Yan X. Recent advances of self-assembling peptide-based hydrogels for biomedical applications. Soft Matter 2019;15:1704-15.

[25] Maude S, Ingham E, Aggeli A. Biomimetic self-assembling peptides as scaffolds for soft tissue engineering. Nanomedicine 2013;8:823-47.

[26] Pugliese R, Gelain F. Peptidic Biomaterials: From Self-Assembling to Regenerative Medicine. Trends in Biotechnology 2017;35:145-58.

[27] Qi GB, Gao YJ, Wang L, Wang H. Self-assembled peptide-based nanomaterials for biomedical imaging and therapy. Advanced Materials 2018;30:1703444.

[28] Rad-Malekshahi M, Lempsink L, Amidi M, Hennink WE, Mastrobattista E. Biomedical applications of self-assembling peptides. Bioconjugate chemistry 2016;27:3-18.

[29] Sarikaya M, Tamerler C, Jen AKY, Schulten K, Baneyx F. Molecular biomimetics: nanotechnology through biology. Nature Materials 2003;2:577-85.

[30] Tamerler C, Kacar T, Sahin D, Fong H, Sarikaya M. Genetically engineered polypeptides for inorganics: A utility in biological materials science and engineering. Materials Science and Engineering: C 2007;27:558-64.

[31] Tamerler C, Khatayevich D, Gungormus M, Kacar T, Oren EE, Hnilova M, Sarikaya M. Molecular biomimetics: GEPI-based biological routes to technology. Biopolymers 2010;94:78-94.

[32] Tamerler C, Sarikaya M. Molecular biomimetics: nanotechnology and bionanotechnology using genetically engineered peptides. Philos Trans A Math Phys Eng Sci 2009;367:1705-26.

[33] Veltri D, Kamath U, Shehu A. Improving Recognition of Antimicrobial Peptides and Target Selectivity through Machine Learning and Genetic Programming. IEEE/ACM Transactions on Computational Biology and Bioinformatics 2017;14:300-13.

[34] Xie S-X, Boone K, VanOosten SK, Yuca E, Song L, Ge X, Ye Q, Spencer P, Tamerler C. Peptide Mediated Antimicrobial Dental Adhesive System. Applied Sciences 2019;9:557.

[35] Yadav N, Chauhan MK, Chauhan VS. Short to ultrashort peptide-based hydrogels as a platform for biomedical applications. Biomaterials science 2020;8:84-100.

[36] Yazici H, Habib G, Boone K, Urgen M, Utku FS, Tamerler C. Self-assembling antimicrobial peptides on nanotubular titanium surfaces coated with calcium phosphate for local therapy. Materials Science and Engineering: C 2019;94:333-43.

[37] Zamuner A, Brun P, Scorzeto M, Sica G, Castagliuolo I, Dettin M. Smart biomaterials: Surfaces functionalized with proteolytically stable osteoblast-adhesive peptides. Bioactive Materials 2017;2:121-30.

[38] Zhang S. Fabrication of novel biomaterials through molecular self-assembly. Nature Biotechnology 2003;21:1171-8.

[39] Wisdom EC, Zhou Y, Chen C, Tamerler C, Snead ML. Mitigation of peri-implantitis by rational design of bifunctional peptides with antimicrobial properties. ACS Biomater Sci Eng 2020;6:2682-95.

[40] Yucesoy DT, Khatayevich D, Tamerler C, Sarikaya M. Rationally designed chimeric solid-binding peptides for tailoring solid interfaces. Medical Devices & Sensors 2020;3:e10065.

[41] Chen X, Zaro JL, Shen W-C. Fusion protein linkers: Property, design and functionality. Advanced Drug Delivery Reviews 2013;65:1357-69.

[42] Liu Z, Ma S, Duan S, Xuliang D, Sun Y, Zhang X, Xu X, Guan B, Wang C, Hu M, Qi X, Zhang X, Gao P. Modification of Titanium Substrates with Chimeric Peptides Comprising Antimicrobial and Titanium-Binding Motifs Connected by Linkers To Inhibit Biofilm Formation. ACS Applied Materials & Interfaces 2016;8:5124-36.

[43] Papaleo E, Saladino G, Lambrughi M, Lindorff-Larsen K, Gervasio FL, Nussinov R. The Role of Protein Loops and Linkers in Conformational Dynamics and Allostery. Chemical Reviews 2016;116:6391-423.

[44] Wriggers W, Chakravarty S, Jennings PA. Control of protein functional dynamics by peptide linkers. Peptide Science: Original Research on Biomolecules 2005;80:736-46.

Appendix A Contributions to Literature

1. **S.K. Woolfolk**, A.K. Cloyd, Q. Ye, K. Boone, P. Spencer, M.L. Snead, C. Tamerler "Peptide enabled nanocomposites offer biomimetic reconstruction of silver diamine treated dental tissues", *Polymers, submitted January, 2022 (In Review)*
2. R. Jarosova, **S.K. Woolfolk**, N. Martinez-Rivera, M.W. Jaeschke, E. Rosa-Molinar, C. Tamerler, M.A. Johnson "Engineered nanoprobes for spatiotemporal imaging of metal ions in living brain tissue", *ChemComm, submitted January, 2022 (In Review)*
3. E. Yuca, S.X. Xie, L. Song, K. Boone, N.J.B. Kamathewatta, **S.K. Woolfolk**, P. Elrod, P. Spencer, C. Tamerler "Reconfigurable Dual Peptide Tethered Polymer System Offers a Synergistic Solution for Next Generation Dental Adhesives", International Journal of Molecular Sciences, 22(12) 6552 (2021).
4. P. Spencer, Q. Ye, N.J.B. Kamathewatta, **S.K. Woolfolk**, B.S. Bohaty, A. Misra, C. Tamerler "Chemometrics-Assisted Raman Spectroscopy Characterization of Tunable Polymer-Peptide Hybrids for Dental Tissue Repair", Frontiers in Materials, 8 (2021).
5. S.X. Xie, L. Song, E. Yuca, K. Boone, R. Sarikaya, **S.K. VanOosten**, A. Misra, Q. Ye, P. Spencer, C. Tamerler "Antimicrobial peptide–polymer conjugates for dentistry", ACS Applied Polymer Materials, 2(3) 1134-1144 (2020).
6. S.X. Xie, K. Boone, **S.K. VanOosten**, E. Yuca, L. Song, X. Ge, Q. Ye, P. Spencer, C. Tamerler "Peptide Mediated Antimicrobial Dental Adhesive System", Applied Sciences, 9(3) (2019).
7. X. Wu, S. Mahalingam, **S.K. VanOosten**, C. Wisdom, C. Tamerler, M. Edirisinghe "New Generation of Tunable Bioactive Shape Memory Mats Integrated with Genetically Engineered Proteins", Macromolecular Bioscience, 17(2) (2017). Feature Cover
8. C. Wisdom, **S.K. VanOosten**, K. Boone, D. Khvostenko, P.M. Arnold, M.L. Snead, C. Tamerler "Controlling the Biomimetic Implant Interface: Modulating Antimicrobial Activity by Spacer Design", Journal of Molecular and Engineering Materials, 4(1) (2016).
9. **S.K. VanOosten**, E. Yuca, B.T. Karaca, K. Boone, M.L. Snead, P.A. Spencer, C. Tamerler "Biosilver nanoparticle interface offers improved cell viability", Surface Innovations, 4(3) 121-132 (2016).
10. S. Zhang, B.T. Karaca, **S.K. VanOosten**, E. Yuca, S. Mahalingam, M. Edirisinghe, C. Tamerler "Coupling infusion and gyration for the nanoscale assembly of functional polymer nanofibers integrated with genetically engineered proteins", Macromolecular Rapid Communications, 36(14) 1322-1328 (2015).
11. B.T. Karaca, J.E. Meyer, **S.K. VanOosten**, M. Richter, C. Tamerler "Modular peptide-based hybrid nanoprobes for bio-imaging and bio-sensing", MRS Proceedings, 1621, 155-161 (2014).